Republic of Iraq
Ministry of Higher Education
and Scientific Research
University of Babylon
College of Engineering
Civil Engineering Department

NONLINEAR FINITE ELEMENT ANALYSIS OF PLANE FRAME COMPOSED OF COMPOSITE MEMBERS

A Thesis

Submitted to the College of Engineering of the University of Babylon
in Partial Fulfillment of the Requirements for the Degree
of Master of Science in Civil Engineering

By

Majid Mohammed-Ali Kadhim Mohi-Aldeen

(B.Sc. in Civil Engineering 2006)

Supervised by
Prof. Dr. Nameer A. Alwash
Ass. Prof. Mustafa B. Dawood

Nov. , 2008

بسم الله الرحمن الرحيم

ومن يتوكلْ علَى الله فَهو حسبه إِن الله بالغُ أَمرِه قَد جعلَ الله لكُل شيءٍ قَدراً

صدق الله العلي العظيم

سورة الطلاق–الآية(3)

ACKNOWELDGMENTS

*In the name of **Allah**, the most **gracious**, the most **merciful***

*At first, thank to **Allah** my **God** who helped and enabled me to complete this research.*

*I wish to express my thanks to my supervisors **Prof. Dr. Namir Alwash** and **Ass. Prof. Dr. Mustafa B. Dawood** for their advice, guidance and encouragement throughout this work.*

A special thank and gratitude to my family and my friends especially my parents for their care, patience and encouragement throughout the research period.

Also I wish to thank my sisters for their encouragement during the research period.

Majid Mohammed Ali

CERTIFICATE OF THE EXAMINING COMMITTEE

We certify as an Examining Committee that we have read this thesis titled "***Nonlinear Finite Element Analysis of Plane Frame Composed of Composite Members***" and examined the student "**Majid Mohammed-Ali Kadhim**" in its content and what related to it, and found it meets the standard of thesis for the degree of Master of science in Civil Engineering (Structural Engineering).

Signature:
Name: ***Prof. Dr. Nameer A. Alwash***
(Supervisor)
Date: / /2009

Signature:
Name: ***Ass.Prof. Dr. Mustafa B. Dawood***
(Supervisor)
Date: / /2009

Signature:
Name: ***Prof. Dr. Bayan S. Obaid***
(Member)
Date: / /2009

Signature:
Name: ***Ass.Prof. Abdul Ridah Saleh***
(Member)
Date: / /2009

Signature:
Name: *Ass.****Prof. Dr. Ali M. Al-Athray***
(Chairman)
Date: / /2009

Approved by the Head of the Civil Engineering Department

Signature:
Name: ***Prof. Dr. Ammar Y. Ali***
(The Head of the Civil Engineering Department)
Date: / / 2009

Approved by the Dean of the College of Engineering

Signature:
Name: ***Ass.Prof. Dr. Salah Tawfeek Al-Bazzaz***
(The Dean of the College of Engineering)
Date: / / 2009

Abstract

In the present work nonlinear finite element analysis has been used to predict the load deflection behavior of composite frame under different static load conditions by using ANSYS (ANalysis SYStem) (version 9) computer program, eight-node brick element has been used to model concrete (plain or reinforced) and steel parts (tube or I-section). The bond between steel structure and concrete has been modeled by using two-node contact element. The full Newton-Raphson method is used for the nonlinear solution algorithm, the materials nonlinearity due to cracking, crushing of concrete, and yielding of steel structure (tube or I-section) are taken into consideration during the analysis. In tension, the crack is represented by a fixed smeared crack with post cracking shear transfer model to simulate the aggregate interlock and dowel actions.

Different composite members (beams and columns) have been analyzed and their results are compared with experimental data and found to give good agreement. In the present study three types of frames (composite frame composed of concrete filled steel tube members, composite frame composed of concrete encased steel members, and reinforced concrete frame) with same cross section area of steel and concrete have been investigated in the present analysis. Among the conclusions obtained, the first type of frames (composed of concrete filled steel tube) is of higher load carrying capacity than the other types of frames by about (36%), while the second type of frames (composed of concrete encased steel) have a higher load carrying capacity than reinforced concrete frame by about (52%).

The parametric studies results in several conditions. One of them, using circular cross section for concrete filled steel tube beam and columns gives higher load carrying capacity in comparison with other shapes (square and rectangular) with the same cross section area (for steel and concrete) by about 6% and 11% respectively for beam and about 17% and 22% for column respectively.

Contents

Notation

A_c	Area of concrete. mm^2
A_s	Area of steel.mm^2
D_i	The inside dimension of steel.mm
D_o	The outside dimension of steel (diameter of circular section or length of a side on a square).mm
E_c	Elastic modulus of concrete. MPa
E_s	Modulus of elasticity of steel. MPa
f'_c	The circular compressive strength of the concrete. MPa
f_{ch}	Ultimate biaxial compressive strength. Mpa
f_{cu}	Cube strength of concrete. MPa
f_{sy}	Yield strength of steel. MPa
f_s'	Allowable steel stress. MPa
f_r	Modulus of rapture. MPa
f_1	Ultimate compressive strength for a state of biaxial compressive superimposed on. MPa
f_2	Ultimate compressive strength for a state of uniaxial compressive superimposed on. MPa
M_o	The ultimate pure bending capacity. N.mm
P_o	The axial force capacity. N
G_s	Shear modulus. MPa
L	Length of column. mm
r_c	Radius of gyration of concrete core. mm
r_s	Radius of gyration of steel tube. mm
ρ_s	Unit mass. Kg/m^3
σ_h	Hydrostatic stress. MPa
v	Poisson's ratio.
ε	Strain at stress f.
ε_o	Strain at the ultimate compressive strength $f'c$.

σ	Stress at any strain ε. MPa
μ	Friction coefficient.
β_o, β_c	Shear transfer coefficient for opened and closed cracks (respectively).

CHAPTER ONE

INTRODUCTION

1.1. Composite Construction

Composite structures are hybrid structures formed by combining two or more elements into a structural system. The composite structure has seen widespread use in recent decades because of the benefits of combining the two construction materials. Reinforced concrete is inexpensive, massive, and stiff, while steel members are strong, lightweight, and easy to assemble.

The earliest use of composite construction was in North America, the year 1894 is stated as the time in which concrete encased beams were first used in a bridge in Iowa and a building in Pittsburgh. The earliest laboratory tests on encased columns took place at Columbia University in 1908, whilst composite beams were first tested at the Dominion Bridge Works in Canada in 1922. By 1930 the New York City building code recognized some benefit of concrete encasement to steelwork by permitting higher extreme fibre stresses in the steel parts of the encased members **[1]**.

Early used in Japan of concrete encasement to improve both fire and earthquake resistance, dating from about 1910. Termed “steel reinforced concrete” or SRC, this form of construction was quickly become popular for buildings of more than 6 stories. Its integrity was demonstrated by the good performance of structures of this type in the great Kanto earthquake of 1923.Any research on the topic in Japan did not start until the 1930s; codes came much later, with the first SRC code produced by the Architectural Institute of Japan (AIJ) appearing in 1958**[1]**. Working on a design guide for composite bridges was started in 1952 but the document was not published until

1959. Beginning with the earliest beam tests in 1929 and column tests in the same year, research studies flourished in the 1950s and 1960s, leading to a heavy concentration since then on understanding the behavior of composite construction when subjected to seismic action. **[2]**

One of the earliest substantial documents devoted to composite construction was the book by Viest *et al* **[2]**. It referred to early usage of the technique in the United States by 1935 and a patent by Kahn dated 1926.

Parallel developments had been taken place in Europe-especially as part of the post-war reconstruction in Germany. Reporting on this in 1957 **[3],** refers to "research in Germany, Switzerland and elsewhere" providing the basis for their "Provisional Regulations for the Design of Girders in Composite Construction" published in July 1950. Four years later the topic was addressed more formally in DIN 1078. Sattler **[4]** reported on numerous examples of the use of composite construction for both bridges and buildings in Germany. This extended to the use of concrete filled tubes as columns but for beams relied on far more complex forms of shear connection than the welded studs which were at that time already being introduced into the United States by the Nelson company. In the discussion to these papers, British researchers Chapman & Johnson referred to both research in progress and buildings under construction that had been designed compositely at Imperial College and Cambridge University. **[4]**

Figure 1.1 shows examples of towers and buildings constructed of composite members in Hong Kong and London

Figure 1.1 Examples of buildings construct of composite members[6]

1.2. Composite Frame

A composite frame is defined in Eurocode4 part1.1 **[5]** "Framed structure for a building or similar construction work, in which some or all of the beams and columns are composite members. The use of reinforced or prestressed concrete or mansory member in bracing system is not excluded".

It is implied by this definition that a composite frame is more similar to a structural steel frame then to one in reinforced or prestressed concrete **[6]**. It is likely to be built by first erection a frame of steel beams and columns, then fixing profile sheeting to the steel work to provide working platform, and finally constructing the reinforced concrete.

1.3. Types of sections

The most common types of steel-concrete composite members are shown in ***Figure 1.2.*** The cross sections can be classified in 3 groups **[7]**:

- Fully encased
- Partially encased
- Concrete filled tube

Composite members are available in many different types of cross-section some of which are shown in ***Figure 1.2***. Among these, the steel section encased in concrete ***Figure 1.2a*** perhaps represents the earliest type of composite cross-section. Initially, due to low grade, concrete was merely used as insulation to provide the steel section's fire resistance.

To eliminate temporary formwork while still using universal sections in composite members, partial encasement may be used ***Figure 1.2b***. In this type of members, concrete is cast between the flanges of the steel section. Since the

steel web is protected from fire attack, fire resistance of this type of composite column is reasonably high.

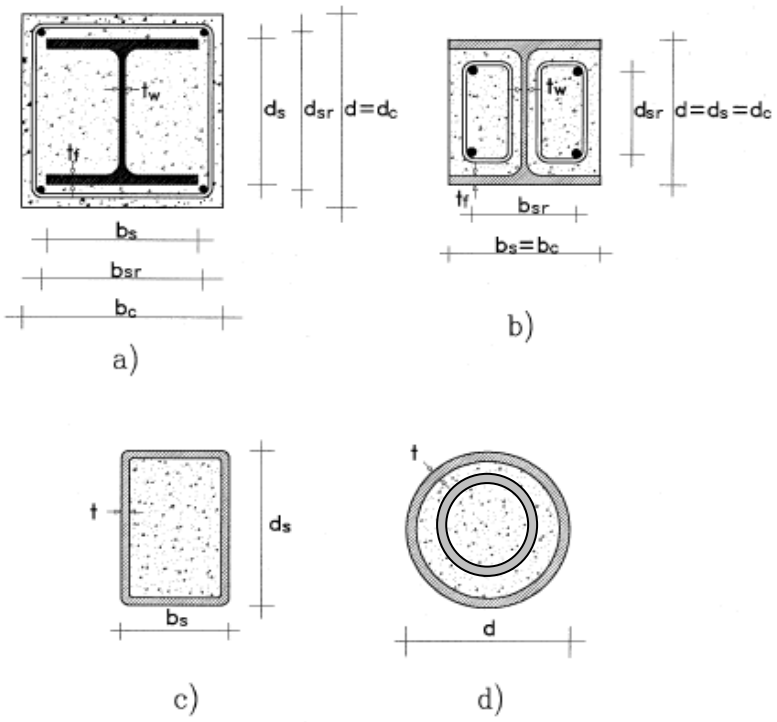

FIGURE 1.2: Typical steel concrete composite members. (a) I steel profile fully encased in concrete. (b) I steel profile partially encased in concrete. (c)Hollow steel section filled of concrete. (d) Circular steel section filled of concrete. [7]

But later research studies showed that by using better quality concrete, significant enhancements in the column strength were possible, enabling smaller steel sections to be used. Nowadays, owing to unattractive appearance and the need for temporary formwork for concrete casting, composite members made of steel sections encased in concrete are less often used than concrete filled hollow sections ***Figure 1.2c***. Moreover, by using steel tubes as permanent formwork, construction speed is increased. Because of the inherently high fire resistance of concrete filled members, fire protection of steel is in many cases not necessary

and the steel can be exposed to achieve attractive appearance. Since construction speed is an important advantage, reinforcement is usually not used. But when required, a convenient reinforcement method is to insert a second tube inside the main one ***Figure 1.2d***.

The present study will confined on concrete fully encased steel section and concrete filled steel tube only.

1.3.1. Concrete Fully Encased Steel structure

In multi-storey building there is need for protection from fire, this is often providing by encasement in concrete. Until 1950, it was normal practice to use a wet mix of low strength, and to neglect the contribution of the concrete to the strength and stability of the member. Then test by Faber, 1956 **[8]** and others showed that savings could be made by using better-quality concrete and designed as composite member. This led to the “cased strut” method of design **[6]**. This was originally Faber, 1956 **[8]** a permissible-stress method for the steel member. The presence of the concrete is allowed for in two ways. It is assumed to resist a small axial load, and to reduce the effective slenderness of the steel member, which increases its resistance to axial load. Resistance to bending moment is assumed to be provided entirely by the steel. No account is taken for the resistance of the longitudinal reinforcement in the concrete.

This type of composite member has been used in Japan for more than 4 decades **[1]**. It also becomes increasingly popular to use the concrete encased steel member in building construction in Taiwan after the Ji-I earth-quake in 1999. A design guide for this type of structural member can be found from the latest edition of the steel reinforced concrete (SRC) structures design standards published by Architectural Institute of Japan **[9]**.

1.3.2. Concrete filled steel tube

Concrete-filled steel tube members become more popular to use in new building construction in the world **[10]**. However, bare steel or reinforced concrete members are still used more extensively than concrete filled steel tube members due to the lack of knowledge and experience that engineers have with concrete filled steel tube structural systems.

Where hollow steel sections are used as a column or beam more persuasive argument for composite action with an internal filling of concrete can be advanced **[11]**. The combination of large diameter high yield steel tube filling with high grade concrete can produce member capable to carrying very large loads. A specific application of such columns occurred at the Almondsbury Interchange **[12]**, where high loads had to be carried on column with the smallest possible lateral dimensions. The maximum load of (32000 kN) was supported by a composite tube of (1033mm) outside diameter and (44.5 mm) thick filled with concrete of cube strength (52 MPa).

1.4. Advantages and disadvantages of composite members

Composite members offer many advantages over bare steel or reinforced members and are becoming increasingly used in multi-storey and tall buildings. This being especially desirable in tall buildings where load is high and space is usually at a premium

1.4.1. Concrete filled steel tube members

In recent years, concrete filled steel tube structures become more widely accepted and used in tall buildings as well as arch bridges, particularly, in the far-east region, like China and Japan. The advantages of the conventional concrete filled steel tube structure include:

i. As a typical composite structural system, due to the composite effects, the advantages of the two materials can be utilized and their disadvantages can be avoided, thus forming a more rational system.
ii. Compared with steel structures, the cost can be reduced by using composite or hybrid systems, since the reduced usage of steel and the increased stiffness as well as improved fire resistance.
iii. The steel tubes can be used as the formwork for casting concrete and the shoring system in construction, thus concrete filled tube structures have much better constructability than concrete structures.
iv. The outer steel shell confines the concrete core, which further increases the compressive strength of the column.
v. The concrete core will delay the local buckling of the outer steel shell, which provides further strength increases in the column section.
vi. Greater useable floor area, higher visibility, and aesthetically pleasing.
vii. Reduced maintenance.

However, the conventional concrete filled tube system also has its own disadvantages, such as,

i. The beam-to-column connections are complicated for concrete filled tube frame structures. In Japan, structural frames using concrete filled tube columns typically end up using steel or SRC beams with specially designed connections, thus increasing the construction cost. Practice in China tends to adopt more concrete filled tube column and RC beam

system with using complicated connections. Such labor-intensive practice is apparently not suitable for the US construction industry.

ii. Due to the fact that the steel tube is used as longitudinal reinforcement to resist axial force or moment, when the steel tube yields under excessive longitudinal stresses, its transverse confinement (particularly in terms of stiffness) to the internal concrete is drastically reduced. This may be considered as the fate of steel as an isotropic material.

iii. As demonstrated in the cyclic loading tests of conventional concrete filled tube columns conducted by Sakino **[13]**, local plastic buckling may occur at the ends of the steel tube followed by the crushing of internal concrete. This type of failure is very difficult to repair if not impossible. Such failure mode also results in unstable hysteretic loading capacity, particularly for columns with higher axial load.

1.4.2. Concrete encased steel section

Concrete encased steel section member embodies several advantages. In general,

i. Encasement of a steel shape increases its stiffness, and energy absorption.
ii. Drastically reduces the possibility of local buckling of the encased steel.
iii. From a technical viewpoint, the fully encased and partially encased columns offer good fire and corrosion resistance properties, owing to the protection offered by concrete.
iv. Concrete represents an effective bound for steel in order to prevent or delay the critical warping.
v. A particular advantage of using this member is the reduction in member cross-sectional area,

Disadvantages of concrete encased steel section are:

i. The member needs for the formwork for casting concrete

ii. No confinement provided for concrete compared to concrete filled steel tube.

1.5. Objectives and Scope

The main objective of this research is to conduct an analytical investigation on the overall behavior of composite frame. This aim is achieved by using the finite element method, when nonlinear three dimensional finite element representations are required. Material nonlinearity due to cracking, crushing, and yielding of steel tube is taken into account and partial bond between steel and concrete is included.

` ANSYS program (ANalysis SYStem) **[14]** using three-dimensional finite element method to solve in numerical solution.

Different types of composite member were chosen for analysis and compare this result with experimental data that provided from other studies. Also parametric studies are carried out to investigate the effect of many factors on the behavior of composite members.

1.6. Layout of Thesis

This study consists of six chapters and appendix as follow:

In Chapter one a general introduction describes composite members and benefit of it as well as problems and the aim of this study. Chapter two includes previous research of the theoretical and experimental studies concerning composite member.

Chapter three describes basic concepts of finite element formulation, the nonlinear techniques that used to solve the nonlinear equations, material behavior (concrete and steel) and models used to represent steel and concrete.

General description of the bond between concrete and steel and represented in ANSYS is given in chapter four. Chapter five includes results of nonlinear analysis of composite members and comparison with experimental data. In addition, many parametric studies were carried out. The conclusions of the research work and recommendations for future work are given in chapter Six.

CHAPTER TWO

LITERATURE REVIEW

2-1 Introduction

This chapter is devoted for reviewing previous experimental work conducted to composite members which is either concrete filled steel tube or encased steel section. Also is carried out in this chapter review of analytical works related to composite members.

2-2 Experimental work

A contribution by **Russell in (1953) [16]** apparently provided the formulas for the National Building Code of Canada 1965 (NBC) and the ACI318-63 building code requirements, which included carrying out test on pinned-ended light and heavy gauge concrete filled pipe columns. All the columns tested experienced an Euler type buckling failure. From the results of his tests, he proposed the following equation to predict allowable loads for pipe columns where the steel has a minimum yield stress of (227.6MPa) and column has an (L\r) ratio ≤120

$$p_{all} = 0.25\, fc' \left(1 - 0.000025 \frac{L^2}{r_c^2}\right) A_c + fs' A_s \quad \text{..... (2-1)}$$

$$fs' = 17000 - 0.485 \frac{L^2}{r_s^2} \quad \text{..... (2-2)}$$

Where:

r_c= radius of gyration of concrete core.

r_s= radius of gyration of steel tube.

fc'= unconfined crushing strength of concrete.

fs'= allowable steel stress.

A_c= area of concrete.

A_s= area of steel.

L= length of column.

Kloppel and Goder in (1957) [17] studied the behavior of concrete filled steel tube with equivalent slenderness ratio of less than 50, also they considered the effect of creep and proposed a design formula. From their tests results, they presented a table of allowable working stresses to predict the working loads of pipe column for the cases of mild steel and high strength steel pipes. Experimentally, however, their test arrangement of hinged bearing only permitted column end rotation in one plane. This may explain some of the discrepancies in their predicted and measured ultimate load. They conducted that "the modulus of elasticity of tube contained concrete can be determined with sufficient accuracy from the uniaxial stress condition".

Furlong in (1967) [18] presented data on the ultimate strength of concrete filled steel sections after tests made at the University of Texas on twenty-two circular and seventeen square composite columns subjected to various amounts of axial loads. These loads were held constant while moments were increased. In addition eight circular

columns and square columns were loaded with axial force only. The columns were of various sizes, yielding stress and crushing strength.

The ultimate strength and ultimate moment capacity were measured. The lower limit p_o and m_o were obtained from:

$$P_o = A_s f_{sy} + A_c f_c' \sqrt{\frac{f_{sy}}{0.0018E_s}} \quad with \ \frac{f_{sy}}{0.0018E_s} \leq 1.00 \quad \ldots\ldots\ldots\ldots (2\text{-}3)$$

For circular shapes

$$M_o - \frac{f_{sy}}{6}\left(D_o^3 - D_i^3\right) \quad \ldots\ldots\ldots\ldots (2\text{-}4)$$

And for square shaped

$$M_o = \frac{f_{sy}}{4}\left(D_o^3 - D_i^3\right) \quad \ldots\ldots\ldots\ldots (2\text{-}5)$$

Where:

D_o = The outside dimension of steel (diameter of circular column or length of a side on a square)

D_i = The inside dimension of steel.

f_c' = The cylinder compressive strength of concrete

M_o = The ultimate pure bending capacity

P_o =The axial force capacity when M=0

f_{sy} = Yield strength of steel.

E_s = Modulus of elasticity of steel

As an interaction diagram was constructed after obtaining the ratio of the measured moment capacity and ultimate strength to P_o andM_o. It

was observed that there was no general relationship among the ratios, but a fair estimation of a lower bound could be described by the formula.

$$(\frac{P_u}{P_o})^2 + (\frac{M_u}{M_o})^2 \leq 1.00 \quad \text{..... (2-6)}$$

Knowles and Park in (1969) [19] made an experimental work to determine the failure load of the axially and eccentrically loaded hollow steel tubes of various slenderness ratio and short unconfined concrete cylinders of approximately the same cross sectional area as the tube cross section.

The stress-strain relationship for the hollow tubes and for concrete specimens was obtained from the tests. With the observation that the concrete specimens were made under conditions as close as possible to those in the core of a tube. These relationships were used to compute the stress tangent modulus curves and from these curve the theoretical ultimate stress-slenderness ratio curves were computed for both the steel tubes and the concrete specimens.

Tomii *et al.* in (1977) [20] investigated (270) circular, octagonal, and square composite columns. Values of (diameter/ thickness) ratio ranged from (19) to (75), and (length\diameter) ratio ranged from (2) to (9). Results of that work suggested that the post-yield behavior for the vertical load may be characterized as either (1) strain hardening (2) perfectly plastic; or (3) degrading stiffness type. Circular and many octagonal shapes were classified as either type (1) or (2), while some of the octagonal and all of the square cross sections were categorized as type (3). At high axial loads, concrete confinement was observed in the circular and many octagonal cross sections, which explain the strain

hardening characteristics for these specimens while square tubes provided very little confinement of the concrete because the wall of the square tube resists the concrete pressure by plate bending, instead of membranes-type hoop stresses. Consequently, there was an axial load increase due to the triaxial compression effects for the square tubes.

Sakino *et al.* in (1985) [13] tested (18) circular specimens with (D\t) ratio ranged between (18) and (192). In the investigation, three otherwise identical specimens were subjected to different load conditions. Axial load was applied to the concrete and steel tube simultaneously for the first specimen group. The load was applied exclusively to the concrete core in the second specimen group, and load application was similar to that in the third group except the inside tube wall was greased before casting the concrete. Results indicated that when the steel tube and the concrete core were loaded simultaneously, the tube provide no confinement until post-yield behavior. In the concrete loaded specimens, some longitudinal stresses were noted in the steel tube even for the columns with the greased wall of the steel tube appeared to the primarily in the biaxial stress state. Test results indicated that the axial stiffness of the concrete loaded columns were about half that of the other tested concrete-filled steel tube, the concrete loaded columns obtained a greater yield and ultimate axial load capacity.

Shakir-Khalil and Zeghiche in (1989) [21] carried out a test in Manchester, U.K. on seven full-scale composite columns (3m) long. Representing a typical storey height in multi storey-building, the columns made of the concrete filled rolled steel hollow rectangular hollow section (120*80*5) mm. The experimental results were compared against the prediction of a finite element numerical analysis, and also with the failure

loads as predicted in accordance with (BS 5400) for the design of composite building.

Shakir-Khalil and Zeghiche concluded that the squash load calculated in accordance with (BS 5400) is a reasonable estimate of the actual failure load of stub column of the concrete filled rectangular hollow section. (BS5400) gave safe predictions for the axially loaded column as well as for columns in uniaxial bending about the major axis, however, in the case of uniaxial bending about the minor axis; both theory and tests showed that (BS5400) predictions were on the unsafe side.

Lu and Kennedy in (1992) [22] tested a series of four flexural hollow structural steel sections and twelve concrete filled steel section were undertaken to assess the general behavior of this composite section. The properties of the test specimens were chosen to examine the effect of different ratios of depth\width and therefore of the proportions of steel and concrete in compression and of different values of shear-span/length as related to the transfer of forces from one to the other when no direct means is provided for this transfer. The test showed that the ultimate flexural strength of the concrete steel section is increased by 10% to 30% over that of the bare steel section depending on the relative proportions of steel and concrete. In all cases slip between the concrete and steel were not determined even though shear-span/length ratios as low as one was used.

Brahmachari in (1997) [23] presented an experimental study for the flexural behavior of steel hollow sections filled with high strength concrete. Steel fibers were mixed with high strength concrete in some of the specimens to examine their effect. The study emphasizes low ductility

and post failure strength of the composite beams due to the brittle behavior of higher strength concretes when compared to normal strength concrete. Spreadsheet graphs were used to present the results such as load versus strains, load versus deflections etc. also tested 2 tubular beam leaved hollow and compared this results with concrete filled steel tubes.

Huang *et al.* in (2002) [24] investigated the axial load behavior of concrete-filled steel tubular (CFT) columns with the width-to-thickness ratios between 40 and 150, and proposed an effective stiffening scheme to improve the mechanical properties of square cross-sectional CFT columns. Seventeen specimens were tested to examine the effects of cross-sectional shapes, width-to-thickness ratios, and stiffening arrangements on the ultimate strength, stiffness, and ductility of CFT columns. Moreover, nonlinear finite element analysis was also conducted to investigate cross-sectional axial stress distribution at the ultimate strength. Comparing the measured ultimate strength with that estimated by using some current specifications suggested that current specifications may considerably underestimate the ultimate strength of circular CFT columns, particularly for columns with a small width-to-thickness ratio. Results in this study demonstrate that the proposed stiffening scheme can significantly enhance the ultimate strength and ductility of square CFT columns.

Prickett and Driver in (2006) [25] tested eleven full-scale PEC columns with high-strength concrete under either concentric or eccentric axial loading. In seven concentric tests, concrete type and link spacing were studied. In four eccentric tests, bending axis and various eccentricities were studied. Test results indicate that the columns attain full composite behavior, but have a more brittle failure mode than those with normal-strength concrete. However, smaller link spacing or the

addition of steel fibers to the concrete improves the failure mode. Then conservative the current design criteria for concentrically-loaded high-strength PEC columns. Load–moment interaction diagrams agree well with test results from the eccentrically-loaded PEC columns in either orientation.

Baig in (2006) [26] presented an experimental study on the behavior of short concrete filled steel tubular columns (CFT) axially loaded in compression to failure. A total of 28 specimens (16 were filled with concrete and 12 were kept hollow) with different cross-sections were tested to investigate the load capacity. The length-to-diameter ratios of these columns were between 4 and 9. Parameters for the tests were tube shape and diameter-to-thickness ratio. Some of the concrete filled columns had internal bracing of #3 deformed bars. The test results are compared with the theoretical results and previous studies. The results show that the confinement effect on concrete does play a role in increasing the compressive strengths to almost 60% in some cases. Based on the test results, an equation to estimate the ultimate axial compressive loading capacities is also proposed for square CFT columns.

Gupta et al. in (2007) [27] presented an experimental and computational study on the behavior of circular concentrically loaded concrete filled steel tube columns till failure. Eighty-one specimens were tested to investigate the effect of diameter and D/t ratio of a steel tube on the load carrying capacity of the concrete filled tubular columns. The effect of the grade of concrete and volume of flyash in concrete was also investigated. The effect of these parameters on the confinement of the concrete core was also studied. Diameter to wall thickness ratio between

25 < D/t < 39, and the length to tube diameter ratio of 3 < L/D < 8 was investigated. Strength results of Concrete Filled Tubular columns were compared with the corresponding findings of the available literature. Also a nonlinear finite element model was developed to study the load carrying mechanism of CFTs using the Finite Element code ANSYS **[14]**. This model was validated by comparison of the experimental and computational results of load–deformation curves and their corresponding modes of collapse. From the experimental and computational study it was found that for both modes of collapse of concrete filled tubular columns at a given deflection the load carrying capacity decreases with the increase in % volume of flyash up to 20% but it again increases at 25% flyash volume in concrete.

Mouli and Khelafi in (2007) [28] concentrated on the bond strength and axial capacity of concrete filled steel columns. A series of tests was performed to consider the behavior of short composite columns under axial compressive loading; two rectangular hollow steel sections (RHS) were used in these tests, namely 120 × 80 × 5 RHS and 150 × 100 × 5 RHS. The RHS sections were filled with normal and lightweight aggregate concrete where natural pouzzolan was used as the lightweight aggregate component in the latter concrete. The main objectives of those tests were to clarify the performance of the lightweight aggregate-concrete filled steel specimens compared with those manufactured from normal concrete. The experimental investigations included tests on short steel and short composite columns. The bond strength and the squash load in composite sections depend on several factors. The cross section and the length of the steel tube, and the type of concrete were considered in the present study. The experimental failure load is seen to be adversely affected when the height of the squash specimens is increased from 100

to 200 mm. The test results reported show that lightweight aggregate concrete offered higher bond strength than normal concrete, but the load–slip behavior of all specimens is similar for both type of concretes, and the bond strength is not influenced by the section of tube steel specimens. Moreover the results of this investigation showed that the contribution of lightweight aggregate concrete to the squash load is shown to be considerable.

Elghazouli and Treadway in (2008) [29] presented an account of the results of a series of tests on partially-encased composite steel/concrete beam–columns. The experimental inelastic behavior of members is examined under idealized conditions representing extreme lateral loading in combination with co-existing axial gravity loads. Members with three different cross-sectional sizes, utilizing Grade S460 steel, were employed in the tests. The specimens were tested under major- or minor-axis bending in conjunction with a constant level of axial loading. The experimental arrangement and test rig constructed for this purpose are described together with the material properties and details of the specimens. The main experimental results from tests carried out on ten composite models are presented and discussed. In addition to providing essential data for validating future analytical and design studies, the experimental results and observations enable a direct assessment of several important factors. Particular emphasis is placed on key parameters related to yield and ultimate capacity as well as on ductility and residual strength considerations.

2-3Theoretical Techniques

Knowel and park in (1970) [12] studied analytically twelve circular and seven square columns with (D/t) ratios of (15), (22), and (59), and (L/D) ratios ranging from (2) to (21). The results indicated that the tangent modulus method accurately predicted the capacity for columns with (L/D<11), but was slightly conservative for column with small slenderness ratio. It was concluded that the increase in the expected capacity for composite columns with (L/D<11) was due to the increase of concrete strength resulting from triaxial confinement effects.

Shakir-khalil and Mouli in (1990) [30] compared the design of rectangular hollow section columns according to both (BS 5950) and (BS 5400). The numerical results of the study were presented with a view to illustrate the increase in the carrying capacity of the bare steel rectangular hollow sections when they are filled with concrete. The comparison between the design, in accordance with the British Standard, of composite and steel columns showed that filling the section with concrete considerably increased the carrying capacity of the column. For the studied steel section and column length, it was found that the percentage increase in column carrying capacity ranged between (12%) and (65%) for (120*80*50) mm, rectangular hollow section, and (250*150*6.3) mm, rectangular hollow section respectively. It was concluded that, the percentage gain was enhanced by increasing both the strength of concrete and the size of the steel section, but was adversely affected when increasing the design strength of steel and the column length.

Schiller and Hajjar in (1996) [31] presented a fiber-based distributed plasticity finite element formulation for conducting nonlinear

analysis of composite frame structure composed of steel wide flange girder framing onto square or rectangular concrete filled steel tube beam-columns. The research focused on the development of the concrete filled tube finite element formulation. A comparable formulation for steel wide flange member is included, and the model is suitable for conducting geometrically and materially nonlinear analysis of complete three-dimensional frame structures or subassemblies. The current implementation included structures subjected to monotonic proportional and non proportional loading; a companion research project has extended this analysis capability to cyclic loading. This formulation is geared for conducting behavior studies of concrete filled tube columns, beams, and beam-columns having a wide range of geometric and material properties for the purpose of developing interaction curves or design recommendations, or for predicting the behavior of experiments of concrete filled tube members or composite subassemblies. The model is also suitable for conducting second order inelastic advanced analysis of composite frame structures for use directly in design or for conducting second order inelastic "push-over" analysis to determine the capacity of frame structure subjected to seismic loading.

Hajjar and Gourley in (1996) [32] presented the development of polynomial equation to represent the three dimensional cross section strength of square or rectangular concrete filled steel tube beam-columns. The equation provided an accurate representation of the cross section strength of concrete filled tube subjected to a combination of axial force, strong axis flexure, and weak axis flexure. This expression is verified against the results of a detailed fibre analysis formulation, and against experimental test of short square concrete filled steel tubes available in the literature. This concrete filled steel tube cross section strength

equation forms a compact expression of the failure surface of square or rectangular concrete filled tubes having a wide range of cross section dimensions and material strengths. The cross section strength surface also provided the basis for abounding-surface concentrated plasticity model in 3D force space for concrete filled tube beam-column, presented in related work by the authors, this beam-column model, in turn, is suitable for conducting monotonic static, cyclic static, or transient dynamic seismic analysis of composite un braced frame structures composed of steel I-girders framing biaxially into concrete filled tube beam-columns.

Brahmachari in (1997) [23] presented analytical work also in two separate methods. The analysis of ultimate moment and deflection of composite beams were performed from the principle of structure mechanics. Finite element analysis was conducted to model the physics behavior and also compare the experimental results. Among the main considerations of the derivations, the steel portion was assumed either elastic-perfectly plastic or perfectly plastic and the concrete carried no strength in the tensile zone. At the interface both full bond and partial bond were assumed for comparison. Efforts were also made to calculate the mid span deflection of the composite beams. Simple analytical expressions derived from this study can be coded to a programmable calculator or in a small spreadsheet program for design use.

Muhsen in (2002) [11] carried out a three dimensional nonlinear finite element analysis of short concrete filled steel tube columns using ANSYS 5.4. The 8-node brick element is used to represent the concrete core and the steel tube and connected by a 4-node interface element. Different types of concrete filled steel tube columns were analyzed and finite element solutions are compared with the available experimental data, and give good agreement with experimental study. The researcher

offers some effects of the important geometric and material parameters on the concrete filled steel tube short columns.

Al-Rodan and Al-Tarawah in (2003) [33] carried out a three-dimensional, geometrically and materially nonlinear finite element (FE) analysis for rectangular hollow sections filled with high strength concrete when used as a beam. The aim of their research was also to verify the newly published design regulations of Eurocode-4**[5]** for high strength concrete. The comparison between the numerical results obtained and the experimental ones demonstrates the validity of the finite element model. The experimental results are also compared to the Eurocode-4**[5]** predictions. It shows that, the design methods of Eurocode-4**[5]** for high strength concrete beams appear generally on the safe side.

Hock and Cheong in (2004) [34] presented a computerized approach to estimate the load-bearing capacity of an externally strengthened RC composite column, particularly with respect to the moment force interaction. Columns are assumed to be subjected to axial loading and uniaxial and/or biaxial bending. The methodology is to analyze the columns using fundamental principles of mechanics and the computations are carried out using spreadsheet. The estimation obtained from this approach is then compared with available experimental results as well as other Standards for its effectiveness. Overall, the approach is relatively successful in predicting the composite strength of the columns.

Han in (2004) [35] developed a mechanic model that can predict the behavior of concrete-filled hollow structural section (HSS) beams. A form of unified theory, where a confinement factor (n) was introduced to describe the composite action between the steel tube and filled concrete, is used in the analysis. A series of concrete-filled square and rectangular

tube beam tests were carried out. The main parameters varied in the tests were the depth-to-width ratio (b) from 1 to 2, and tube depth to wall thickness ratio from 20 to 50. The load vs. lateral deflection relationship was established for concrete-filled HSS beams both experimentally and theoretically. The predicted curves of load vs. mid-span deflection are in good agreement with the presented test results. Formulas which should be suitable for incorporation into building codes are developed for calculating the moment capacity of concrete-filled HSS beams. Comparisons are made with predicted beam capacities and flexural stiffness using the existing codes.

Giakoumelis and Lam in (2004) [36] presented the behavior of circular concrete-filled steel tubes (CFT) with various concrete strengths under axial load. The effects of steel tube thickness, the bond strength between the concrete and the steel tube, and the confinement of concrete are examined. Measured column strengths are compared with the values predicted by Eurocode 4, Australian Standards and American Codes. 15 specimens were tested with 30, 60 and 100 N/mm2 concrete strength, with a D/t ratio from 22.9 to 30.5. All the columns were 114 mm in diameter and 300 mm in length. The effect due to concrete shrinkage is critical for high-strength concrete and negligible for normal strength concrete. All three codes predicted lower values than that measured during the experiments. Eurocode 4 gives the best estimation for both CFT with normal and high-strength concrete.

Bahjet in (2005) [37] presented a nonlinear three-dimensional finite element analysis of composite beams of concrete encaesed steel section using the analysis system computer program (ANSYS V. 5.4). Nine composite beams with different cross sectional dimension are analyzed and compared with available experimental data, the analysis

give good agreement with experimental study. Many parametric study carried out to investigate the effects of the concrete compressive strength, the width of the flange of the I-steel section that used in the model, on the stiffness of each structure, in addition to the effect of Poisson's ratio of concrete and the finite element mesh refinement.

Mohamed *et al.* in (2006) [38] compared the performance of axially loaded concrete filled steel tube (CFST) columns cast using a conventionally vibrated normal concrete (NC) and a self-consolidating concrete (SCC) made with a new viscosity-modifying admixture (VMA). A total of 16 columns with a standard compressive strength of approximately 50 MPa for both SCC and NC were tested by applying concentric axial load through the concrete core. Test results showed that the ease of placement and time of casting were considerably improved for columns with SCC compared to those with NC. The strength of SCC columns was found comparable to that of their NC counterparts as the maximum strength enhancement in NC columns ranged between 1.1 and 7.5% only. The ductility of comparatively shorter columns (H/D ranging between 3.1 and 4.8) with both SCC and NC was similar. However, slender NC columns (H/D ranging between 6.3 and 9.5) showed higher ductility compared to their SCC counterparts. Ductility also decreased with the increase of slenderness ratio (H/D) of columns. No significant differences in strain development was found due to the presence of SCC or NC or due to the presence of longitudinal and hoop reinforcement. The confined strength f'(cc) of SCC was found to be lower than that of NC, and f'(cc) also decreased with the increase of slenderness of the columns.

Pi and Brain in (2006) [39] formulated total Lagrangian finite element model for the nonlinear inelastic analysis of both composite beams and columns. An accurate rotation matrix is used in the position

vector analysis and nonlinear strain derivations. The slip between the steel and concrete components due to the flexible shear connection at their interface is considered as an independent displacement in the formulation which makes it easier to assign the corresponding proper slip conditions at the connections between composite beams and columns. The effects of nonlinearities and slip on the deformations and strains in the steel and concrete components, and so on the stress resultants (i.e., internal forces), stiffness, and strength of the composite member are thus combined together in the formulation. The constitutive models for steel and concrete in this investigation are based on the longitudinal normal stress and the shear stress induced by the slip between the steel and concrete components. Hence, these models include the effects of the slip at the interface on the von Moses yield surface, associated flow rule and isotropic hardening rule. These constitutive models can be used in association with any type of uniaxial stress–strain curves for steel and concrete, including hot-rolled or cold-formed steel, and confined or unconfined concrete. The constitutive models are expressed in terms of engineering stresses and strains. The total Lagrangian formulation is applicable for these constitutive models directly, and most convenient for the slips at the interface between the steel and concrete components.

Tort and Hajjar in (2007) [10] developed a computational study to reliability-based performance-based seismic design guidelines of RCFT members. A three-dimensional geometrical and material nonlinear mixed distributed-plasticity finite element formulation was developed for RCFT beam-columns as part of complete composite frame structures. Translational degrees-of-freedom for the steel tube and the concrete are defined separately to allow for differential slip displacement along the element length between the constituent materials, modeling cyclic

interface and load transfer response ranging from perfect slip to complete bond. The material nonlinearity of the steel tube and the concrete core is accounted for through assigning comprehensive cyclic nonlinear stress-strain relations. Using an experimental database developed by the authors that documents detailed progression of damage in RCFT members and frames, a comprehensive verification study for the mixed finite element formulation is conducted on RCFT members under various loading conditions that highlights the complex interrelationship between the constitutive materials and the progression of damage with these composite members.

Sapountzakis and Mokos in (2007) [40] developed a boundary element method for the construction of the 14*14 stiffness matrix and the nodal load vector of a member of arbitrary homogeneous or composite cross section taking into account both warping and shear deformation effects. To account for shear deformations, the concept of shear deformation coefficients is used. In this investigation the definition of these factors is accomplished using a strain energy approach. Seven boundary value problems are formulated and solved employing a pure BEM approach, that is only boundary discretization is used. Numerical results are presented to illustrate the method and demonstrate its efficiency and accuracy. The influence of the warping effect especially in composite members of open form cross section is analyzed through examples demonstrating the importance of the inclusion of the warping degrees of freedom in the analysis of a space frame. Moreover, the discrepancy of both the deflections and the internal forces of a member of a spatial structure arising from the ignorance of the shear deformation effect necessitate the inclusion of this additional effect, especially in thick walled cross section members.

Xiong and Zha in (2007) [41] presented a comprehensive numerical investigation on the behavior of CFST columns under initial stresses by the non-linear finite element method. The investigation includes several parametrical studies such as initial stress ratio, slenderness ratio, eccentricity ratio, etc. In the practical construction of concrete-filled steel tubular (CFST) structures, the steel tubes usually have already had some initial stresses before they work together with the core-concrete. The initial stress should affect the behavior of the whole member. Numerical analysis results are verified with published experimental ones. Recommendations on how to consider the effect in design formulae are also suggested.

Han *et al*. in (2007) [42] investigated the behaviors of concrete-filled thin-walled steel tubular members subjected to combined loading, such as compression and torsion, bending and torsion, compression, bending and torsion. ABAQUS software is used in this paper for the finite element analysis (FEA). A comparison of results calculated using this modeling shows generally good agreement with test results. The FEA modeling is then used to investigate the influence of important parameters that determine the ultimate strength of the composite members under combined loading, such as compression and torsion, bending and torsion, compression, bending and torsion. The parametric studies provide information for the development of formulae for calculating the ultimate strength of the composite members subjected to combined loading.

Liang *et al*. in (2007) [43] studied the critical local and post-local buckling behavior of steel plates in concrete-filled thin-walled steel tubular beam–columns by using the finite element analysis method. Geometric and material nonlinear analyses are performed to investigate the critical local and post-local buckling strengths of steel plates under

compression and in-plane bending. Initial geometric imperfections and residual stresses presented in steel plates, material yielding and strain hardening are taken into account in the nonlinear analysis. Based on the results obtained from the nonlinear finite element analyses, a set of design formulas are proposed for determining the critical local buckling and ultimate strengths of steel plates in concrete-filled steel tubular beam–columns. In addition, effective width formulas are developed for the ultimate strength design of clamped steel plates under non-uniform compression. The accuracy of the proposed design formulas is established by comparisons with available solutions. The proposed design formulas can be used directly in the design of composite beam–columns and adopted in the advanced analysis of concrete-filled thin-walled steel tubular beam–columns to account for local buckling effects.

Dundar *et al.* in (2008) [44] presented an experimental investigation of the behavior of reinforced concrete columns and a theoretical procedure for analysis of both short and slender reinforced and composite columns of arbitrarily shaped cross section subjected to biaxial bending and axial load. In the proposed procedure, nonlinear stress–strain relations are assumed for concrete, reinforcing steel and structural steel materials. The compression zone of the concrete section and the entire section of the structural steel are divided into adequate number of segments in order to use various stress–strain models for the analysis. The slenderness effect of the member is taken into account by using the Moment Magnification Method. The proposed procedure was compared with test results of 12 square and three L-shaped reinforced concrete columns subjected to short-term axial load and biaxial bending, and also some experimental results available in the literature for composite

columns compared with the theoretical results obtained by the proposed procedure and a good degree of accuracy was obtained.

As shown, there is no research as found towards the study of the analysis of composite frame composed of composite members.

CHAPTER THREE

FINITE ELEMENT MODELING

3-1 Introduction

The behavior of any structural member under load depends on the behavior of the components of this member. In composite members which are made up of concrete and steel, the behavior of composite members depend on concrete and steel and composite action of them. Steel can be considered homogenous material and its material well defined. On the other hand, concrete is homogenous material made up of cement, mortar and aggregates. Its mechanical properties scatter more widely and cannot be defined easily.

In the case of reinforced concrete structures, the effect of large deformations can be neglected for the majority of cases. This is due to the early onset of material nonlinearity, with large deformations that occurring only close to the structural collapse, especially in composite members where slippage and separation between different materials may become noticeable. In the present study, the sources of material nonlinearity are cracking of concrete, yielding of steel, plastic deformation of concrete and steel, crushing of concrete and reduction in composite action due to failure of adhesion materials or due to slipping or separation at interface between the components.

At nonlinear stage of behavior, it is not possible to solve the governing equilibrium equations directly. Therefore, resort has to be made to more sophisticated solution strategies. In the present work, the combined

incremental-iterative solution technique is used. The solution techniques adopted are operated under a load control increment scheme.

3.2. Material Modeling

As stated before the performance of any member under load depends to a large extent on the behavior and the type of materials used to construct the members. Composite members are made of different materials (e.g. concrete and steel), which are brought together to constitute a composite system. The steel can be considered as a homogeneous material that exhibits a similar stress-strain relationship in tension and compression. But, the behavior of concrete is very much dependent on the properties of each of its components; namely, cement mortar, aggregates and air voids. Therefore, it is a material with a grossly heterogeneous internal structure.

3.2.1 Concrete

Concrete exhibits a large number of microcracks, especially, at the interface between coarser aggregates and mortar, even before subjected to any load. The presence of these microcracks has a great effect on the mechanical behavior of concrete, since their propagation during loading contributes to the nonlinear behavior at low stress levels and causes volume expansion near failure. Many of these microcracks are caused by segregation, shrinkage or thermal expansion of the mortar.

Some microcracks may develop during loading because of the difference in stiffness between aggregates and mortar. Since the aggregate-mortar interface has a significantly lower tensile strength than mortar, it constitutes the weakest link in the composite system. This is the primary reason for the low tensile strength of concrete. The response of a structure under load depends to a large extent on the stress-strain relation of the constituent

materials and the magnitude of stress. Since concrete is used mostly in compression, the stress-strain relation in compression is of primary interest. Such a relation can be obtained from cylinder tests with a height to diameter ratio of 2 or from strain measurements in beams **[45]**.

The concrete stress-strain relation exhibits nearly linear elastic response up to about 30% of the compressive strength. This is followed by gradual softening up to the concrete compressive strength, when the material stiffness drops to zero. Beyond the compressive strength, the concrete stress-strain relation exhibits strain softening until failure takes place by crushing.

Concrete can behave as either a linear or nonlinear material depending on the nature and the level of the induced stresses. Many experimental studies on the behavior of concrete under uniaxial and multiaxial loading conditions have been performed. The aims of such investigations have been to understand the complex response of concrete for various imposed stress conditions and to provide the necessary data required to develop accurate numerical models for use in nonlinear finite element analysis of concrete structures.

3.2.1.1 Uniaxial Behavior of Concrete

3.2.1.1.1 Uniaxial Behavior under Compression Load

The compressive strength of concrete in the uniaxial state is usually based on standard (150 mm × 300 mm) cylinders cured under standard laboratory conditions and tested at a specified rate of loading at 28 days of age **[46]**. Different researchers have used several models for stress-strain curves in their works; the following four mathematical models for uniaxial stress-strain curve in compression are explained.

i. Hognestad Model.[47]

One of the earliest, widely used mathematical models for uniaxial stress-strain curve is the one proposed by Hognestad as shown in ***Figure 3.1.a.*** The value of initial modulus of elasticity (*E*) can be calculated from the empirical formula given by the ACI committee-318-08 ***Equation (3.4)***, requirement for reinforced concrete. The ascending part of the stress-strain curve is a parabola. Beyond the maximum compressive stress, the model is represented by a straight line with ultimate strain (ε_{cu}) equal to 0.0038 **[48]** after which crushing of the concrete is assumed.

ii. BS-8110 Model. [49]

Another widely used model for the stress-strain relationship of concrete in compression is that proposed in the BS 8110 as shown in ***Figure 3.1.b.*** where the variation of curved portion of the stress-strain relationship is given by:

$$\sigma = 5500.f_{cu}\varepsilon - 11.3 * 10^{6}.\varepsilon^{2} \qquad 3.1$$

With initial modulus of elasticity (*Ei*) equal to:

$$Ei = 5500.\ (fcu)^{0.5} \qquad 3.2$$

Where:

(*fcu*) in (MPa).

fcu: cube strength of concrete

iii. Bangash model [50]

The stress-strain curve for concrete is linearly elastic up to about 30 percent of the maximum compressive strength as shown in ***Figure 3.1.c***. above this point, the stress increases gradually up to the maximum compressive strength $\sigma_{cu,}$ the curve descends into a softening region, and eventually crushing failure

occurs at an ultimate strain ε_{cu} . In tension, the stress-strain curve for concrete is approximately linearly elastic up to the maximum tensile strength. After this point, the concrete cracks and the strength decreases gradually to zero **[50]**.

iv.Xiong and Zha Model [41]

A typical uniaxial compressive stress-strain curve is shown in ***Figure 3.1.d.*** It can be noted that the concrete behaves as a linear elastic material when the stress level is less than about 30 percent of the uniaxial compressive strength f_c' . This stress level is called the point of onset of localized cracking.

For stress levels ranging between ***0.3 f_c'*** and ***0.5 f_c'*** the stress-strain curve exhibits a slight non-linearity due to the extension of stress concentrations at crack tips. When the stress level increases from ***0.5 f_c'*** to ***0.75 f_c'*** , mortar cracks and other cracks continue and grow slowly with a gradual increase in curvature of the curve. Beyond this level of stress, the rate of crack propagation increases rapidly and the stress-strain curve bends sharply until the peak stress level is reached. Beyond the peak stress level, concrete shows a softening response to reach 0.15 ***f_c'*** after this curve continue in reducing linearly until strain reach $10\epsilon_0$ **[41]**

All the first three models have been used for unconfining concrete (in concrete encased steel member) in the present study, to compare results and chose the best of them, and fourth model used for confining concrete (for concrete core in concrete filled steel tube member)

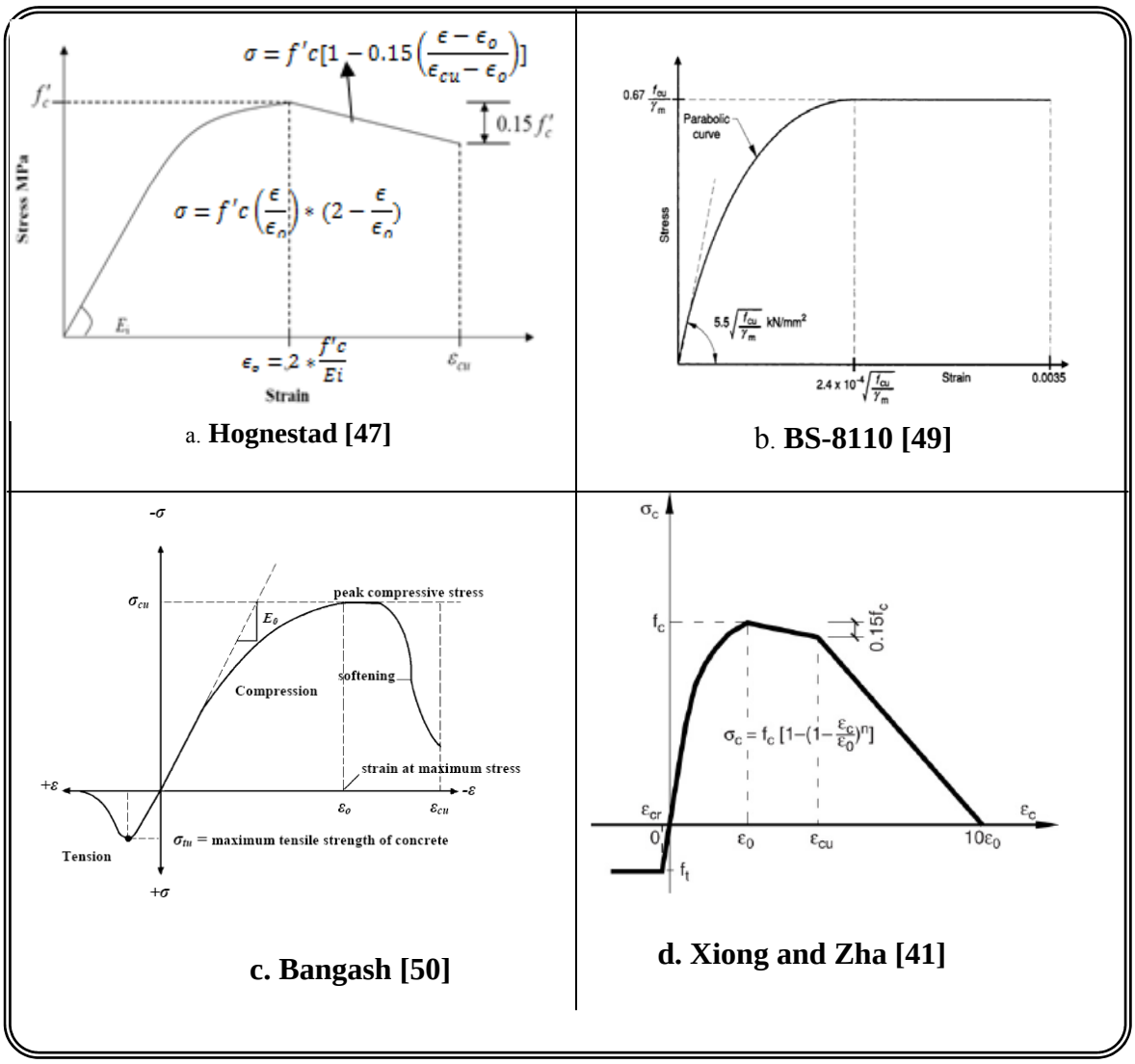

Figure 3.1 *typical uniaxial stress-strain of concrete in compression*

The **modulus of elasticity** of concrete (E_c) is generally taken to be a function of the compressive strength, f_c', with a slightly higher value of the modulus corresponding to a higher compressive strength, as shown in ***Figure 3.2***. In lieu of actual test data, the modulus of elasticity, E_c, can be calculated with a reasonable accuracy from the empirical formula **[51]** .

$$E_c = 0.043(w_c)^{1.5}(f_c')^{0.5} \qquad 3.3$$

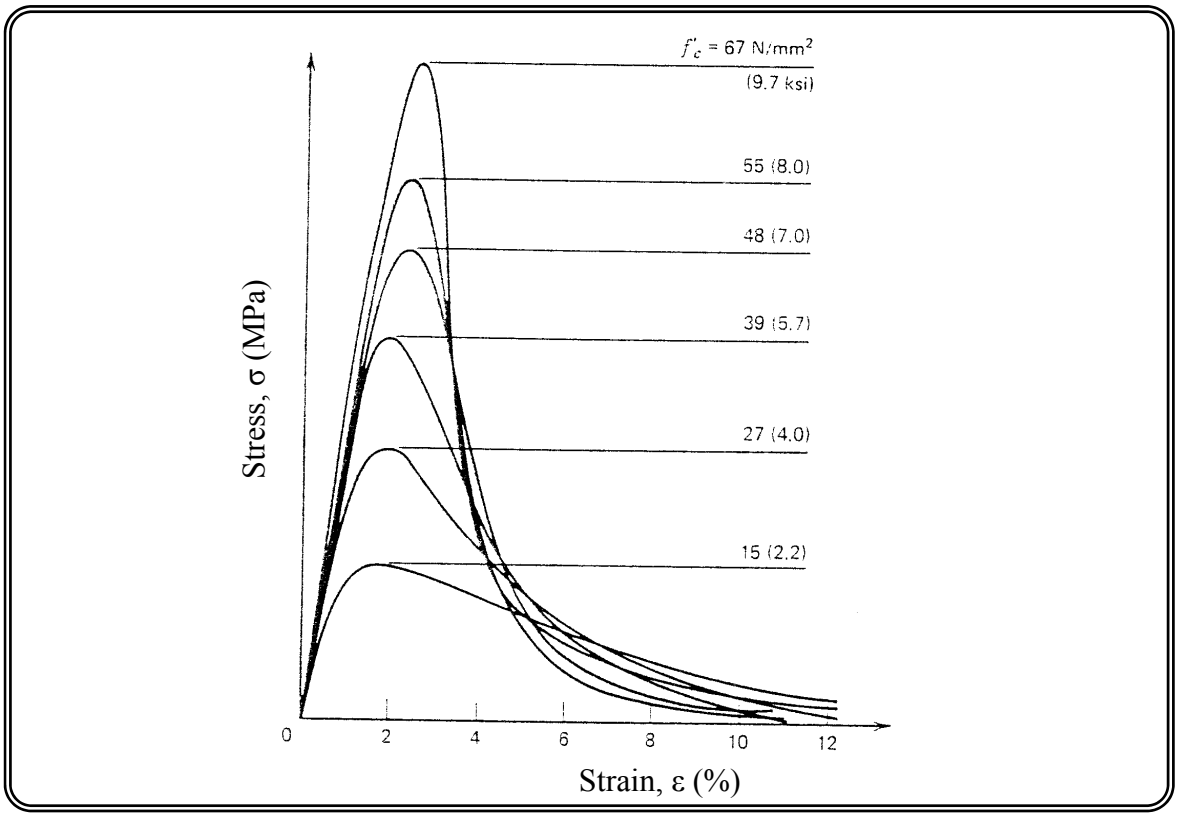

Figure 3.2 *Uniaxial compressive stress-strain curves for concrete with different strengths* ***[52]***

In which, w_c is the air-dry unit weight of concrete in kg/m³, f_c' is the cylinder compressive strength of concrete in MPa and E_c is the modulus of elasticity of concrete in MPa.

For the normal weight concrete based on a dry unit weight (2200-2500 kg/m^3), E_c can be permitted to be taken as **[51]**:

$$E_c = 4700\sqrt{f_c'} \quad \text{(MPa)} \qquad 3.4$$

Poisson's ratio (υ) of concrete under uniaxial compressive load ranges from about 0.15 to 0.22; a representation value is 0.19 or 0.2. Under uniaxial loading, the ratio ν remains constant until approximately 80% of fc^- at which stress the apparent Poisson's ratio begins to increase **[51, 52]**.

3.2.1.1.2. Uniaxial Behavior under Tension Load

The general mechanical behavior of concrete under uniaxial tensile loading shows many similarities to the behavior observed in uniaxial compression. Typical stress-strain curves for concrete in uniaxial tension are shown in ***Figure 3.3***. In general, at a stress less than 60% of the tensile strength, the creation of new micro-cracks is negligible. So, this stress level will correspond to a limit of elasticity. Above this level of stress, the bond microcracks start to grow **[53]**.

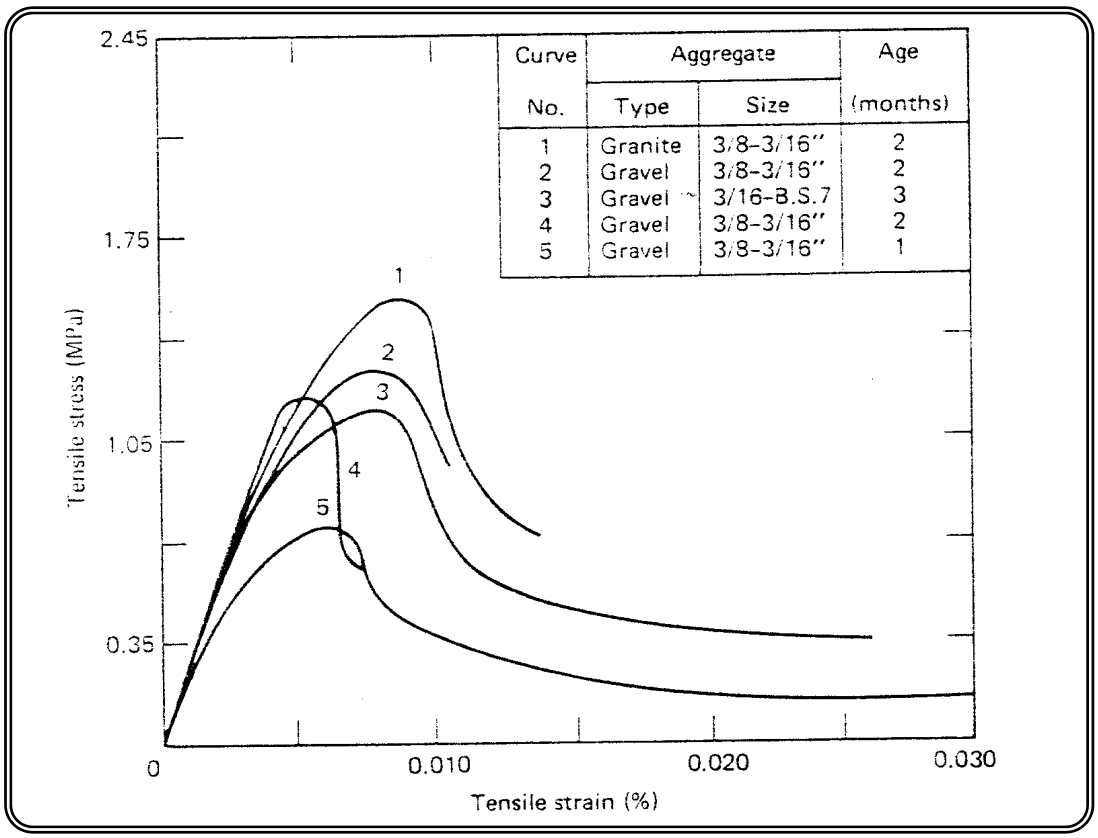

Figure 3.3 *Typical tensile stress-strain curves for concrete* ***[53]***.

The direction of crack propagation for uniaxial tension is transverse (normal) to the stress direction. The growth of every new crack will reduce the available load-stress capacity and this reduction causes an increase in the stresses at critical crack tips. The failure in tension is caused by a few

connected cracks rather than by numerous cracks, as it is for compressive states of stress.

The ratio between uniaxial tensile strength (f_t) and compressive strength f_c' may vary considerably but usually ranges from 0.05 to 0.1. The modulus of elasticity under uniaxial tension is somewhat higher and Poisson's ratio somewhat lower than in uniaxial compression **[52]**.

The direct tensile strength of concrete is difficult to measure and is normally taken as 0.3 to $0.4\sqrt{f_c'}$. Many times, either the modulus of rupture,f_r, or the split cylinder strength (f_t) is used to approximate the tensile strength of concrete. The value of the modulus of rupture of concrete varies quite widely but is normally as in ***Equation (3.5)***. The split cylinder tensile strength is usually somewhat lower, at approximately 0.45 to $0.55\sqrt{f_c'}$ in N/mm^2, f_r can be permitted to be taken as **[51]**:

$$f_r = 0.62\lambda\sqrt{f_c'} \qquad 3.5$$

Where: *fr* and *f'c* in MPa

λ =0.75 for all lightweight concrete

λ =0.85 for sand-lightweight concrete

λ =1 for normal weight concrete

3.2.1.2 Biaxial Behavior of Concrete

Under different combinations of biaxial loading, concrete exhibits strength and stress-strain behavior somewhat different from that under uniaxial condition. For biaxial compression states, the maximum strength increases approximately 25 % at a stress ratio of $\sigma_2/\sigma_1 = 0.5$ and 16 % at an equal biaxial compression state ($\sigma_2/\sigma_1 = 1$) **[52]**.

Under biaxial tension, concrete exhibits a constant tensile strength, or perhaps a slightly increased tensile strength, compared with values obtained under uniaxial loading. Under biaxial compression-tension, the compressive strength decreases almost linearly as the applied tensile stress is increased. ***Figure 3.4*** illustrates a typical biaxial strength envelope for concrete subjected to proportional biaxial loading **[52]**.

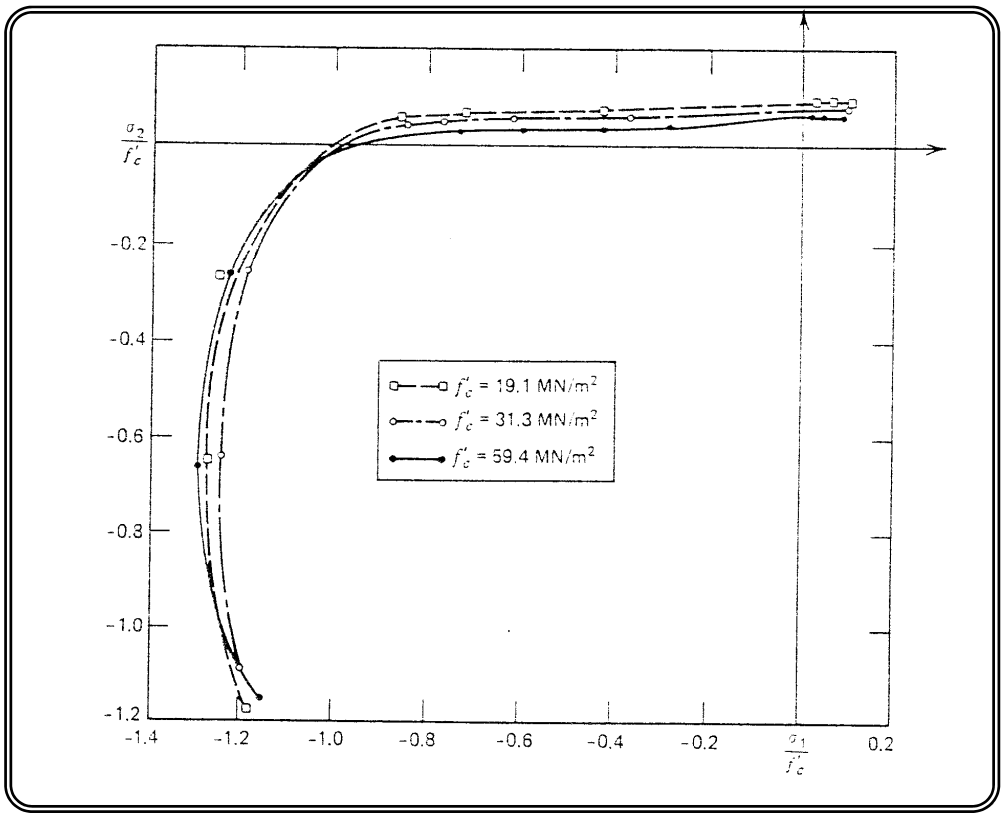

Figure 3.4 *Biaxial strength envelope of concrete* ***[54]***

3.2.1.3 Triaxial Behavior of Concrete

Experimental test data for the triaxial stress-strain behavior of plain concrete has been obtained by Richart *et al.* (1928) **[55]** at low or moderate volumetric (hydrostatic or confining) stresses, and by Balmer (1949) **[56]** at very high confining stresses. Typical stress-strain curves from the tests by Balmer (1949) **[56]** are shown in ***Figure 3.5***. These curves show that concrete, depending on the hydrostatic stress, can behave as a quasi-brittle,

plastic softening, or plastic hardening material. This is mainly because under high hydrostatic stresses, the possibility of bond cracking to occur is greatly reduced and the failure mode shifts from cleavage to crushing of cement paste (or mortar between aggregates). The ultimate axial strength is found to increase considerably with increasing the confining stress **[56]**, as shown in ***Figure 3.5.***

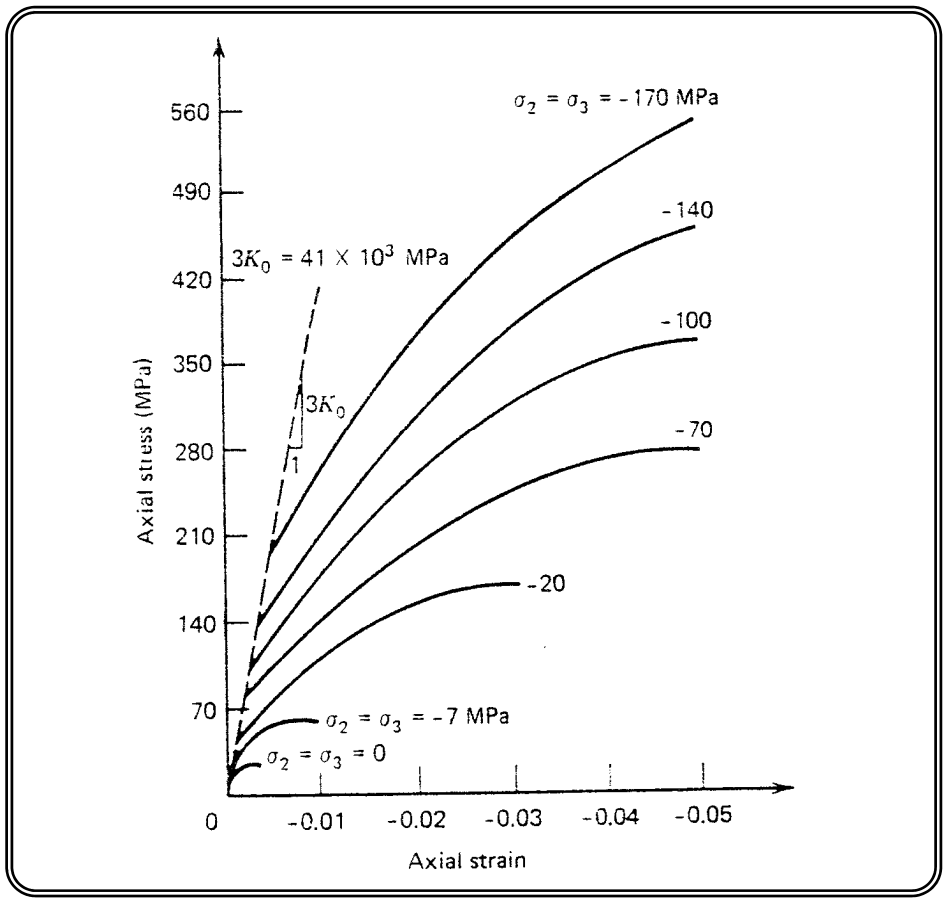

Figure 3.5 *Triaxial stress-strain relationship for concrete* ***[56]***

Under triaxial loading, experiments indicate that concrete has a fairly consistent failure surface that is a function of the three principal stresses. If isotropy of concrete is assumed, the elastic limit (onset of stable crack propagation), the onset of unstable crack propagation, and the failure limit all can be represented as a surface in three-dimensional principal stress space.

The shapes of the elastic limit surface and failure surface are shown schematically in ***Figure 3.6***. **[52]**

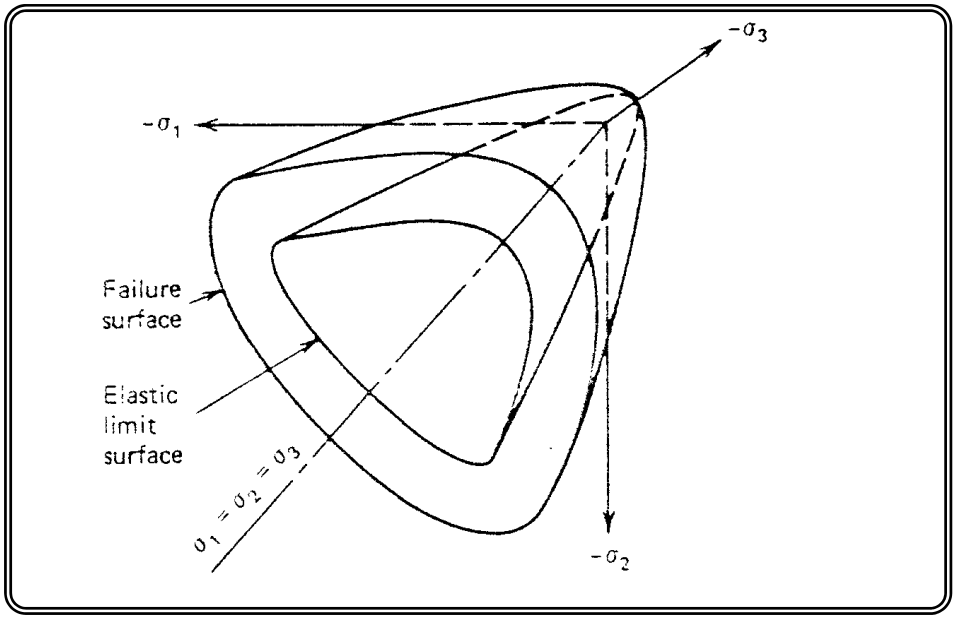

Figure 3.6 *Schematic representations of the elastic limit and failure surfaces of concrete in the three-dimensional principal stress space* ***[52]***

3.2.1.4 Crack Model

The first reinforced concrete finite element model which includes the effect of cracking was developed by **[57]**, who carried out a linear elastic analysis of beams with predefined crack patterns. The cracks were modeled by separating the nodal points of the finite element mesh and thus creating a discrete crack model ***Figure 3.7a***. With the change of topology and the redefinition of nodal points the narrow band width of the stiffness matrix is destroyed and a greatly increased computational effort results in this model. Moreover, the lack of generality in crack orientation has made the discrete crack model unpopular. In spite of these shortcomings, the use of discrete crack models in finite element analysis offers certain advantages over other methods. For those problems that involve a few dominant cracks, the discrete

crack approach offers a more realistic description of the cracks, which represent strain discontinuities in the structure. Such discontinuities are correctly characterized by the discrete crack model. The need for a crack model that offers automatic generation of cracks and complete generality in crack orientation, without the need of redefining the finite element topology, has led the majority of investigators to adopt the smeared crack model. Rather than representing a single crack, as shown in ***Figure 3.7a***, the smeared crack model represents many finely spaced cracks perpendicular to the principal stress direction, as illustrated in ***Figure 3.7b***. This approximation of cracking behavior of concrete is quite realistic, since the fracture behavior of concrete is very different from that of metals. In concrete, fracture is preceded by microcracking of material in the fracture process zone, which manifests itself as strain softening. This zone is often very large relative to the cross section of the member due to the large size of aggregate Figure 3.8a. In a steel member fracture is preceded by yielding of material in the process zone which is concentrated near the crack tip and has a relatively small size Figure 3.8b. In this case a discrete crack model is a more realistic representation of actual behavior.

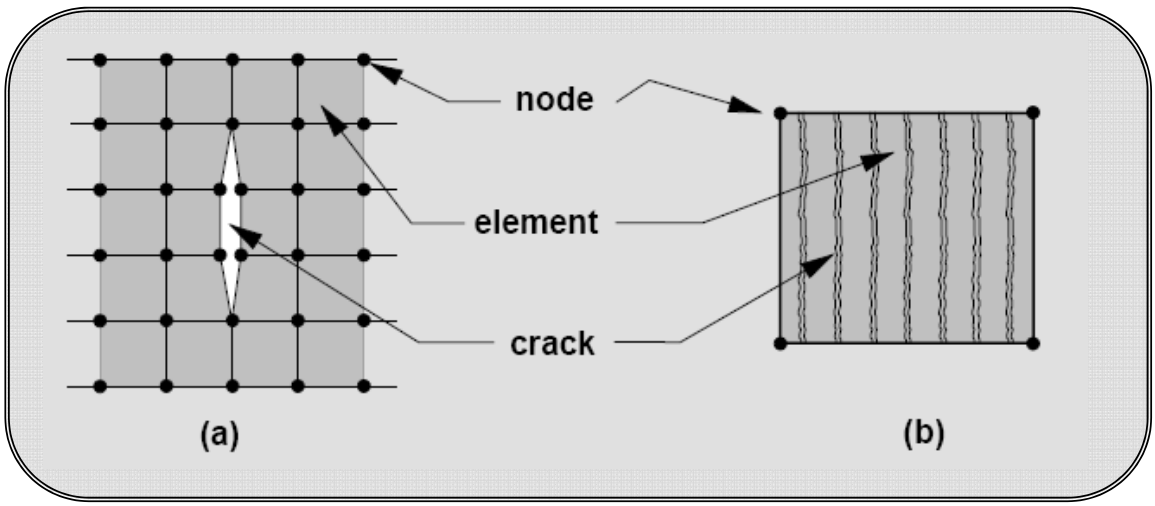

Figure 3.7 *cracking models: a) discrete crack, b) smeared crack* **[58]**

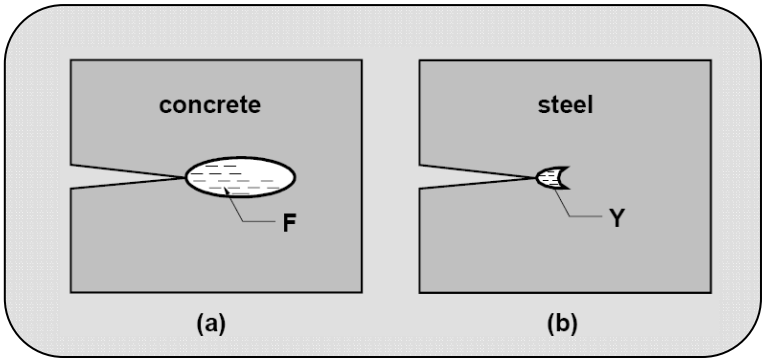

Figure 3.8 *relative size of crack process zone*
a) Fraction zone (F) of concrete, b) yielding zone (Y) of steel ***[45]***

The smeared crack model was first used by Rashid (1968) **[58]** represents cracked concrete as an elastic orthotropic material with reduced elastic modulus in the direction normal to the crack plane. With this continuum approach the local displacement discontinuities at cracks are distributed over some tributary area within the finite element and the behavior of cracked concrete can be represented by average stress-strain relations. In contrast to the discrete crack concept, the smeared crack concept fits the nature of the finite element displacement method, since the continuity of the displacement field remains intact. Although this approach is simple to implement and is, therefore, widely used, it has nevertheless a major drawback, which is the dependency of the results on the size of the finite element mesh used in the analysis **[59, 60]**. When large finite elements are used, each element has a large effect on the structural stiffness. When a single element cracks, the stiffness of the entire structure is greatly reduced. Higher order elements in which the material behavior is established at a number of integration points do not markedly change this situation, because, in most cases, when a crack takes place at one integration point, the element stiffness is reduced enough so that a crack will occur at all other integration points of the element in the next iteration. Thus, a crack at an integration point does not

relieve the rest of the material in the element, since the imposed strain continuity increases the strains at all other integration points. The overall effect is that the formation of a crack in a large element results in the softening of a large portion of the structure. The difficulty stems from the fact that a crack represents a strain discontinuity which cannot be modeled correctly within a single finite element in which the strain varies continuously. Many research efforts have been devoted to the solution of this problem based, in particular, on fracture mechanics concepts **[60, 61, and 62]**.

The success fracture mechanics theory **[63]** had in solving different types of cracking problems in metals, ceramics and rocks has lead to its use in the finite element analysis of reinforced concrete structures. If it is accepted that concrete is a notch-sensitive material, it can be assumed that a cracking criterion which is based on tensile strength may be dangerously unconservative and only fracture mechanics theory provides a more rational approach to the solution of the problem. In its current state of development, however, the practical applicability of fracture mechanics to reinforced concrete is still in question and much remains to be done. Intensive research in this area is presently undertaken by several researchers **[60, 61, 62, 64]**

.

In ANSYS computer program, the presence of a crack at an integration point is represented through modification of the stress-strain relations by introducing a plane of weakness in a direction normal to the crack face. Also, a shear transfer coefficient is introduced which represents a shear strength reduction factor for those subsequent loads which induce sliding (shear) across the crack face.

3.2.1.5 Crushing Modeling

In ANSYS computer program, the material is assumed to crush at an integration point if the material at that point fails in uniaxial, biaxial, or triaxial compression. In concrete element, crushing is defined as the complete deterioration of the structural integrity of the material (e.g. material spalling). Under conditions where crushing has occurred, material strength is assumed to have degraded to an extent such that the contribution to the stiffness of an element at the integration point in question can be ignored.

3.2.1.6 Used Model

3.2.1.6.1FEM input data

For concrete, ANSYS computer program requires input data for material properties, as follows **[14]**:

Ultimate uniaxial compressive strength (f_c')

Elastic modulus (E_c)

Ultimate uniaxial tensile strength (modulus of rupture,f_r)

Poisson's ratio (υ)

Shear transfer coefficient for opened and closed cracks (β_o and β_c respectively)

Ultimate biaxial compressive strength (f_{ch}) ($1.2f_c'$)

Hydrostatic stress (σ_h) ($1.57f_c'$)

Ultimate compressive strength for a state of biaxial compressive superimposed on (f_1) ($1.45f_c'$)

Ultimate compressive strength for a state of uniaxial compressive superimposed on (f_2) ($1.725f_c'$)

Friction coefficient μ

Compressive uniaxial stress-strain relationship for concrete

An effort was made to estimate the ultimate uniaxial compressive and tensile strength (f_c' and f_r) of test reinforced concrete beams. Details about these values and others, related with chapter five.

From the ultimate uniaxial compressive strength (f_c'), obtained from appropriate tests, the elastic modulus of concrete (E_c) for each beam model was calculated according to ACI 318-08 by using ***Equation 3.4***, the modulus of rupture of concrete was calculated according to ACI318-08 by using ***Equation 3.5***. Poisson's ratio for concrete was assumed to be 0.2 **[50, 65]** for all reinforced concrete beams.

The shear transfer coefficient, β, represents conditions of the crack face. The value of β ranges from 0.0 to 1.0, with 0.0 representing a smooth crack (complete loss of shear transfer) and 1.0 representing a rough crack (no loss of shear transfer) **[14]**

The value of β_o used in many studies of reinforced concrete and composite steel-concrete structures, however, varied between 0.05 and 0.25 **[50, 66, 67]**. A number of preliminary analyses were attempted in this study with various values for the shear transfer coefficient within this range, but convergence problems were encountered at low loads with β_o less than 0.2. Therefore, the shear transfer coefficients for closed and opened cracks, used in this study, were taken equal to 0.99 and 0.2 respectively for all examples.

5.2.1.6.2Compressive Uniaxial Stress-Strain Relationship for Concrete

The ANSYS computer program requires the uniaxial stress-strain relationship for concrete in compression. For numerical expressions **[68]**, the following ***Equations 3.6*** and ***3.7***, were used along with ***Equation 3.8*** **[69]** and

Equation 3.4 **[51]** to construct the uniaxial compressive stress-strain curve for concrete.

$$f = \frac{E_c \varepsilon}{1 + \left(\frac{\varepsilon}{\varepsilon_o}\right)^2} \tag{3.6}$$

$$\varepsilon_o = \frac{2 f'_c}{E_c} \tag{3.7}$$

$$E_c = \frac{\sigma}{\varepsilon} \tag{3.8}$$

Where:

σ = stress at any strain ε, MPa

ε = strain at stress f .

ε_o = strain at the ultimate compressive strength f'_c

Figure 3.9 shows the simplified compressive uniaxial stress-strain relationship that was used in this study.

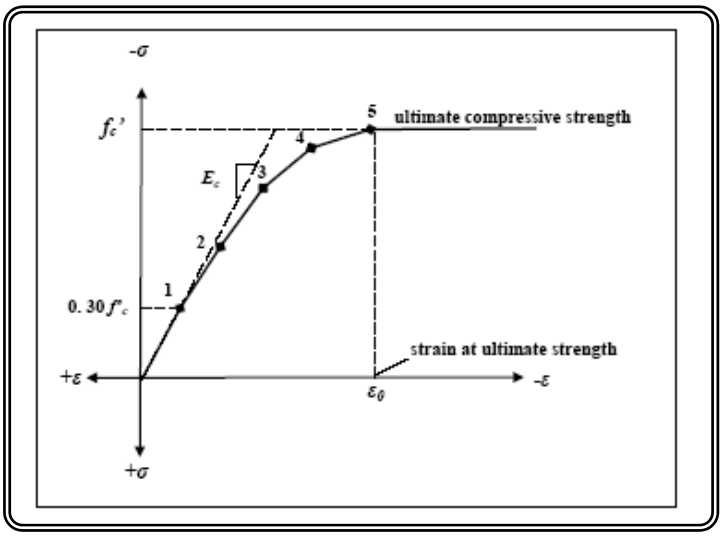

Figure 3.9 *Simplified compressive uniaxial stress-strain curve for concrete* ***[66]***

The simplified stress-strain curve for concrete model is constructed from six points connected by straight lines. The curve starts at zero stress and strain. Point of number 1, at $0.30 f'_c$, is calculated for the stress-strain

relationship of the concrete in the linear range (***Equations 3.8 and 3.4***). Point of numbers 2, 3, and 4 are obtained from ***Equation 3.6***, in which ε_o is calculated from ***Equation 3.7***. Point of number 5 is at ε_o and $f\acute{c}$. In this study, an assumption was made of perfectly plastic behavior after point of number 5 **[66]**.

5.2.1.7 Failure Criterion for Concrete

The model to be used is capable of predicting failure for concrete materials. Both cracking and crushing failure modes are accounted for. The two input strength parameters (i.e., ultimate uniaxial tensile and compressive strengths) are needed to define a failure surface for the concrete. Consequently, a criterion for failure of the concrete due to a multiaxial stress state can be calculated **[70]**.

A three-dimensional failure surface for concrete is shown in Figure 3.10. The most significant nonzero principal stresses are in the x and y -directions, represented by σ_{xp} and σ_{yp}, respectively. Three failure surfaces are shown as projections on the $\sigma_{xp} - \sigma_{yp}$ plane. The mode of failure is a function of the sign of σ_{zp} (principal stress in the z -direction).

For example, if σ_{xp} and σ_{yp} are both negative (compressive) and σ_{zp} is slightly positive (tensile), cracking would be predicted in a direction perpendicular to σ_{zp}. However, if σ_{zp} is zero or slightly negative, the material is assumed to crush **[11]**.

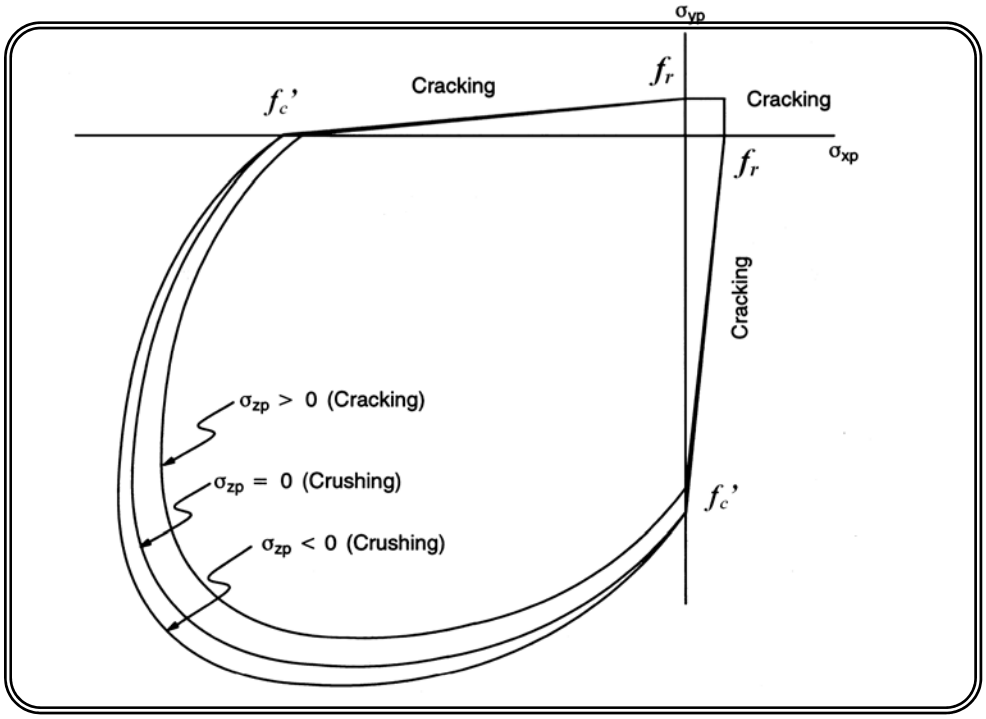

Figure 3.10 *3D-failure surface for concrete* ***[14]***

In a concrete element, cracking occurs when the principal tensile stress in any direction lies outside the failure surface. After cracking, the elastic modulus of the concrete element is set to zero in the direction parallel to the principal tensile stress direction. Crushing occurs when all principal stresses are compressive and lies outside the failure surface; subsequently, the elastic modulus is set to zero in all directions **[14]**, and the element effectively disappears.

During this study, it was found that if the crushing capability of the concrete is turned on, the finite element beam models fail prematurely. Crushing of the concrete starts to develop in elements located directly under the loads. Subsequently, adjacent concrete elements will crush within several load steps as well, significantly reducing the local stiffness.

3.2.2 Steel

Compared to concrete, steel is a much simpler material to represent. Its strain-stress behavior can be assumed to be identical in tension and in compression. A typical uniaxial stress-strain curve for a steel specimen loaded monotonically in tension is shown in ***Figure 3.11.***

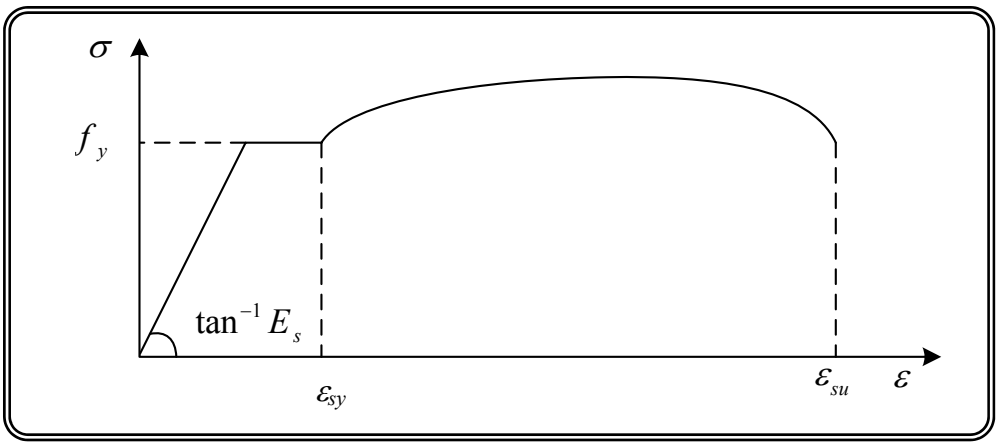

Figure 3.11 *Typical stress-strain curve for steel* ***[52]***

The stress-strain diagram may for simplicity consist of two branches: the first branch starts from the origin with a slope equal to E_s, up to f_y. A second branch is horizontal or, for practical use of computers, is assumed to have a very small slope such as 10^{-2} E and this last case is limited to the strain 0.01 according to EC4 **[5]**. Therefore, the following two cases can be used:

For design calculations, the relation between stress and strain of structural steel may be idealized as elastic-perfectly plastic, as shown in ***Figure 3.12.***

To avoid possible computational difficulties when using a computer, the alternative bilinear stress-strain relationship indicated in Figure 3.13 may be used.

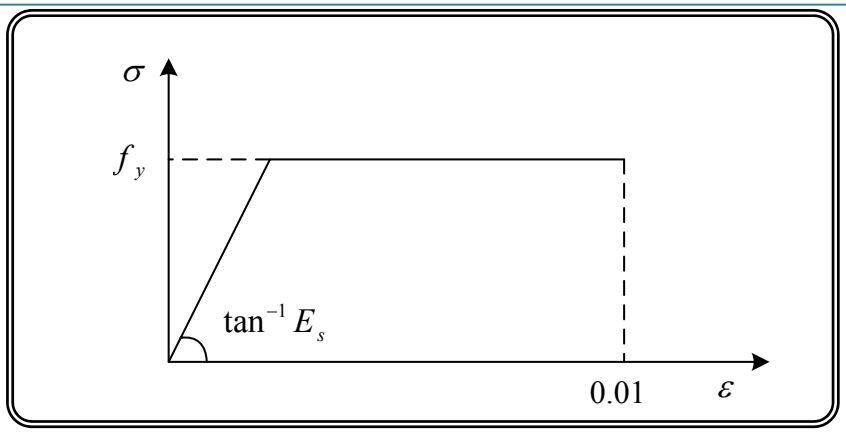

Figure 3.12 *Elastic-perfect plastic stress-strain relationships* ***[52]***

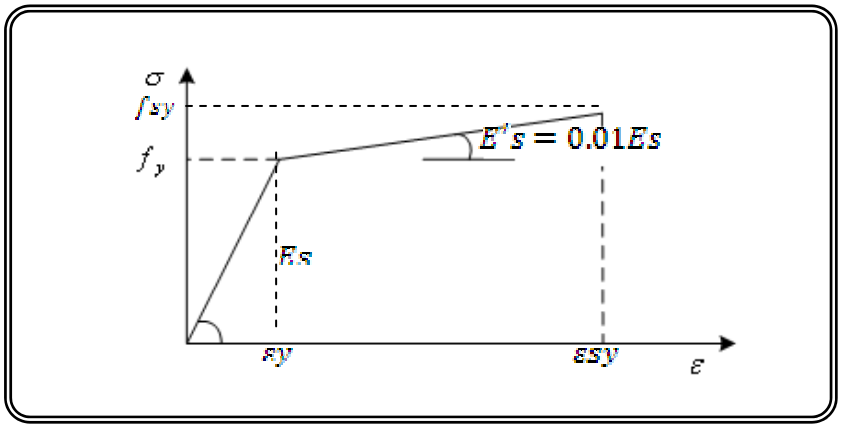

Figure 3.13 *Idealization for computer calculations* ***[41]***.

The material coefficients to be adopted in calculations for the steels covered by this study will be taken, as follows (according to ACI-318-08) **[51]**:

Modulus of elasticity Es=200000N/mm^2

Shear modulus $G_s = E / 2(1+2\gamma_s)$

Poisson's ratio $\upsilon_s = 0.3$

Unit mass $\rho_s = 7800\,\text{kg/m3}$

The value of steel yield strength (f_y) and ultimate tensile strength (f_u), corresponding to steel, are carried out from tensile test, as shown in chapter five.

3.3 Model Generation

The ultimate purpose of finite element analysis is to recreate mathematically the behavior of an actual engineering system. In other words, the analysis must use an accurate mathematical model of a physical prototype. In the broadest sense, this model comprises all the nodes, elements, material properties, real constants, boundary conditions, and other features that are used to represent the physical system.

In ANSYS terminology **[14]**, the term model generation usually takes on the narrower meaning of generating the nodes and elements that represent the spatial volume and connectivity of the actual system. Thus, model generation in this discussion will mean the process of defining the geometric configuration of the model's nodes and elements.

In the following 7 elements described to be used in the model: the first element (SOILD65) is for concrete, (SOILD45) and (SHELL43) are for steel, and (CONTAC52), (COMBIN39), and (CONTA173 and TARGE170) are for bond modeling. In the last, one element is chosen to represent every type of materials that depending on the agreements with experimental data gives.

3 .3.1 SOLD65 Element Description

SOLID65 (or 3-D reinforced concrete solid) is used for the 3-D modeling of solids with or without reinforcing bars (rebar). The solid is capable of cracking in tension and crushing in compression. In concrete applications, for example, the solid capability of the element may be used to model the concrete, while the rebar capability is available for modeling

reinforcement behavior. Other cases for which the element is also applicable would be reinforced composites (such as fibre glass), and geological materials (such as rock). The element is defined by eight nodes having three degrees of freedom at each node: translations of the nodes in x, y, and z-directions. Up to three different rebar specifications may be defined.

The most important aspect of this element is the treatment of nonlinear material properties. The concrete is capable of cracking (in three orthogonal directions), crushing, plastic deformation, and creep. The rebars are capable of tension and compression, but not shear. They are also capable of plastic deformation and creep. This 8-node brick element is used, in this study, to simulate the behavior of concrete (i.e. plain concrete). The element is defined by eight nodes and by the isotropic material properties. The geometry, node locations, and the coordinate system for this element are shown in ***Figure 3.14.***

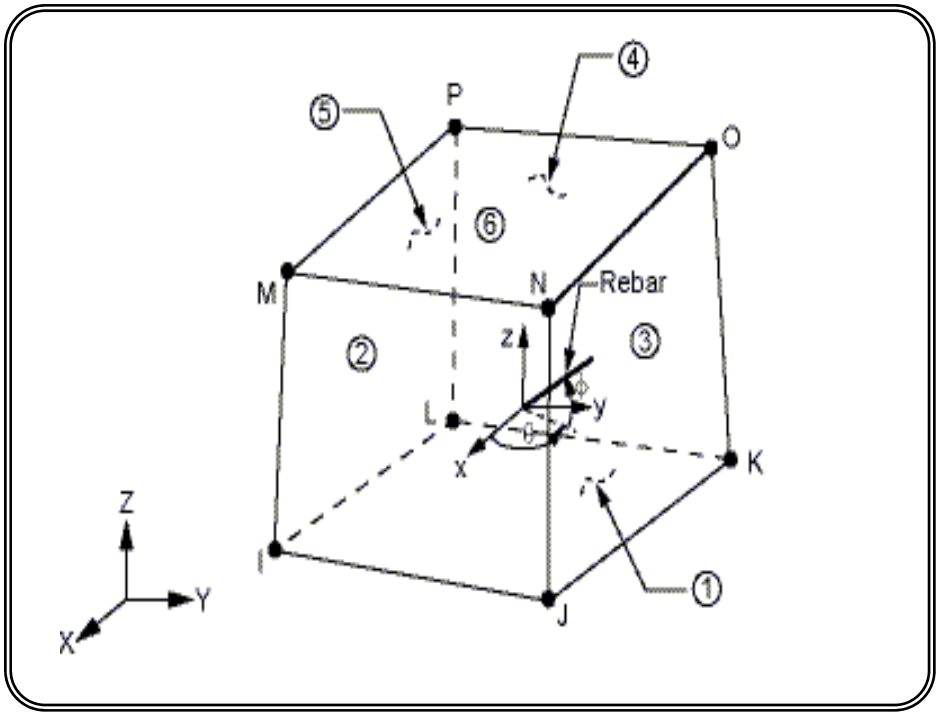

Figure 3.14 *SOLID65 geometry* ***[14]***

3.3.2 SOLID45 Element Description

An eight-node solid element, SOLID45, was used for the steel plates at the supports in the beam models. The element is defined with eight nodes having three degrees of freedom at each node –translations in the nodal x, y, and z directions. The geometry and node locations for this element type are shown in ***Figure 3.15***. The element has plasticity, creep, swelling, stress stiffening, large deflection, and large strain capabilities. A reduced integration option with hourglass control is available.

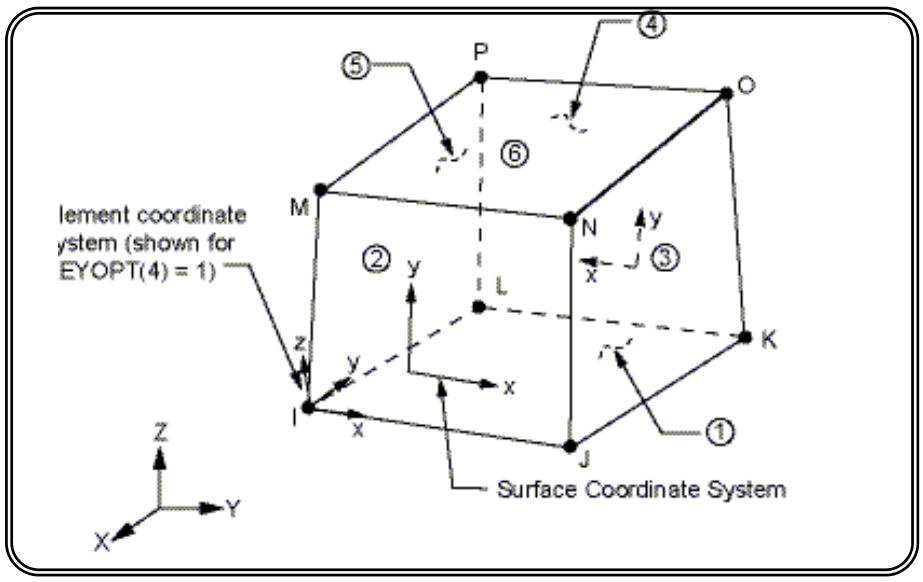

Figure 3.15**: SOLID45 geometry* ***[14]

3.3.3 SHELL43 Element Description

SHELL43 is well suited to model linear, warped, moderately-thick shell structures. The element has six degrees of freedom at each node: translations in the nodal x, y, and z directions and rotations about the nodal x, y, and z axes as shown in ***Figure 3.16***. The deformation shapes are linear in both in-plane directions. For the out-of-plane motion, it uses a mixed interpolation of tensorial components. The element has plasticity, creep, stress stiffening, large deflection, and large strain capabilities.

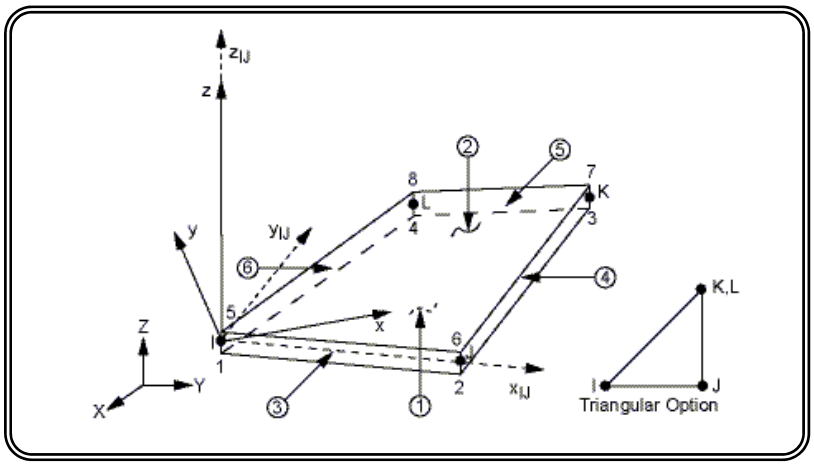

Figure 3.16 *SHELL43 Geometry* ***[14]***

3.3.4 CONTAC52 Element Description

CONTAC52 represents two surfaces which may maintain or break physical contact and may slide relative to each other. The element is capable of supporting only compression in the direction normal to the surfaces and shear (Coulomb friction) in the tangential direction. The element has three degrees of freedom at each node: translations in the nodal x, y, and z directions as shown in ***Figure 3.17***. The element may be initially preloaded in the normal direction or it may be given a gap specification. A specified stiffness acts in the normal and tangential directions when the gap is closed and not sliding, the element is defined by two nodes.

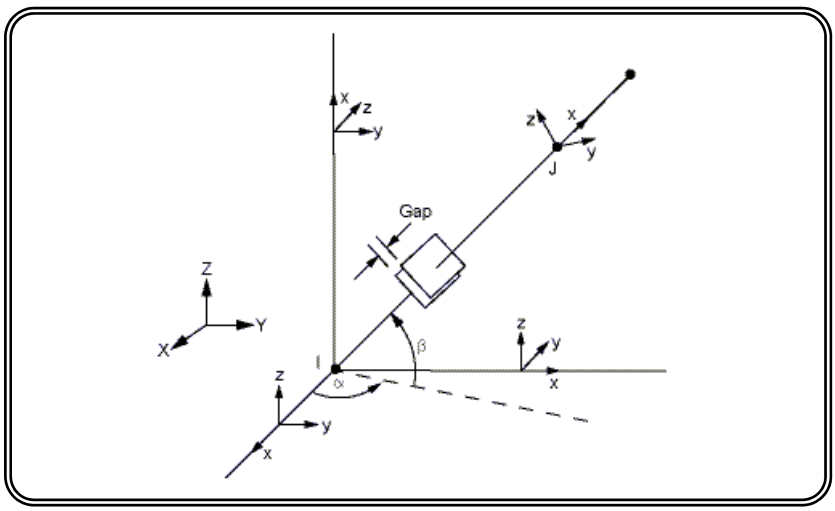

Figure 3.17.*CONTAC52 Geometry* ***[14]***

3.3.5 COMBIN39 Element Description

COMBIN39 is a unidirectional element (or nonlinear spring) with nonlinear generalized force-deflection capability that can be used in any analysis. The element has longitudinal capability in 1-D, 2-D, or 3- D applications. The longitudinal option is a uniaxial tension-compression element with up to three degrees of freedom at each node: translations of the nodes in x, y, and z-directions. No bending or torsion is considered. The torsional option is a purely rotational element with three degrees of freedom at each node: rotations about the nodal x, y, and z-axes. No bending or axial loads are considered. The element has a large displacement capability for which there can be two or three degrees of freedom at each node. The element is defined by two node points and a generalized force-deflection curve. The points on this curve (D1, F1, etc.) represent force (or moment) versus relative translation (or rotation) for structural analyses. This element is used, in this study, to simulate the behavior of the shear connectors in resisting the horizontal shear between the concrete and the steel plates. The element is defined by two node points and a generalized force-deflection curve. The geometry, node locations, and the coordinate system for this element are shown in ***Figure 3.18***.

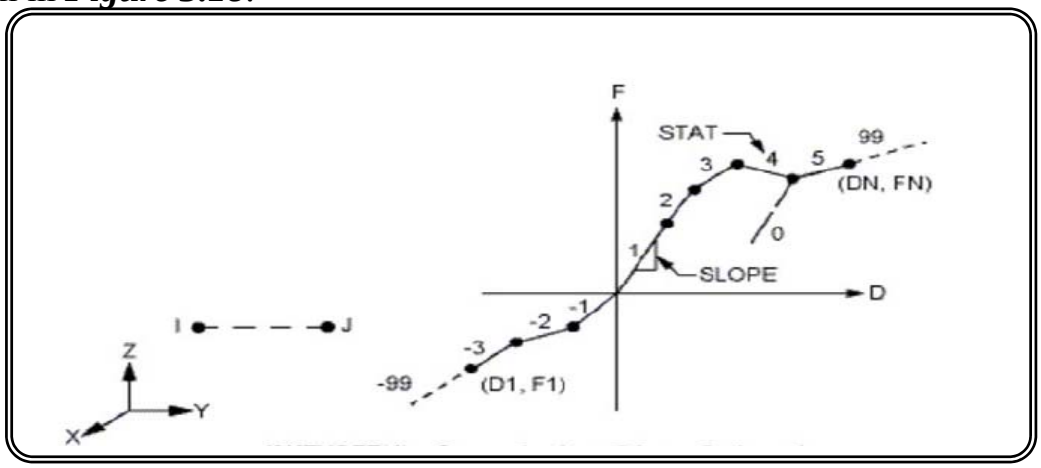

Figure 3.18 *COMBIN39 Geometry* ***[14]***

3.3.6 TARGE170 Element Description

In studying the contact between two bodies, the surface of one body is conventionally taken as a contact surface and the surface of the other body as a target surface. The "contact-target" pair concept has been widely used in finite element simulations. For rigid-flexible contact, the contact surface is associated with the deformable body; and the target surface must be the rigid surface. For flexible-flexible contact, both contact and target surfaces are associated with deformable bodies. The contact and target surfaces constitute a "Contact Pair". TARGE170 is used to represent various 3-D target surfaces for the associated contact elements (CONTA173). The contact elements themselves overlay the solid elements describing the boundary of a deformable body that is potentially in contact with the rigid target surface, defined by TARGE170. Hence, a "target" is simply a geometric entity in space that senses and responds when one or more contact elements move into a target segment element. The target surface is modeled through a set of target segments; typically several target segments comprise one target surface. Each target segment is a single element with a specific shape or segment type, as shown in ***Figure 3.19***. 4 node quadrilateral element is used in this study.

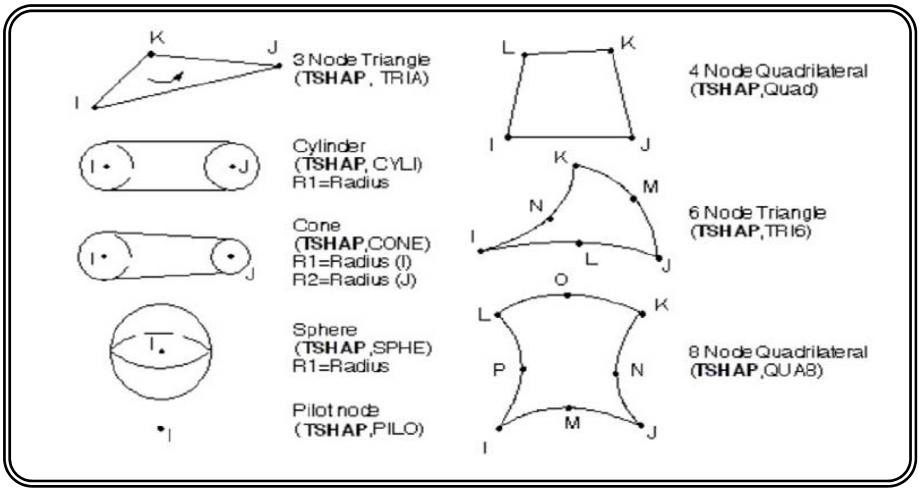

Figure3.19 *TARGE170 geometry* ***[14]***

3.3.7CONTA173 Element Description

CONTA173is used to represent contact and sliding between 3-D "target" surfaces (TARGE170) and a deformable surface, defined by this element. The element is applicable to 3-D structural and coupled field contact analyses. This element is located on the surfaces of 3-D solid or shell elements without mid-side nodes. It has the same geometric characteristics as the solid or shell element face with which it is connected. Contact occurs when the element surface penetrates one of the target segment elements (TARGE170) on a specified target surface. The element is defined by four nodes; the node ordering is consistent with the node ordering for the underlying solid or shell element, as shown in ***Figure 3.20***.

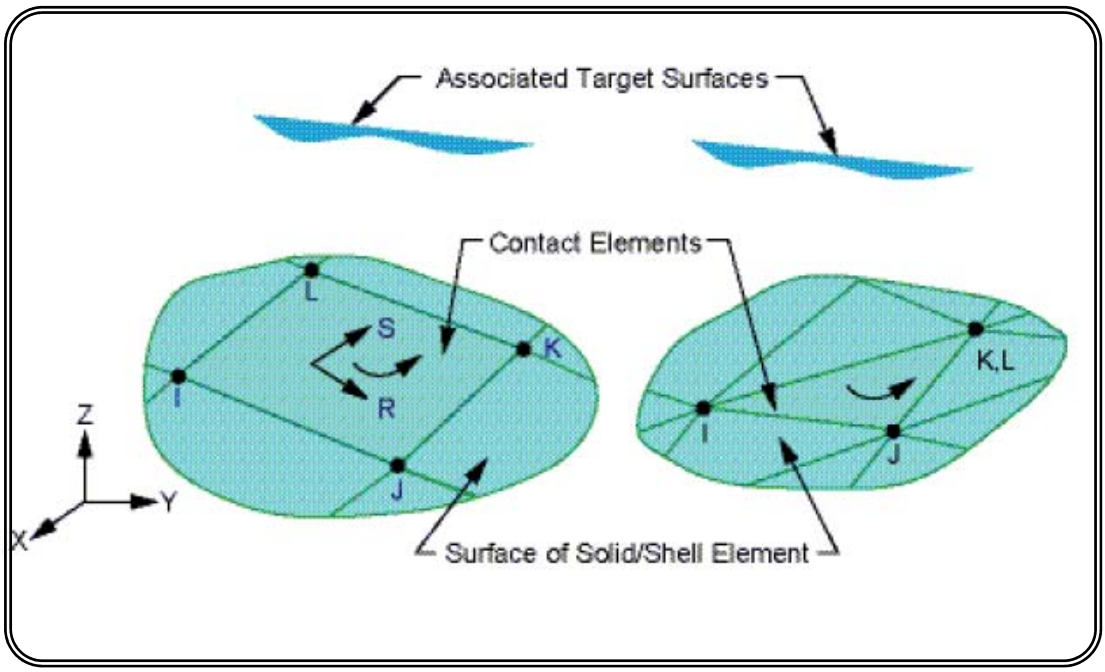

Figure3.20 *CONTA173 Geometry* ***[14]***

3.4 Nonlinear Solution Techniques

The finite element discrimination process yields a set of simultaneous equations **[14]**:

$$[K]\{U\} = \{F^a\} \qquad 3.9$$

Where:

[K] = Stiffness matrix.

{U} = Vector of nodal displacements

$\{F^a\}$ = Vector of applied loads

For linear elastic problems ***equation 3.10*** is used to find the solution of the unknown displacement {U}. In the case of nonlinear system, the stiffness matrix [K] is a function of the unknown displacement (or their derivatives). Then the ***Equation 3.9*** cannot be exactly computed before determination of the unknown displacement {U}.

There are several techniques for solving the nonlinear ***equation 3.10***; the basic techniques can be classified into:

1. Incremental or stepwise procedure, ***Figure (3.21a).***
2. The iterative or Newton-procedure, ***Figure (3.21b).***
3. Incremental-iterative procedure, ***Figure (3.21c).***

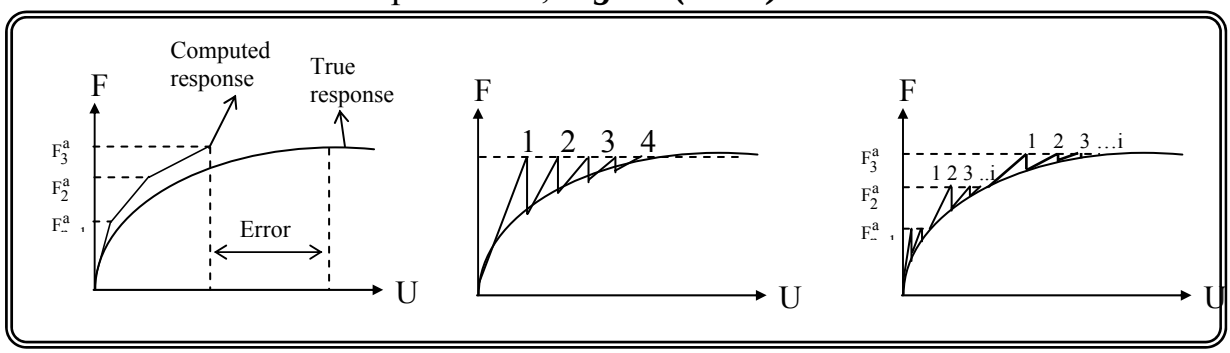

Figure (3.21) *Basic technique for solving the nonlinear equation: (a) Incremental (b) Iterative (c) Incremental-iterative.* ***[14]***

In the incremental procedure, the load is applied in several small increments, and the structure is assumed to respond linearly within each increment with its stiffness recomputed based on the structural geometry and member end actions at the end of the previous load increment. This is a simple procedure, which requires no iterations, but errors are likely to accumulate after several increments unless very fine increments are used, ***Figure (3.21a).***

In the iterative procedure, the total load is applied in one increment at the first iteration, the out of balance forces are then computed and used in the next iteration to obtain progressively improved solution. The iterative process is continued until the final converged solution would be in equilibrium, such that the internal load vector would equal the applied load vector or within some tolerance. This process can be written as:

$$[K_i^T]\{\Delta U_i\} = \{F^a\} - \{F^{nr}\} \quad (3.10)$$

$$\{U_{i+1}\} = \{U_i\} + \{\Delta U_i\} \quad (3.11)$$

Where:

$[K_i^T]$ = Stiffness matrix

i = Subscript representing the current equilibrium iteration.

$\{F^{nr}\}$ = Internal load vector

This procedure fails to produce information about the intermediate stage of loading. For structural analysis including path-dependent nonlinearities (such as plasticity), the solution process requires that some intermediate increments be in equilibrium in order to correctly follow the load path. This can be achieved by using the combined incremental-iterative method.

In the combined-iterative procedure, a combination of the incremental and iterative scheme is used. The load is applied incrementally, and iterations

are performed in order to obtain converged solution corresponding to the stage of loading under consideration, ***Figure (3.21c)***

The incremental-iterative solution procedures have been used in this study: Full Newton-Raphson procedure. The stiffness matrix is formed at every iteration. The advantage of this procedure may give more accurate result. The disadvantage of this procedure is that a large amount of computational effort may be required to form and decompose the stiffness matrix, ***Figure (3.22).***

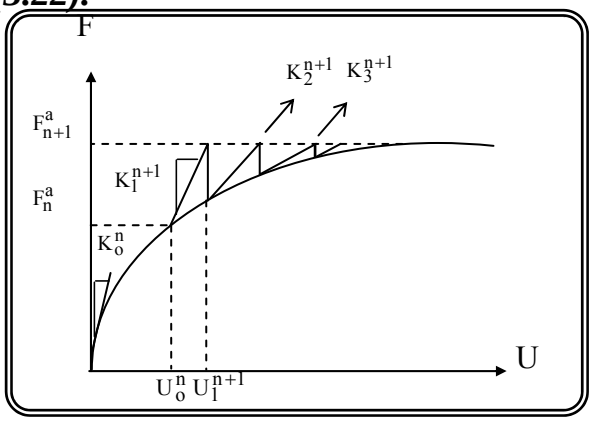

Figure (3.22) *Incremental-iterative procedures full Newton-Raphson procedure* ***[14]***.

In some nonlinear static analyses, if Newton-Raphson method is used alone, the tangent stiffness matrix may become singular (or non-unique), causing severe convergence difficulties. Such occurrences include nonlinear buckling analyses in which the structure either collapses completely or "snaps through" to another stable configuration. For such situations, an alternative iteration scheme must be activated, the arc-length method, to help avoid bifurcation points and track unloading **[14]**.

From the previous discussion, a nonlinear analysis in the ANSYS computer program can be organized into three levels of operation:

The "top" level consists of the load steps that it defines explicitly over a "time" span. Loads are assumed to vary linearly within load steps (for static analyses), as shown in ***Figure 3.23***.

Within each load step, it can direct the program to perform several solutions (substeps or time steps) to apply the load gradually.

At each substep, the program will perform a number of equilibrium iterations to obtain a converged solution.

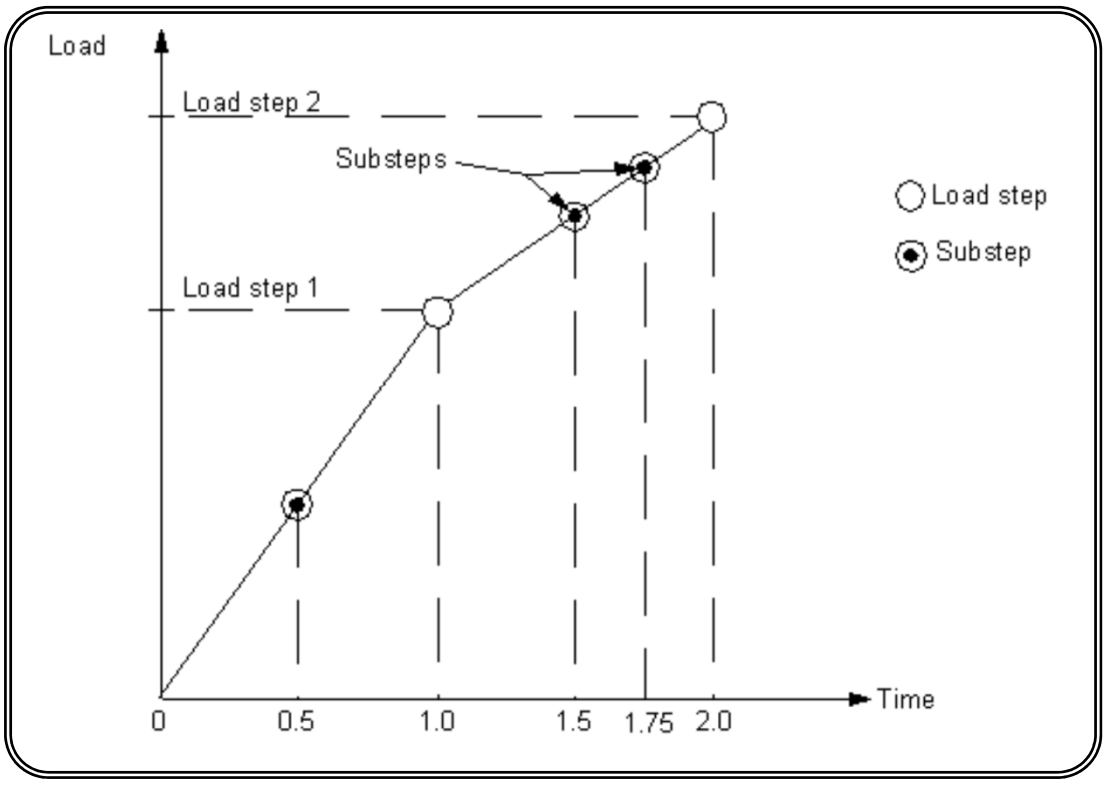

Figure 3.23 *Load step, substeps and time.***[14]**

The ANSYS program gives a number of choices when designating a convergence criterion. Convergence checking can be based on forces, moments, displacements, or rotations, or on any combination of these items. Additionally, each item can have a different convergence tolerance value. For multiple degree-of-freedom problems, it also has a choice of convergence norms. It should almost always employ a force-based (and, when applicable, moment-based) convergence tolerance. Displacement-based (and, when applicable, rotation-based) convergence checking can be added, if desired, but should not be usually used alone.

3.5. Analysis Termination Criterion

In the physical test under load control, collapse of a structure takes place when no further loading can be sustained. This is usually indicated in the numerical tests by successively increasing iterative displacements and a continuous growth in the dissipated energy. Hence, the convergence of the iterative process cannot be achieved. A maximum number of iterations for each increment is specified to stop the nonlinear solution if the convergence limit has not been achieved for this study. It has been observed that a maximum number of about (50-100) iterations are generally sufficient to predict the solution divergence or failure. This maximum number of iterations depends on the type of the problem, extent of nonlinearities, and on the specified tolerance.

CHAPTER FOUR

BOND BETWEEN STEEL AND CONCRETE

4.1 Introduction

Bond is the interaction between concrete and steel. The force transfers from concrete to steel or vice versa through three different phenomena:

1. Chemical adhesion between steel and mortar paste.
2. Friction and wedging action of small dislodging sand particles between steel and attaching concrete.
3. Mechanical interaction between concrete and steel.

Usually bond in composite member is derived primarily from the first two mechanisms, even though there is some mechanical interlocking caused by the roughness of the surface.

4.2 Load-Slip Relation

There are two types of experiment used in the determination of the bond load-slip relation:-

4.2.1 push-out Test

This method adopted by standard ASTM, at which the force is applied at concrete core which is embedded in a steel tube.

Normally bottom of the steel column left without filling of concrete to keep for the travel of concrete core. A displacement transducer was attached to steel tube to record the travel of the concrete core. A photograph showing all details of the test set up shown in ***Figure 4.1*** **[23]**.

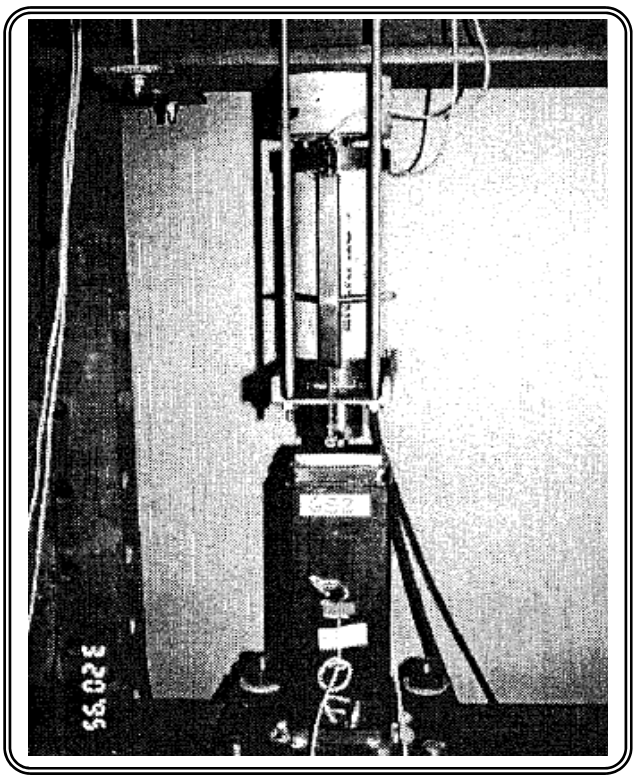

Figure 4.1 *push out test set up* **[23]**

4.2.2 Slip Measurement: In other type of test, the relative slip is determined from the change in the concrete to steel travel that records by gauges put in the steel and concrete ends. This method is very sensitive to experimental errors **[22]**, the location of the gauges is shown in ***Figure 4.2***

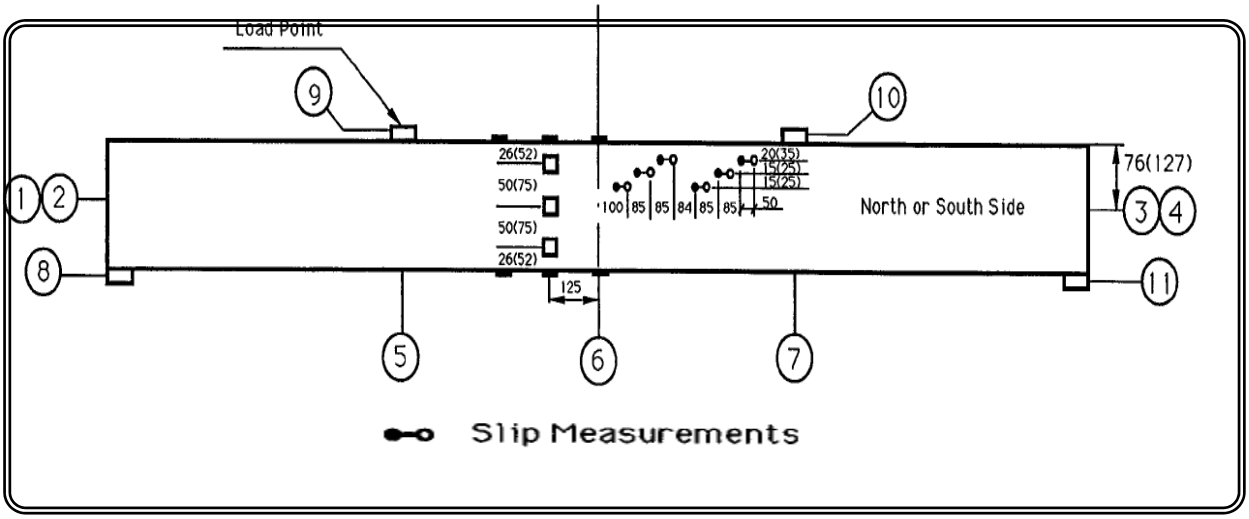

Figure 4.2 *test 2 setup shown the gauges locations* **[22]**

4.3. Bond in Composite Members

In the analysis and design of composite columns and beam-columns complete compatibility of stains between steel and concrete is assumed in the codes of practices **(Eurocode4, 1994; ACI318-08) [5, 51]**. A number of studies **[18, 12, 73, and 74]** indicated that the bond between steel and concrete has little effect in relation to the performance of columns and beam-columns. However, when longitudinal shear stresses are predominate as in the case of the flexural member **[23]**, bond strength may have significant role when no shear connectors are provided.

However, in the present study, partial bond is assumed for beams, beam-column and columns.

4.3.1 Slip Due to Axial Load

Clearly if sufficient axial force is applied to only steel or concrete of a concrete filled steel tube slip may be induced. In this case, the two materials are assumed to have the same transverse displacements and rotation. Slip stress is only caused by differential axial strains between the steel and concrete layers. In case of frame composed of steel girder (I section) and concrete filled steel tube columns, as shown in ***Figure 4.3,*** in which only portion of the column end will connected, this induced axial force at the column end. These tests often exhibit bond strength and initial slip stiffness which are higher than those observed in push-out test on concrete filled steel tube sections, due to primarily to the added frictional resistance from punching which occurs as the tube starts to deform or buckle in the connection region.

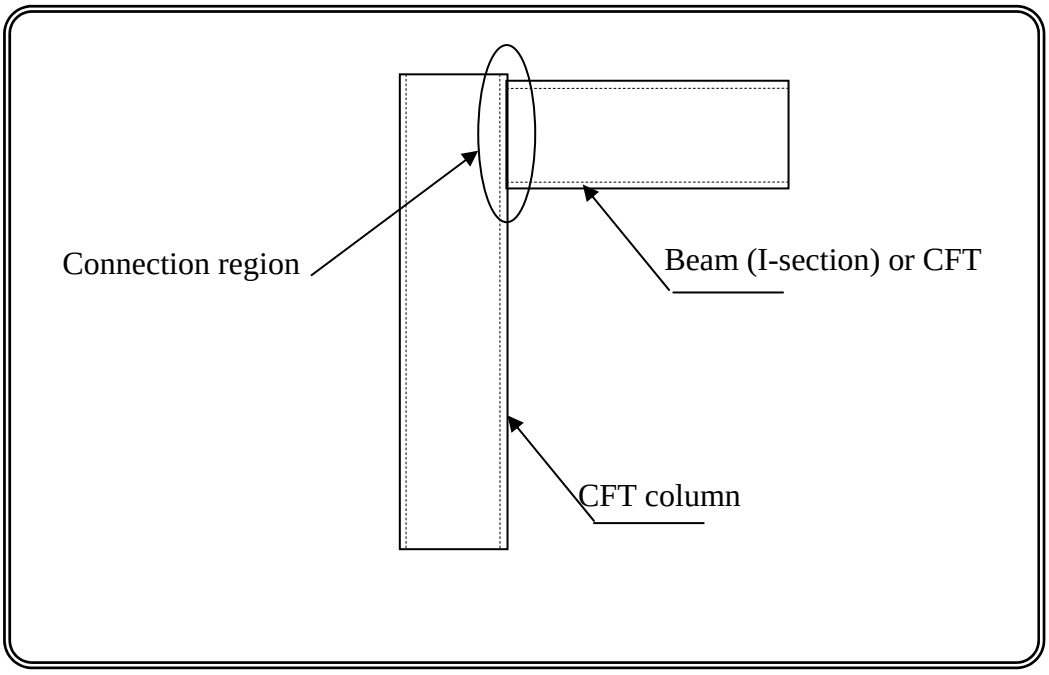

Figure 4.3 *Beam to column connection.***[23]**

4.3.2 Slip Due to Flexure

A second application is slip caused by composite beam action during flexure. This mechanism is triggered by cracking of the concrete core in tension which results in an unsymmetrical section **[75]**. The eccentricity of the uncracked concrete section with respect to the steel section causes longitudinal stress to develop in the materials under pure flexural loading then results in unsymmetrical section ***Figure 4.4.***

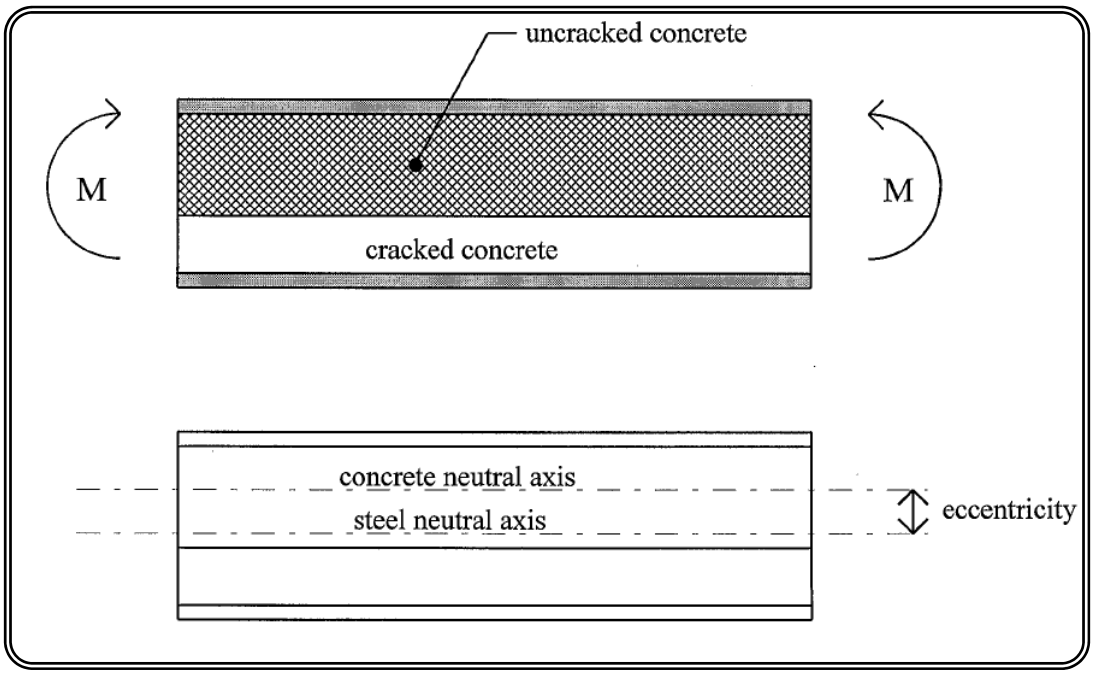

Figure 4.4 *unsymmetrical section caused by concrete cracking*

4.4 Bond Strength

Previous studies **[76, 77]** indicated that push-out behavior primarily depends on the imperfection of the steel. These imperfections are the roughness of the inside surface, the shape, and size of cross section of the steel hollow section. In the codes of practices **(Eurocode4, 1994; ACI318-08) [5, 51]** the value of bond strength in concrete filled steel tube section is recommended as 0.4 MPa, however, this bond strength is based on normal strength concrete as a filler material. When one used high strength concrete as a filler material, bond strength decreased significantly and become almost 0.2 MPa **[77, 23]**. The reason may be that the presence of higher cement content present in higher strength concrete causes high shrinkage **[78]**.

4.5 Bond Modeling

A full bond is often assumed in the design of concrete filled steel tubular section for the simplification of analysis **[23]**.

In ANSYS package a special technique is adopted, the solution begins with equal values of normal stiffness KN, for positive and negative regions. The solution is repeated with different values of normal stiffness KN, according to the regions of positive and negative uplift. This procedure is continued until convergence in the length of the regions in the negative and positive uplift is achieved.

In the present study, three types of interface elements are used to represent bond zone as following:

4.5.1- COMBIN39

Nonlinear spring (see element description in chapter three) was used to model bond zone. This element was connected node to node between the steel and concrete, and the length (as used) of the nonlinear spring element is 0.2 mm.

Nonlinear spring allows for multi-linear element stiffness, this stiffness can be generated by force displacement curve which is the input of nonlinear spring element. This force-displacement curve is obtained from load-slip curve from push-out test of concrete filled steel tubes.

The initial bond stiffness was determined from the results of push-out tests. This bond model is applied throughout the contact surface between steel and concrete. This approaches that is used for the simplification of the

modeling is questionable due to the fact that the bond may be different in the compressive zone compared to tensile zone of flexural member. Bond modeling at the interface in two shearing directions is assumed as mentioned above. The stiffness of nonlinear spring in the normal direction was calculated from the stiffness of concrete which is the weaker of the two materials (steel and concrete) in the composite section **[23]**, and the stiffness was derived from the crushing strength and shortening value of concrete.

4.5.2 CONTAC52

The geometry, node locations, and the coordinate system for this element are shown in Figure 3.17. The element is defined by two nodes, two stiffnesses (KN and KS), an initial gap or interference, and an initial element status. The stiffnesses of contact element, 1- KN taken from the weaker of two materials (concrete normally) 2- KS is the slope of load-slip curve obtained from push-out test. The interface is assumed to be perpendicular to the I-J line or to the specified gap direction. The element coordinate system has its origin at node I and the x-axis is directed toward node J or in the user-specified gap direction. The interface is parallel to the element y-z plane.

The normal stiffness, KN, should be based upon the stiffness of the surfaces in contact. In some cases (such as initial interference analyses, non convergence, or over penetration), it may be useful to change the KN value between load steps or in a restart in order to obtain an accurate, converged solution. The sticking stiffness, KS, represents the stiffness in the tangential direction when elastic Coulomb friction is selected ($\mu > 0.0$ and). The coefficient of friction μ is input as material property MU and is evaluated at the average of the two node temperatures. Stiffnesses may also be computed

from the maximum expected force divided by the maximum allowable surface displacement. KS defaults to KN.

One can specify the gap direction by means of real constants NX, NY, and NZ (the global Cartesian X, Y, and Z components of the gap direction vector). If the gap direction is not specified, the program will calculate the direction based on the initial positions of the I and J nodes, such that a positive normal displacement (in the element coordinate system) of node J relative to node I tends to open the gap. One should always specify the gap direction if nodes I and J have the same initial coordinates, if the model has an initial interference condition in which the underlying elements' geometry overlaps, or if the initial open gap distance is very small. If the gap is initially geometrically opened, the correct normal (NX, NY, NZ) usually points from node I toward node J **[14]**.

The only material property used is the interface coefficient of friction μ. A zero value should be used for frictionless surfaces. Temperatures may be specified at the element nodes (for material property evaluation only). The node I temperature T(I) defaults to TUNIF. The node J temperature defaults to T(I).

The force deflection relationships for the interface element can be separated into the normal and tangential (sliding) directions. The element condition at the beginning of the first substep is determined from the START parameter. If the interface is closed and sticking, KN is used in the gap resistance and KS is used for sticking resistance. If the interface is closed but sliding, KN is used in the gap resistance and the constant friction force μFN is used for the sliding resistance.

In the normal direction, when the normal force (FN) is negative, the interface remains in contact and responds as a linear spring. As the normal force becomes positive, contact is broken and no force is transmitted.

CONTAC52 can be used to specify a "weak spring" across an open interface, which is useful for preventing rigid body motion that could occur in a static analysis. The weak spring stiffness is computed by multiplying the normal stiffness KN by a reduction factor. The default reduction factor of 1E-6 can be overridden with real constant.

In the tangential direction, for FN < 0 and the absolute value of the tangential force (FS) less than μ|FN|, the interface sticks and responds as a linear spring. For FN < 0 and FS = μ|FN|, sliding occurs. If contact is broken, FS = 0.

CONTAC52 offer only the pure penalty method (see Appendix A), in which one must specify the contact stiffness. The normal stiffness KN should be based upon the stiffness of the surface in contact.

4.5.3 CONTA173

Surface to surface contact element geometry is shown in ***Figure3.20.*** The element was needed to:

4.5.3.1 Selecting a Contact Algorithm

ANSYS **[14]** offers several different contact algorithms: (see Appendix A)

The augmented Lagrangian method (which is the default) is an iterative series of penalty methods. The contact tractions (pressure and frictional stresses) are augmented during equilibrium iterations so that the final penetration is smaller than the allowable tolerance. Compared to the

penalty method, the augmented Lagrangian method usually leads to better conditioning and is less sensitive to the magnitude of the contact stiffness. However, in some analyses, the augmented Lagrangian method may require additional iterations, especially if the deformed mesh becomes too distorted. The pure Lagrange multiplier method enforces zero penetration when contact is closed and “zero slip” when sticking contact occurs. The pure Lagrange multiplier method does not require contact stiffness, FKN and FKS. Instead it requires chattering control parameters, FTOLN and TNOP. This method adds contact traction to the model as additional degrees of freedom and requires additional iterations to stabilize contact conditions. It often increases the computational cost compared to the augmented Lagrangian method. An alternative algorithm is the Lagrange multiplier method applied on the contact normal and the penalty method (tangential contact stiffness) on the frictional plane. These methods enforce zero penetration and allow a small amount of slip for the sticking contact condition. It requires chattering control parameters, FTOLN and TNOP.

The Lagrange multiplier also introduces more degrees of freedom which may result in spurious modes for modal and linear eigen value buckling analyses. The augmented Lagrangian method would be a better choice for these analysis types.

4.5.3.2. Determining Contact Stiffness

For the augmented Lagrangian method and penalty method, normal and tangential contact stiffnesses are required. The amount of penetration between contact and target surfaces depends on the normal stiffness. The amount of slip in sticking contact depends on the tangential stiffness. Higher stiffness values decrease the amount of penetration/slip, but can lead to ill-

conditioning of the global stiffness matrix and to convergence difficulties. Lower stiffness values can lead to a certain amount of penetration/slip and produce an inaccurate solution. Ideally, one wants a high enough stiffness that the penetration/slip is acceptably small, but a low enough stiffness that the problem will be well-behaved in terms of convergence.

Set the Real Constants and Element KEYOPTS ANSYS provides default values for contact stiffnesses (FKN, FKT), allowable penetration (FTOLN), and allowable slip (SLTO). In most cases, one does not need to define the contact stiffness.

4.5.3.2.1 Using FKN and FTOLN

For certain contact problems, one may choose to use the real constant FKN to define a normal contact stiffness factor. The usual factor range is from 0.01-1.0, with a default of 1.0. The default value is appropriate for bulk deformation. If bending deformation dominates, It is recommend to use a smaller value (0.1). In cases where the underlying element has a **TB** plasticity material defined (whether plasticity is active or not), the contact normal stiffness will be reduced by a factor of 100. Use real constant FTOLN in conjunction with the augmented Lagrangian method. FTOLN is a tolerance factor to be applied in the direction of the surface normal. The range for this factor is less than 1.0 (usually less than 0.2), with a default of 0.1, and is based on the depth of the underlying solid, shell, or beam element . This factor is used to determine if penetration compatibility is satisfied.

4.5.3.2.2 Using FKT and SLTO

ANSYS automatically defines a default tangential contact stiffness that is proportional to MU and the normal stiffness FKN. The default tangential

stiffness corresponds to a default value of FKT = 1.0. A positive value for FKT is a factor; a negative value indicates an absolute value of tangential stiffness. ANSYS updates tangential contact stiffness based on current contact normal pressure, PRES, and maximum allowable elastic slip, SLTO (FKT = MU* PRES/SLTO). The real constant SLTO is used to control maximum sliding distance when FKT is updated at each iteration. ANSYS provides default tolerance values which work well in most cases. one can override the default values for SLTO (1% of average contact length in pair) by defining a scaling factor (positive value when using command input) or an absolute value (negative value when using command input). A larger value will enhance convergence but compromise accuracy. Based on the tolerance, current normal pressure, and friction coefficient, the tangential contact stiffness FKT can be obtained automatically. In certain cases users can override FKT by defining a scaling factor (positive input value) or absolute value (negative input value) .

4.6 Friction model

In the basic Coulomb friction model, two contacting surfaces can carry shear stresses up to a certain magnitude across their interface before they start sliding relative to each other **[14]**. This state is known as sticking. Coulomb friction model defines an equivalent shear stress τ , at which sliding on the surface begins as a fraction of the contact pressure p ($\tau = \mu p + COHE$, where μ is the friction coefficient and $COHE$ specifies the cohesion of sliding resistance). Once the shear stress is exceeded, the two surfaces will slide relative to each other. This state is known as sliding. The sticking/sliding calculations determine a point of transition from sticking to sliding or vice versa.

For frictionless, rough, and bonded contact, the contact element stiffness matrices are symmetric. Contact problems involving friction produce usually unsymmetric stiffness. Using an unsymmetric solver is more computationally expensive than a symmetric solver for each iteration. For this reason, ANSYS uses a symmetrization algorithm by which most frictional contact problems can be solved by using solvers for symmetric systems. If frictional stresses have a substantial influence on the overall displacement field and the magnitude of the frictional stresses is highly solution dependent, the symmetric approximation to the stiffness matrix may provide a low rate of convergence. In such cases, the unsymmetric solution option is chosen to improve convergence **[14]**.

One of the material properties used for contact elements is input via the interface coefficient of friction, μ, for the Coulomb friction model. $\mu = 0$ is used for frictionless contact. For rough or bonded contact, ANSYS assumes infinite frictional resistance regardless of specified value of μ, μ can be specified as a function of temperature in certain cases. If the underlying element is a super element, the material property must be the same as the one used for the original elements that were assembled into the super element.

ANSYS provides one extension of classical Coulomb friction: TAUMAX is maximum contact friction with units of stress. This maximum contact friction stress can be introduced so that, regardless of the magnitude of normal contact pressure, sliding will occur if the friction stress reaches this value. TAUMAX is typically used when the contact pressure becomes very large (such as in bulk metal forming processes). TAUMAX defaults to 1.0E20. Empirical data is often the best source for TAUMAX. Its value may

be close to $\frac{\sigma_y}{\sqrt{3}}$, where σ_y is the yield stress of the material being deformed.

TAUMAX (N/mm^2) = $\frac{f_c'}{\sqrt{3}}$ is used in this study

Another real constant used for the friction law is the cohesion, COHE (default COHE = 0, adopted in this study), has units of stress. It provides sliding resistance, even with zero normal pressure; this is shown in ***Figure 4.6***

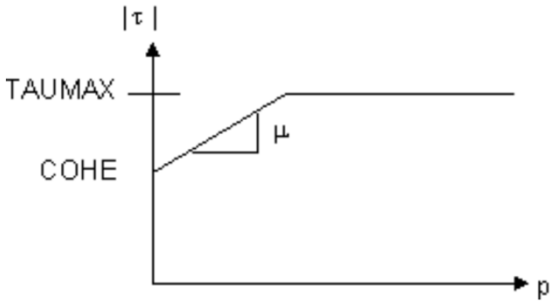

FIGURE 4.6 Sliding contact resistance **[14]**.

CHAPTER FIVE

APPLICATIONS AND DISCUSSION

5.1. Introduction

The main purpose of this chapter is to study the validity, accuracy, and efficiency of computational model developed by using the ANSYS software, and the second purpose is discussion of the results obtained by analysis.

In this chapter many examples are explained about composite members. The results (except example 5) are compared with those from experimental study. Only the first example is used to check the validity of the model and to select elements types used in the model.

No available experimental data for studying the behavior of composite frame composed of composite members. Therefore; composite columns and beams are used to study the validity of the model.

5.2. Example 1: Concrete Filled Steel Tube Beam

(Koushik Brahmachari in 1997) **[23]** Presented experimental study for hollow steel section filled with high strength concrete.

5.2.1. Model Geometry, Loading, and Boundary Condition

The **Figure 5.1** shows the details of beam geometry. The composite beam depth (150mm), width (100mm), thickness of steel tube (4mm), and span between supports (2750mm).A simply supported beam set up is adopted with a hinge and a roller at each ends. Load is applied on the top surface of beam at the mid span. Material properties of beam are given in ***table 5.1***

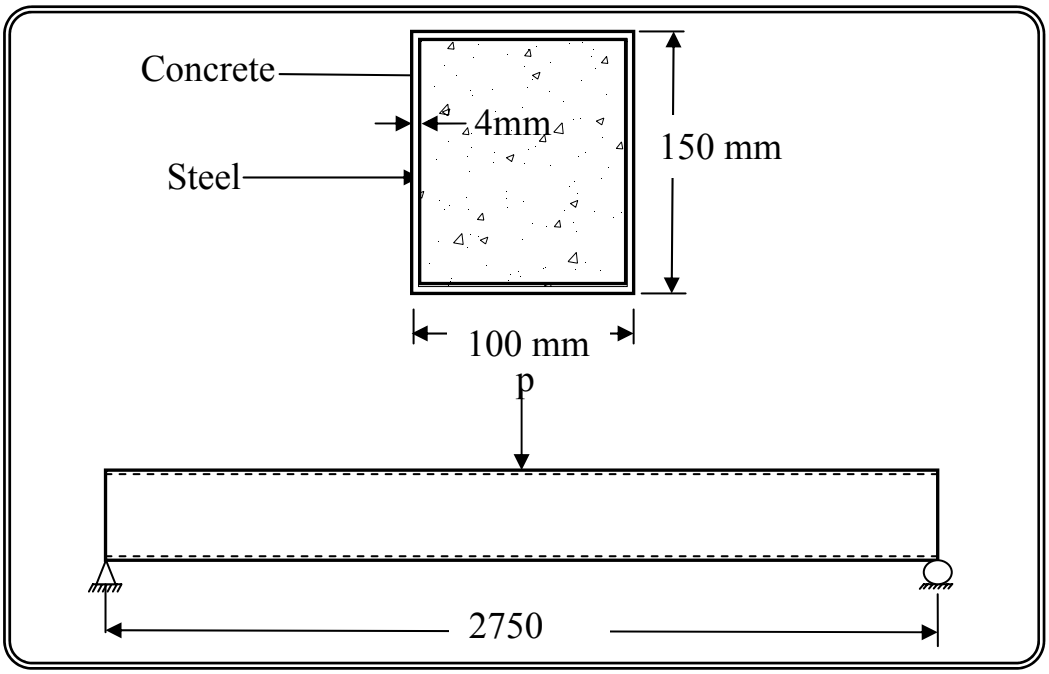

Figure 5.1 *simply support composite beam*

Table 5.1 *material properties*

Concrete		Steel	
Young's modulus, *Ec* (MPa)	45690	Young's modulus, (MPa) E_s	200000*
Compressive strength, *fć*(MPa)	94.5*	Yield stress(MPa) *fy*	434*
Tensile strength, f_t (MPa)	4*	Poisson's ratio, ν	0.3
Poisson's ratio, ν	0.2		
f_{cb} (MPa)	113.4		
f_1 (MPa)	137		
f_2 (MPa)	163		
σ_h^a (MPa)	148.4		
β_o	0.2		
β_c	0.99		

* According to experimental data **[23]**

5.2.2. Finite Element Idealization

In the present study, brick element 8-node (SOLID65) is used to represented concrete core, brick element 8-node (SOLID45) or 4-nodes shell element (SHELL43) in other case are used in representation of steel tube, and contact element (one of three elements COMBIN39, CONTAC52 or CONTA173 as shown later in this chapter).

The finite element analysis has been carried out in general using 8-point (2 x 2 x 2) integration rule for the reinforced concrete brick elements and 4-point (2 x 2) integration rule for the steel shell elements and for the interface elements, with a convergence tolerance of 0.1%. The full Newton-Raphson method has been adopted in the analysis; all mesh details are shown in ***Figure 5.2,***

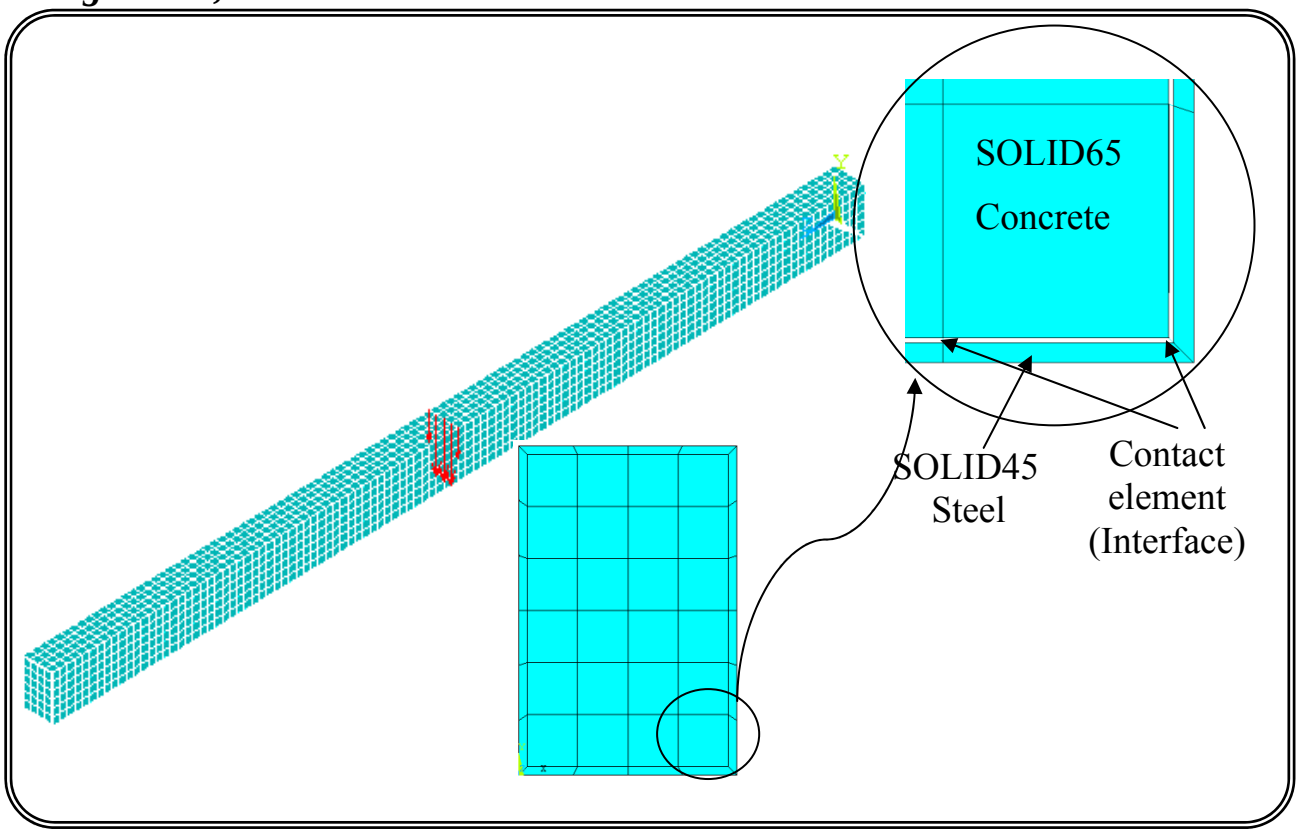

Figure5.2. *Finite element idealization of composite beam*

Load slip curve as obtained by push-out test (Koushik Brahmachari in1997) gives slip (2mm) at force (5 kN), slip (3.3 mm) at force (10 kN),slip (5 mm) at force (12.5 kN) ,and slip (25mm) at force (14.5 kN).

5.2.3. Factors Affecting Model Choice

In order to choose the best model and to get the best agreement between experimental and numerical model, many factors which affect the model are taken into consideration and the best model is adopted as following:

5.2.3.1. Effect of Number of Elements (Mesh Size)

In order to investigate the effect of number of elements for concrete filled steel tube beam, four meshes size adopted as following

Mesh a: total number of elements =1440

Mesh b: total number of elements=3864

Mesh c: total number of elements=7060

Mesh d: total number of elements=20021

Effect of the number of elements on the load-deflection response and ultimate load of the concrete filled steel tube beam are shown in the ***Figure 5.4.*** While the all mesh cases give good agreement with experimental work, Mesh d give the best agreement, but with little difference from Mesh c and more analyzed time, therefore Mesh c has been used in the present study. ***Figure 5.3*** show detail of mesh size for four cases

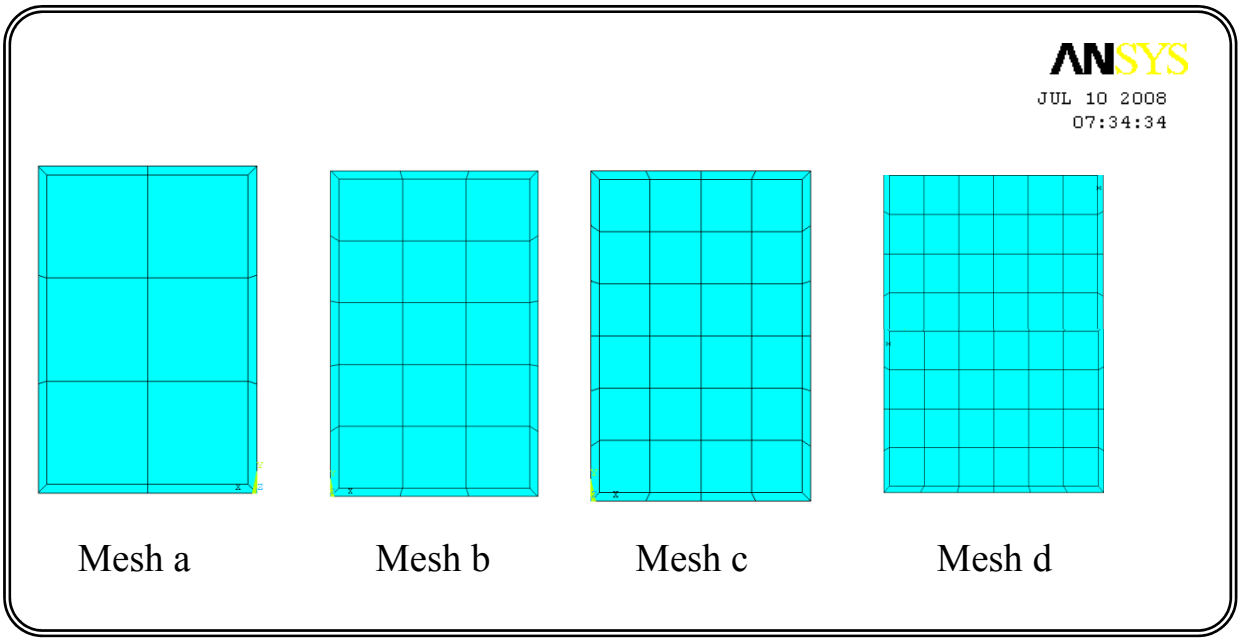

Figure 5.3 *Mesh size detail of composite beam*

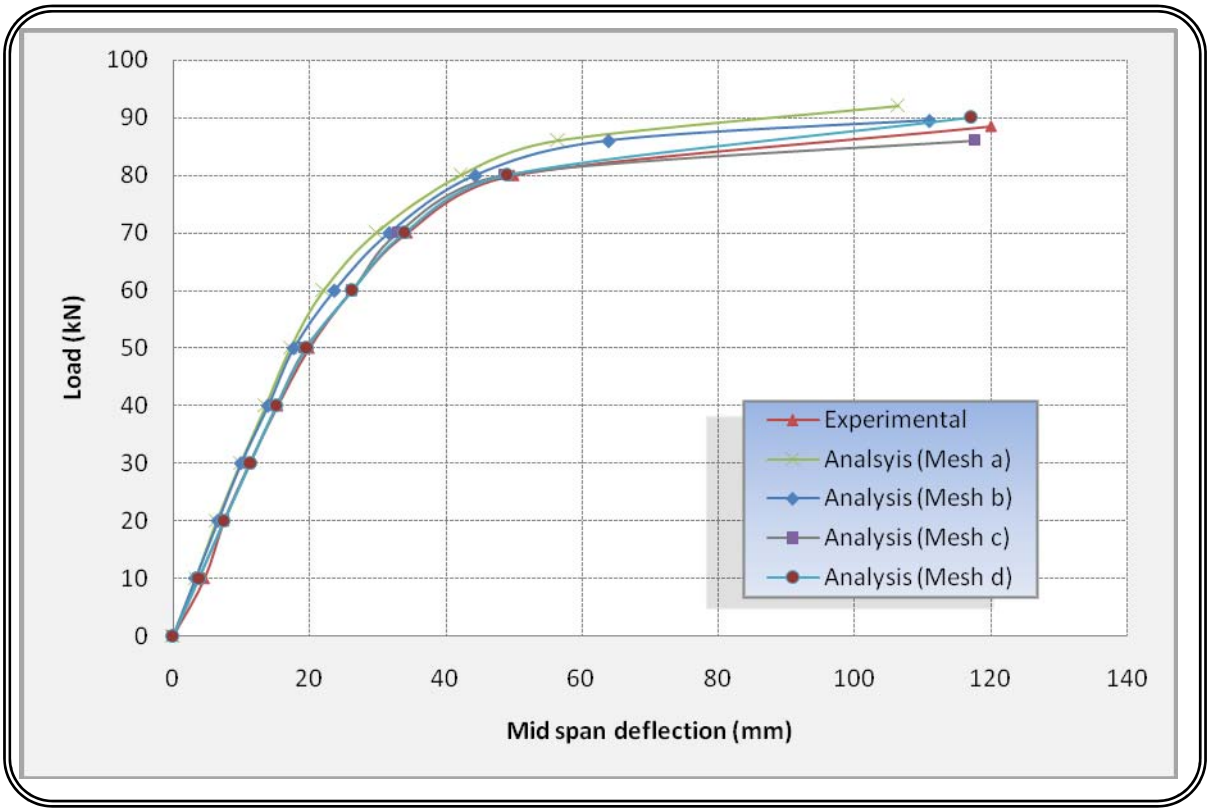

Figure 5.4 *effect of number of elements on composite beam.*

5.2.3.2. Effect of Contact Element

In the present study three types of contact element are tested and results are compared with experimental (tested by **[23]**) as in Figure 5.4. The contact elements which are tested are: nonlinear spring element (COMBIN39), contact element node to node (CONTAC52), and contact element surface to surface (CONTA173). From ***Figure 5.5*** CONTAC52 gives good agreement with experimental result more than other elements. The percentage difference is less than 2% with CONTAC52 and 8% to 10% with CONTA173 and COMBIN39 respectively. So CONTAC52 (node to node element) is adopted for all considered cases. This is because the (CONTAC52) is initially defined by two parameters normal and sticking stiffness, after first load step these parameters were updated depending on stiffness of contact materials. This property led to that CONTAC52 give better results from other contact elements type. On the other hand, (CONTA173) gave more error because this element is automatically defined all parameters and this make that the user can not able to change the stiffness of this element according to experimental data. Finally COMBIN39 was nonlinear spring and has constant stiffness value input by user and can not vary to the last load step and COMBIN39 is non-zero length element and represented it needs gap between steel and concrete. In CONTAC52 the value of stiffness was applied to resist tension force only but in flexural member (as the example) the top mid-span region was under compressive force. In such regions, concrete core is separated from steel tube.

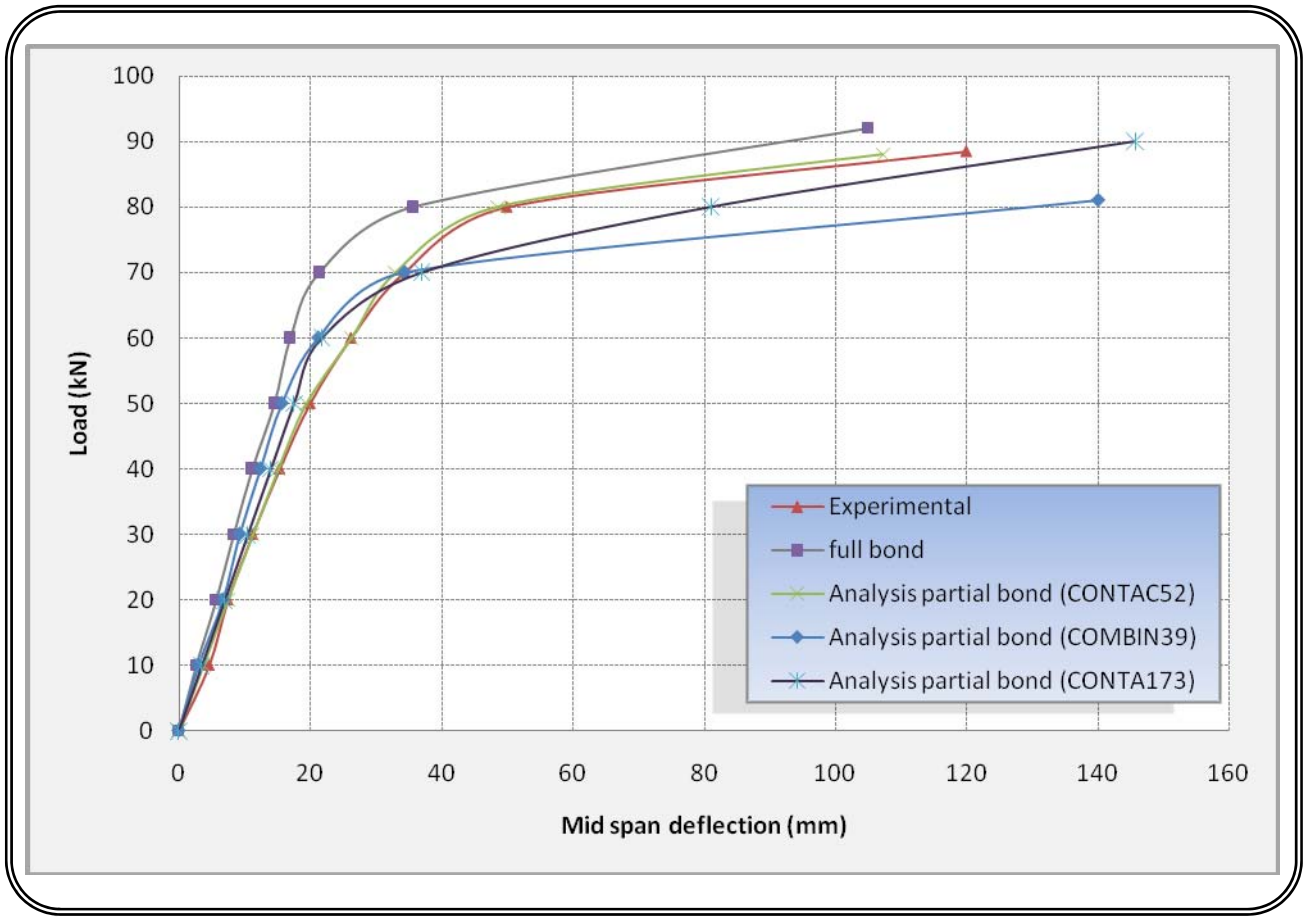

Figure 5.5 *effects of contact elements on load deflection response composite beam.*

5.2.3.3. Effect of Steel Representation

In the present study, two types of elements are tested to represent steel tube. The first one is 8-node brick element (SOLID45) and the other one is 4-node shell element (SHELL43). All details about beam models are shown in ***Table 5.2.*** (SOLID45) gave best agreement with experimental study (error 2%) while the error is 11% when using (SHELL43) as shown in ***Figure 5.6.***

Table 5.2 *composite beam models*

Case	Concrete element	Steel element	Bond case
Case a	SOILD65	SOLID45	Full bond
Case b	SOILD65	SOLID45	Partial bond
Case c	SOILD65	SHELL43	Full bond
Case d	SOILD65	SHELL43	Partial bond

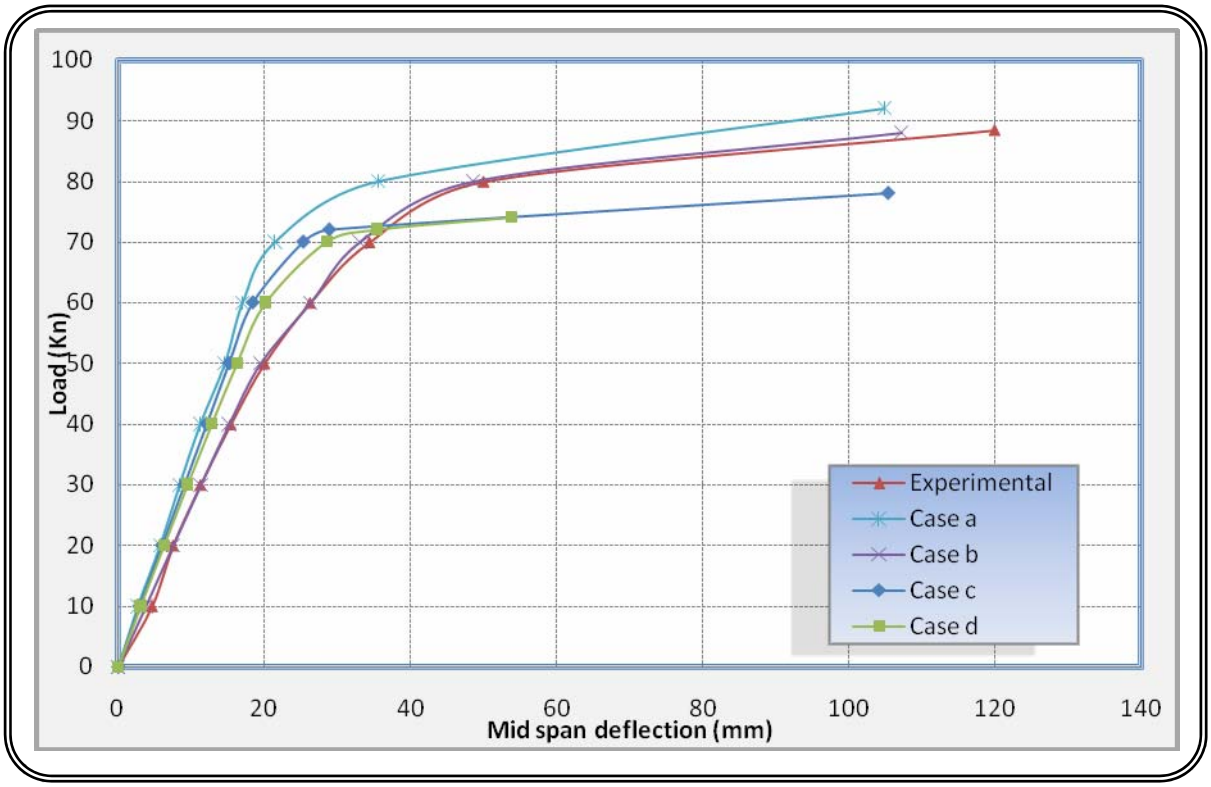

Figure 5.6 *effect of steel representation on composite beam*

Figure 5.6.show the comparison between SOLID45 and SHELL43 in represented steel tube. SOLID45 gave better agreement with experimental results because the element SOLID45 in analysis will not suffer from volumetric locking which can be caused by plasticity, as in SHELL43.

5.2.4 The adopted Model:

From the previous section (section 5.2.3) the model used in all other examples is given as follows:

SOLID65 for concrete core

SOILD45 for steel tube

CONTAC52 for interface model

Mesh a (total number of elements 7060 and side length of brick element 25 mm).

Figure 5.7 shows the load-deflection curve of composite beam by using full bond and partial bond analysis compared with experimental test.

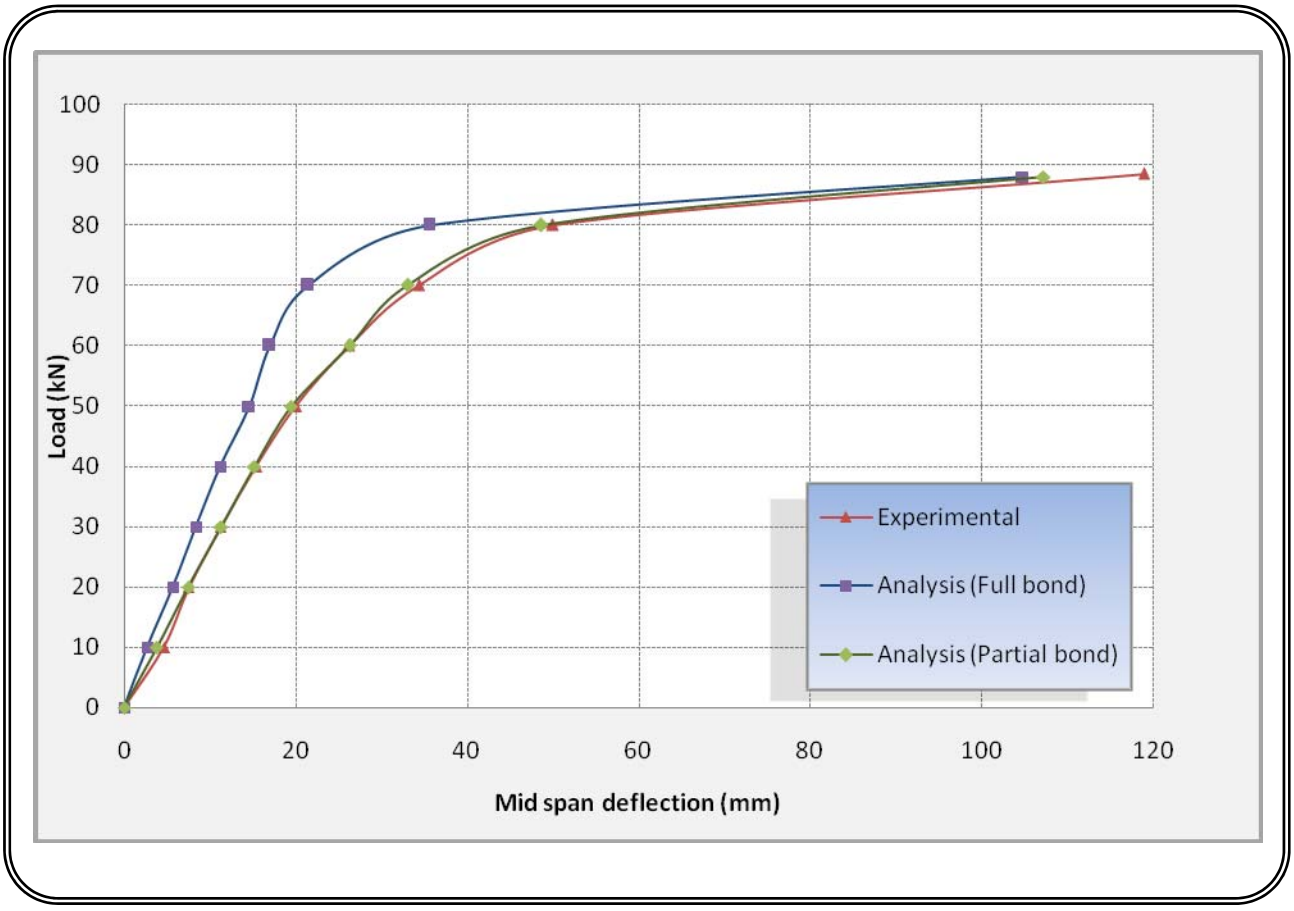

Figure 5.7 *load-deflection curves on composite beam*

5.3. Example 2: Concrete Filled Steel Tube Beams

A total of 5 concrete filled steel SHS (Square Hollow Section) and RHS (Rectangular Hollow Section) beam specimens were tested by (Han, 2004) **[35]**. In present example normal strength concrete was used and steel tubes were manufactured from mild steel sheet.

5.3.1. Model Geometry, Loading, and Boundary Condition

A summary of the specimens is presented in ***table 5.3***.where the section sizes and materials properties are given **[35]**. The specimens are designed with a wide range of width-to-depth ratio (from 1 to 2). The tube depth to wall thickness ratio is ranged from 30 to 50. All the specimens are 1100 mm in length. A four point bending rig is used to apply moment ***Figure 5.8a***. The in plane displacements are measured at location along the specimen by three displacement transducers. Eight strain gauges were used for each specimen to measure stains at the mid span. ***Figure 5.8b*** gives a general view of the test setup.

A load interval of less than one-tenth of the estimated load capacity was used; each load interval was maintained for about 2-3 minutes. At each load increment, the strain reading and the deflection measurements were recorded.

All dimensions and materials properties of 5 concrete filled steel tube beams are given in ***table 5.3*** as in experimental study

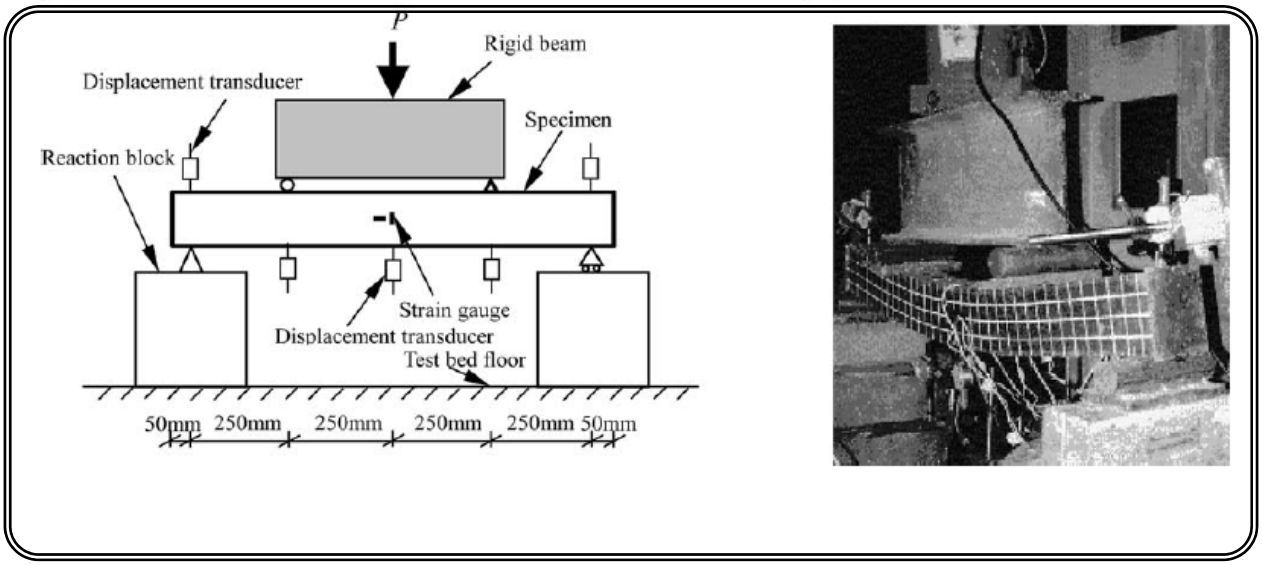

Figure 5.8 *Arrangement of beam tests*

Table 5.3 *Geometry and materials properties of composite beams*

No	Section Dimensions (mm)			(MPa)				μ concrete	μ steel
	H	B	t	f'_c	f_y	E_c	E_s		
1	120	120	3.84	21.8	330	26700	200000	0.2	0.3
2	120	120	5.86	25	321	26700	200000	0.2	0.3
3	150	120	2.93	27.6	293.8	26700	200000	0.2	0.3
4	120	90	2.93	27.6	293.8	26700	200000	0.2	0.3
5	120	60	2.93	27.6	293.8	26700	200000	0.2	0.3

The modulus of elasticity of concrete is determined from ***equation 3.3***in chapter three and other parameters are obtained from experimental data.

5.3.2 Finite Element Idealization

As in the previous example, brick element 8-nodes SOLID65 has been used to represent concrete core, brick element 8-nodes SOILD45 has been used to represent steel tube, and interface is modeled by using contact element 2-nodes CONTAC52. All details of elements that used in model explained in chapter three. The full Newton-Raphson method has been adopted in the analysis of all composite beams, and all other data used in previous example are the same used in present example. The idealization of concrete filled steel tube beam is shown in ***Figure 5.9.***

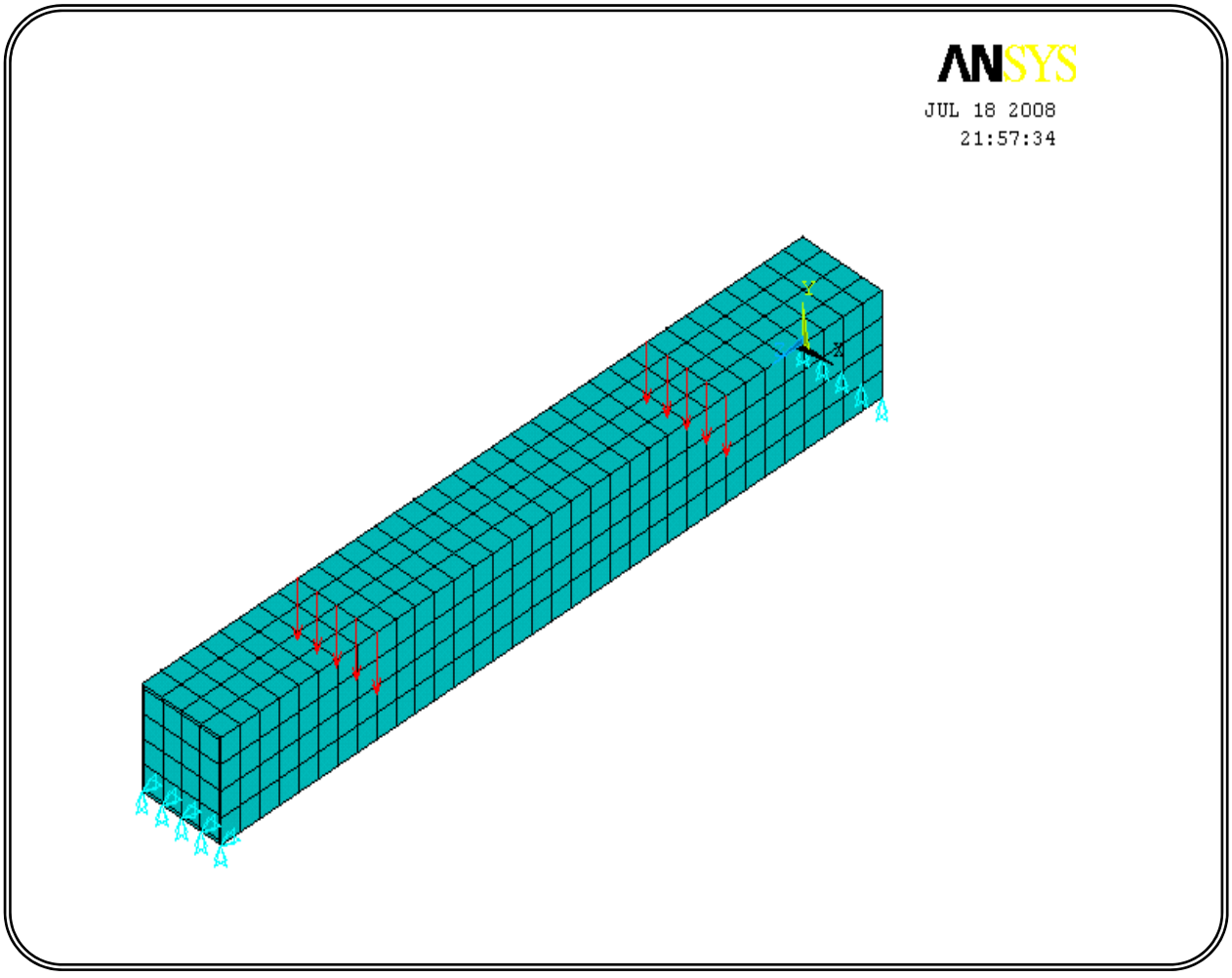

Figure 5.9 *Finite element idealization of composite beam*

5.3.3 Results of Analysis

In the present example. The load is divided into 100 load steps. All steps have the same interval. The moment plotted against deflection at mid span and results are compared with experimental study for all composite beams.

Finite element analysis with partial bond gives better agreement (more than full bond) when compared with experimental study as shown in Figures 5.10-14..

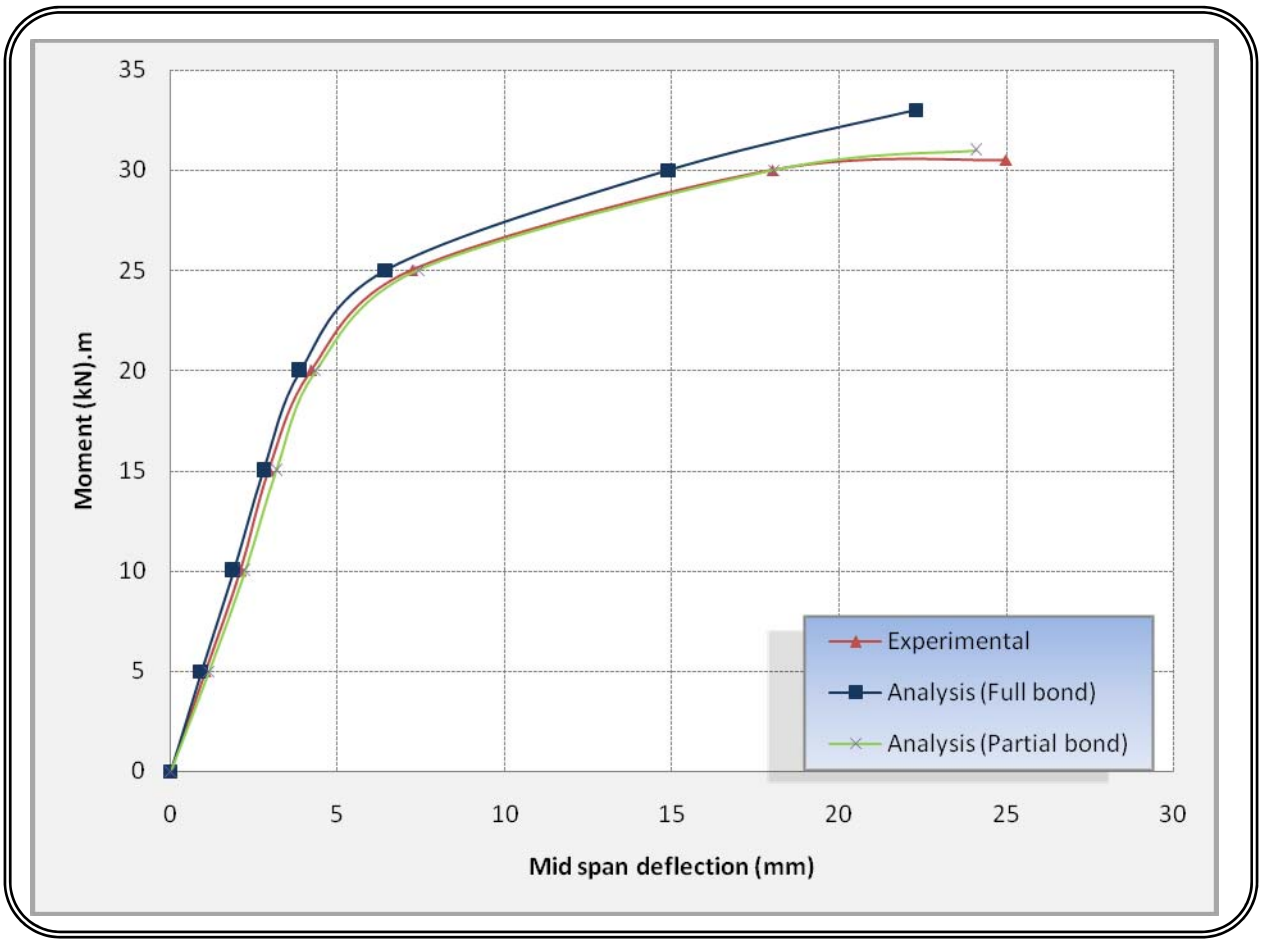

Figure 5.10 *Moment-deflection curve of composite beam 1.*

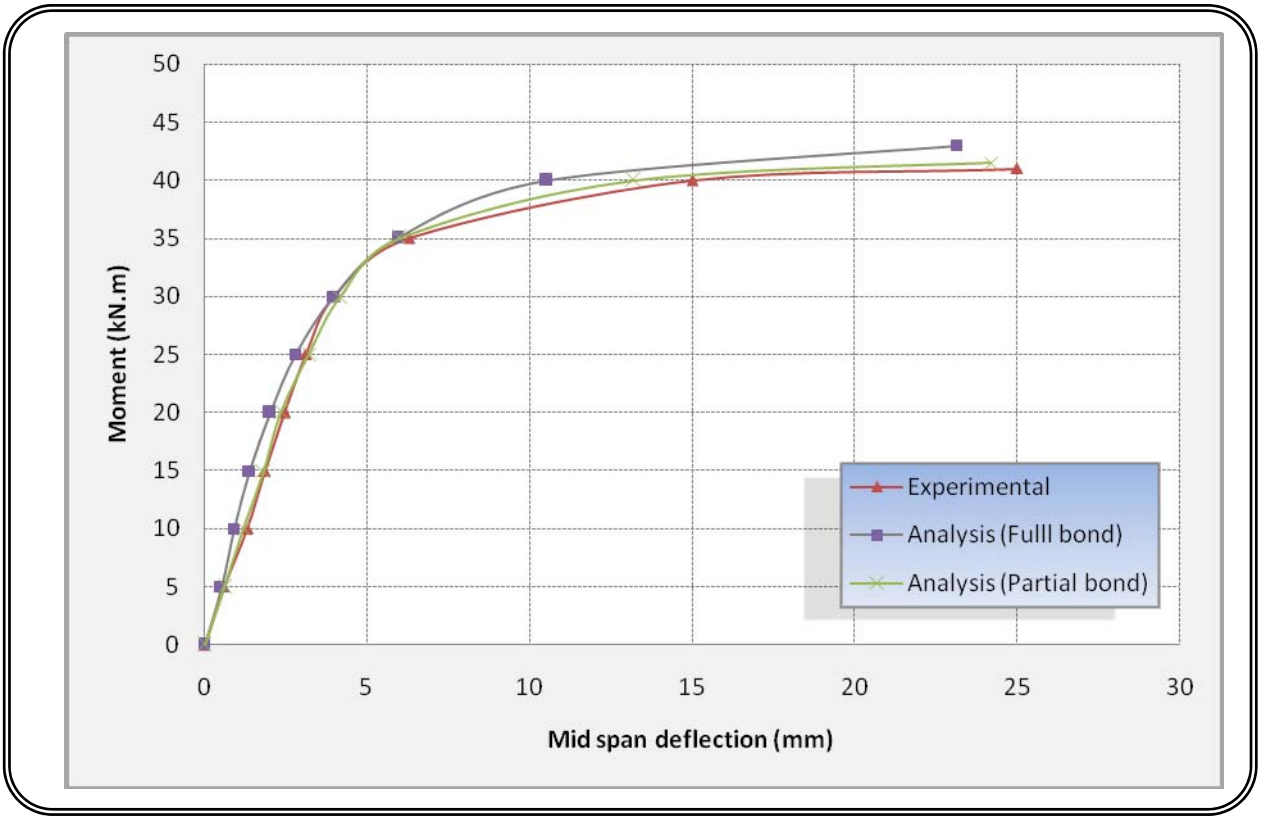

Figure 5.11 *Moment-deflection curve of composite beam 2.*

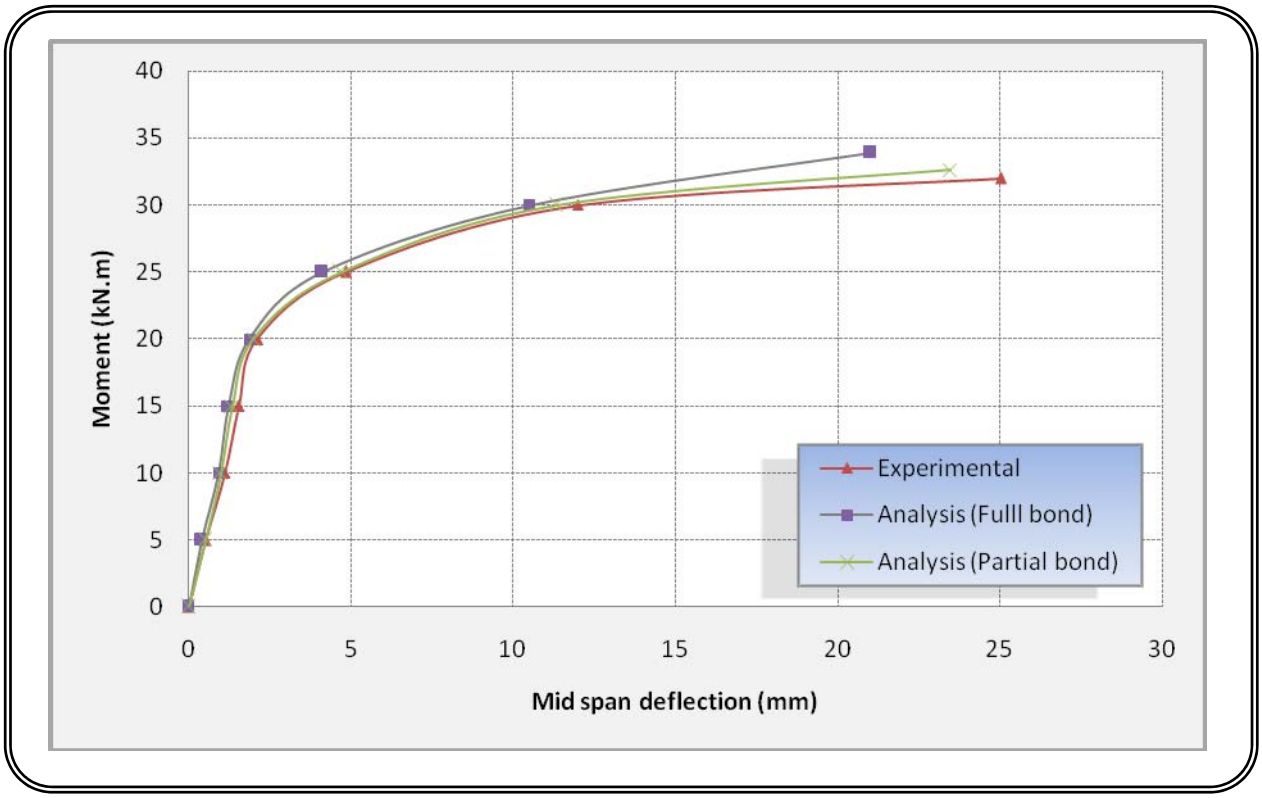

Figure 5.12 *Moment-deflection curve of composite beam 3.*

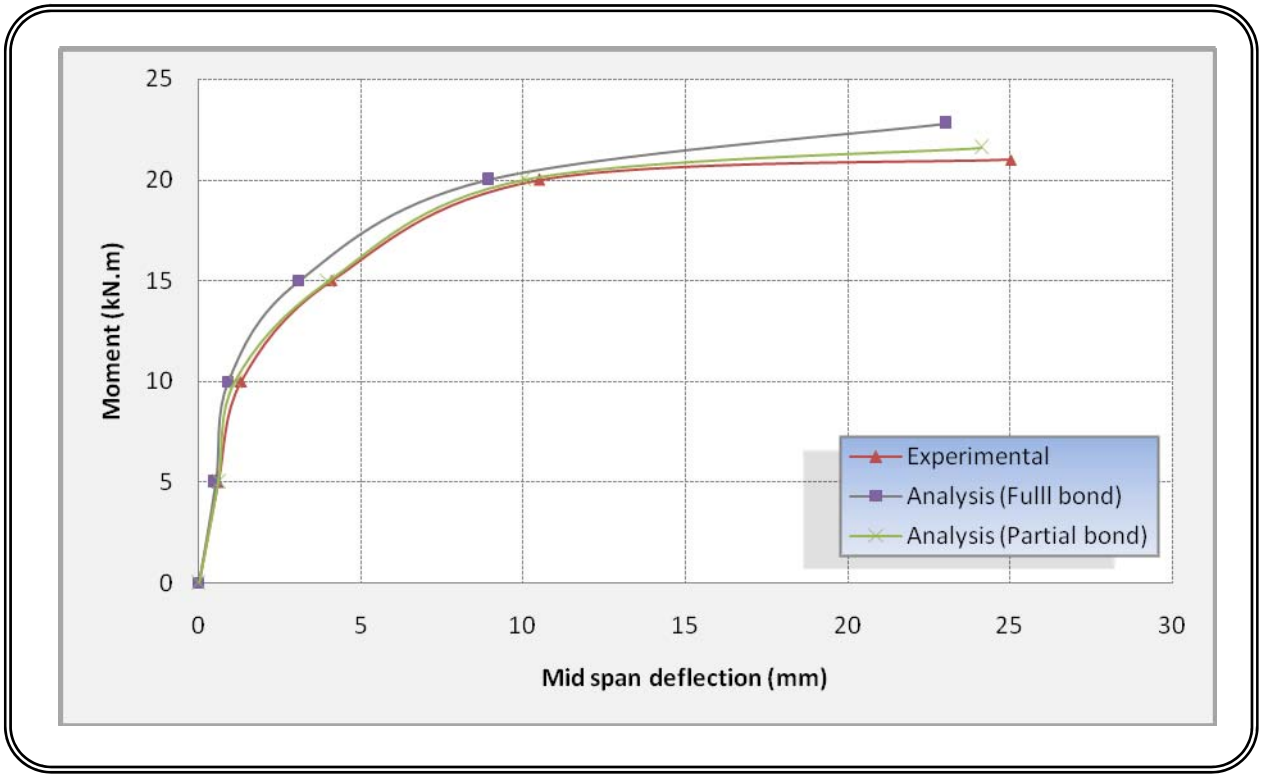

Figure 5.13 *Moment-deflection curve of composite beam 4.*

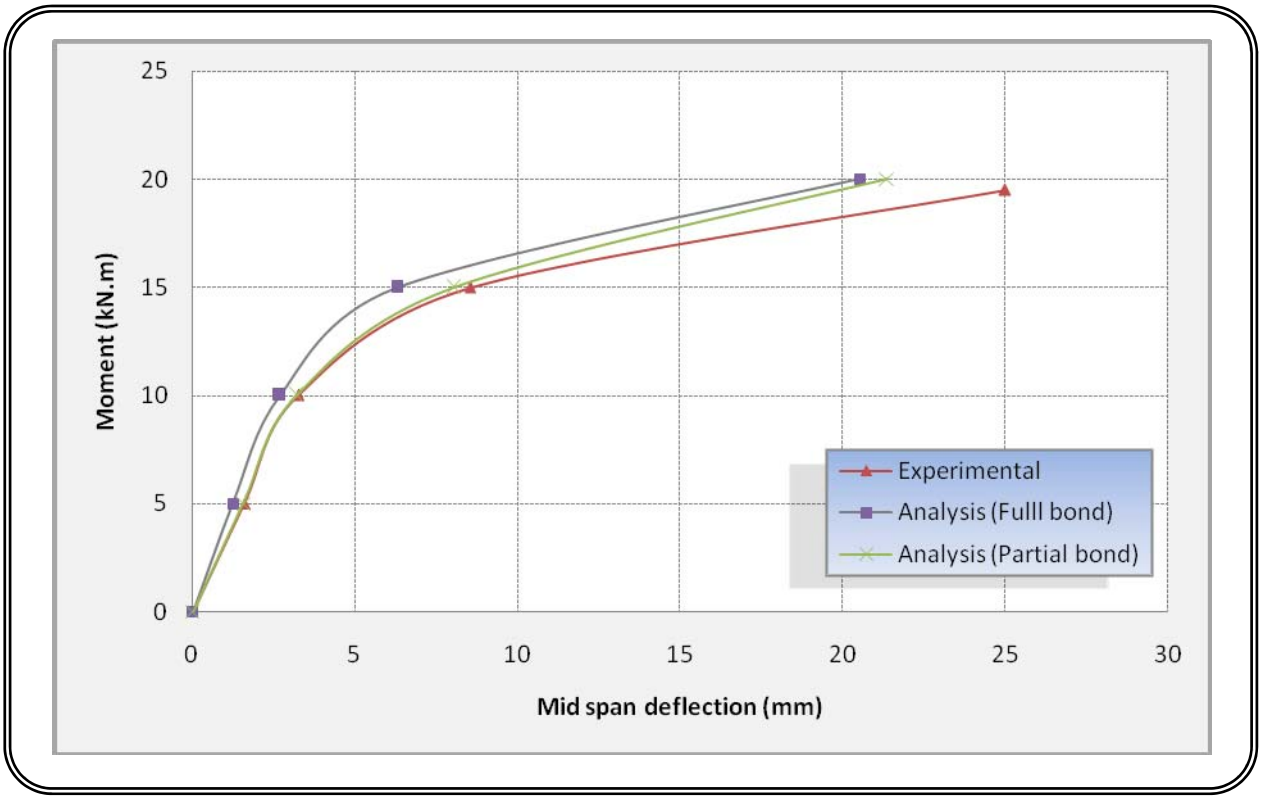

Figure 5.14 *Moment-deflection curve of composite beam 5.*

As shown in ***Figures 5.10*** and ***5.11*** the increase of ultimate moment of composite beam (beam2) is about 24% in comparison composite beam (beam1) [when the area of steel tube (of beam2) was about double the area of steel tube (for beam 1)].

Figures 5.12, 5.13, and ***5.14*** show moment - deflection curve for different cross section of steel with constant thickness of steel tube and materials properties. The decreasing of beam width for beam 4and 5 to 0.75 and 0.5 of width of beam3 respectively led to decreasing the ultimate moment of composite beam (beam4) and (beam5) to about 35% and 15% of beam3 respectively. The different value of ultimate moment decreasing is caused by increasing the confinement ratio of composite beam (beam5) because increasing depth\width ratio (D\b=2) twice depth\width ratio (D\b=1) for (beam3).

5.4. Example 3: concrete encased steel beam

In this example concrete encased steel beam that was tested by (Bahjet, 2005), **[37]**, is considered. 9 beams were tested with different dimensions and materials properties. In present study, 3 beams of them have been analyzed to compare with experimental study.

5.4.1. Model Geometry, Loading, and Boundary Condition

Table 5.4 shows the dimensions and materials properties of the specimens. Each specimen has a 3 m clear span and a rectangular section of 300×500 mm reinforced by deformed bars 19 mm (*fy* =414 MPa) in diameter deployed at four corners. Deformed bars 10 mm in diameter are used as stirrups and are all spaced every 150 mm along the span of the specimen. ***Figure 5.15***.showing cross-sections of the analyzed and tested beams.

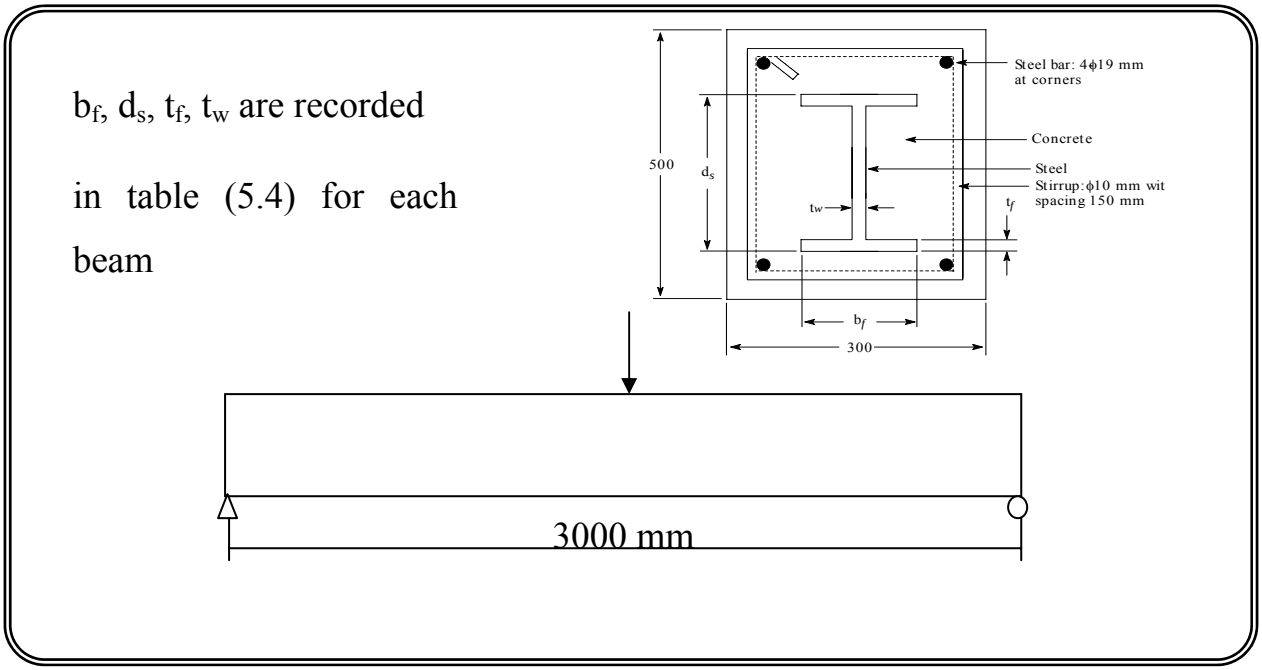

Figure5.15. *Typical composite concrete encased I-section steel beam*

Table 5.4 *Geometry and material properties of composite beams*

No	Section Dimensions (mm)				(MPa)				ν concrete	ν steel
	d_s	b_f	t_w	t_f	f'_c	f_y	E_c	E_s		
1	294	200	8	12	21.8	330	26700	200000	0.2	0.3
2	294	200	6	8	25	321	26700	200000	0.2	0.3
3	294	200	4.5	6	27.6	293.8	26700	200000	0.2	0.3

Concrete behavior used in this example is different from other examples because there is no confinement provided by steel structure as in concrete filled steel tube (in other examples). Hognestad model of uniaxial stress-strain of concrete in compression was used to represent concrete in this example, and same steel model used in all examples.

5.4.2. Finite Element Idealization

Finite element model used in this example is the same as it is used in previous examples. Steel reinforcement is represented by the same element used to represent concrete (SOLID65) by giving the volume ratio of steel to total element volume and angle of bar reinforcement to x-axis and y-axis. Brick element (SOLID65) used smeared model in representing steel reinforcement. ***Figure 5.16*** show finite element idealization of composite beam

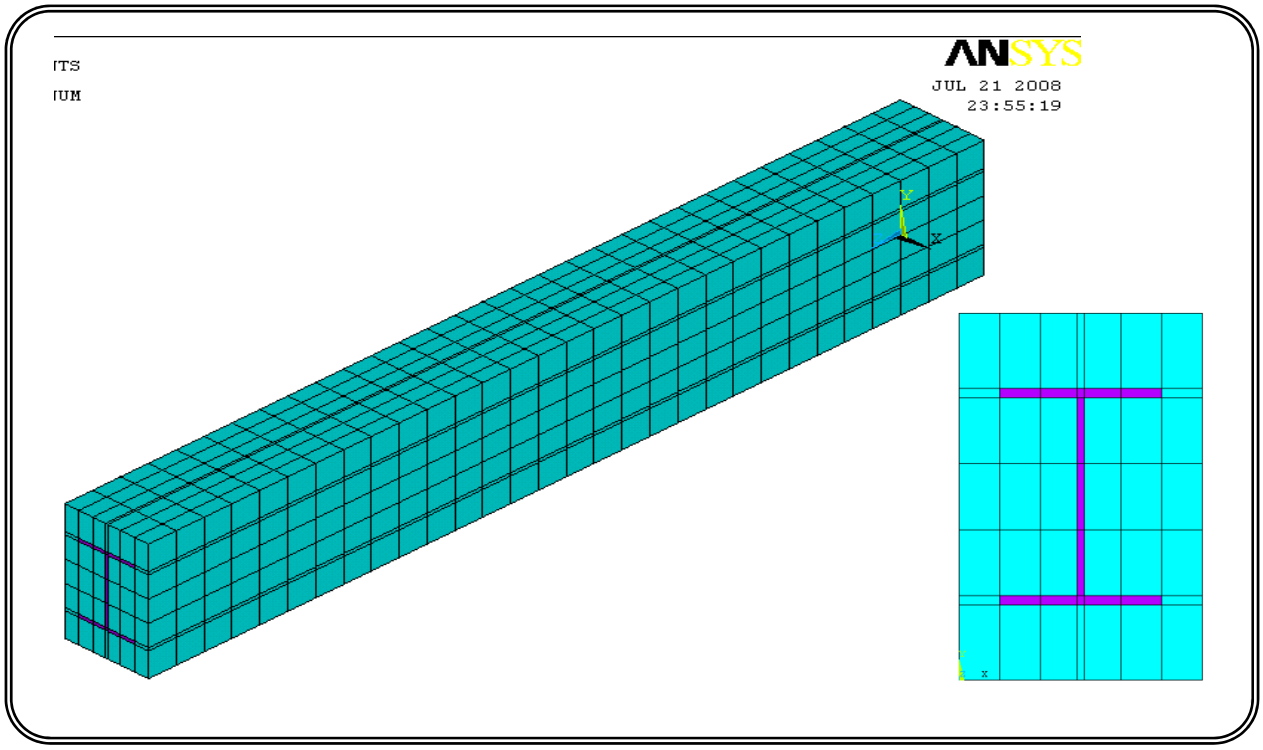

Figure 5.16 *Finite element idealization of composite beam*

5.4.3 Results of Analysis

The results of analysis of concrete encased I-steel beam show good agreement with experimental study while the difference between them is about 2-3 % for partial bond between steel and concrete and about 4-11 % for full bond analysis. All these results are shown in ***Figure 5.17, 5.18,*** and ***5.19.***

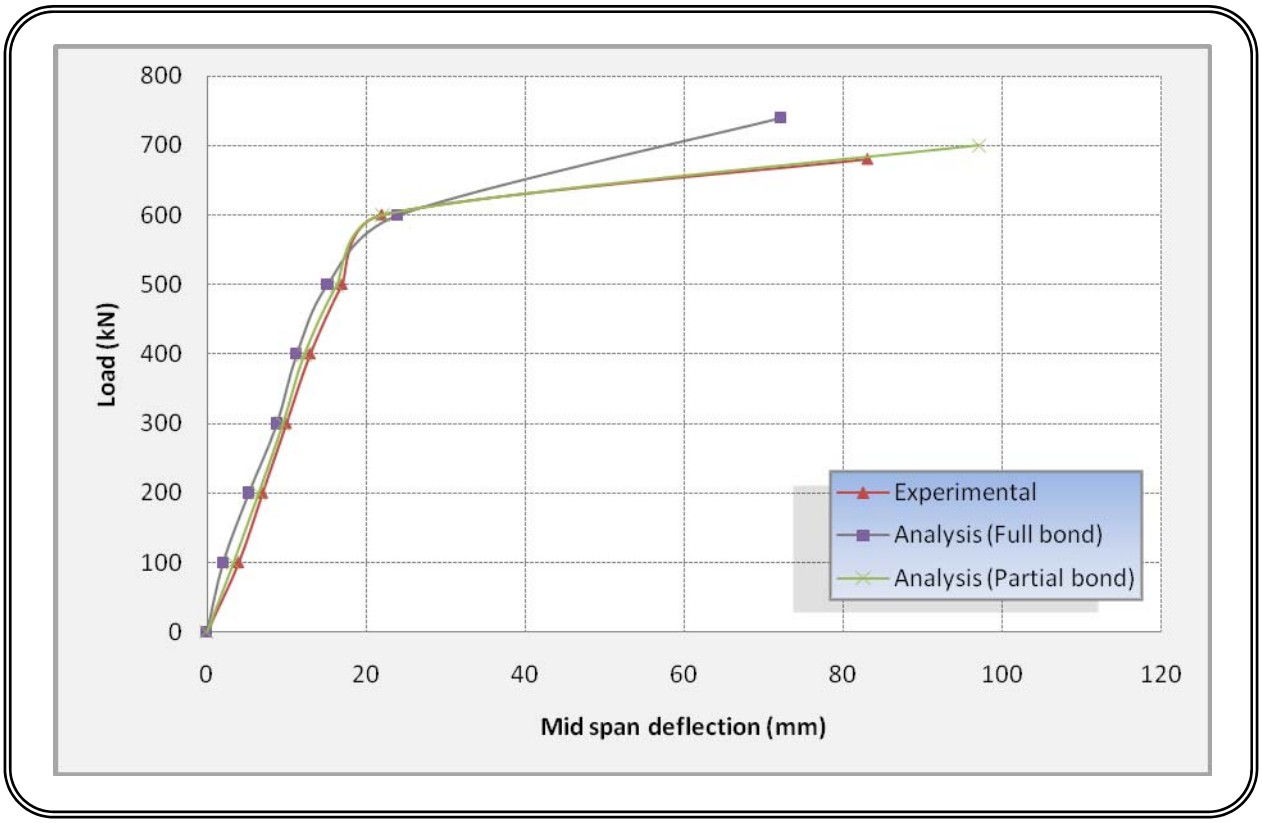

Figure 5.17 *Load-deflection curve of composite beam1.*

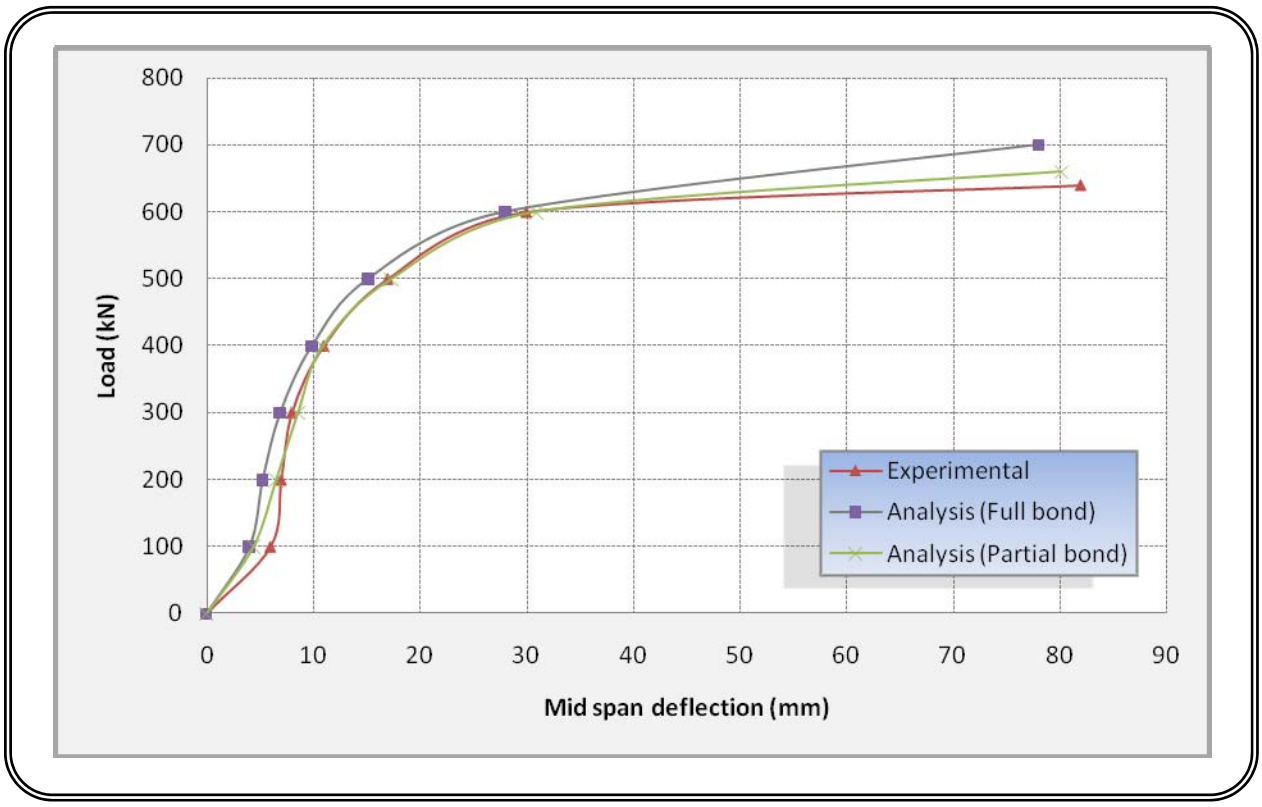

Figure 5.18 *load-deflection curve of Composite beam2.*

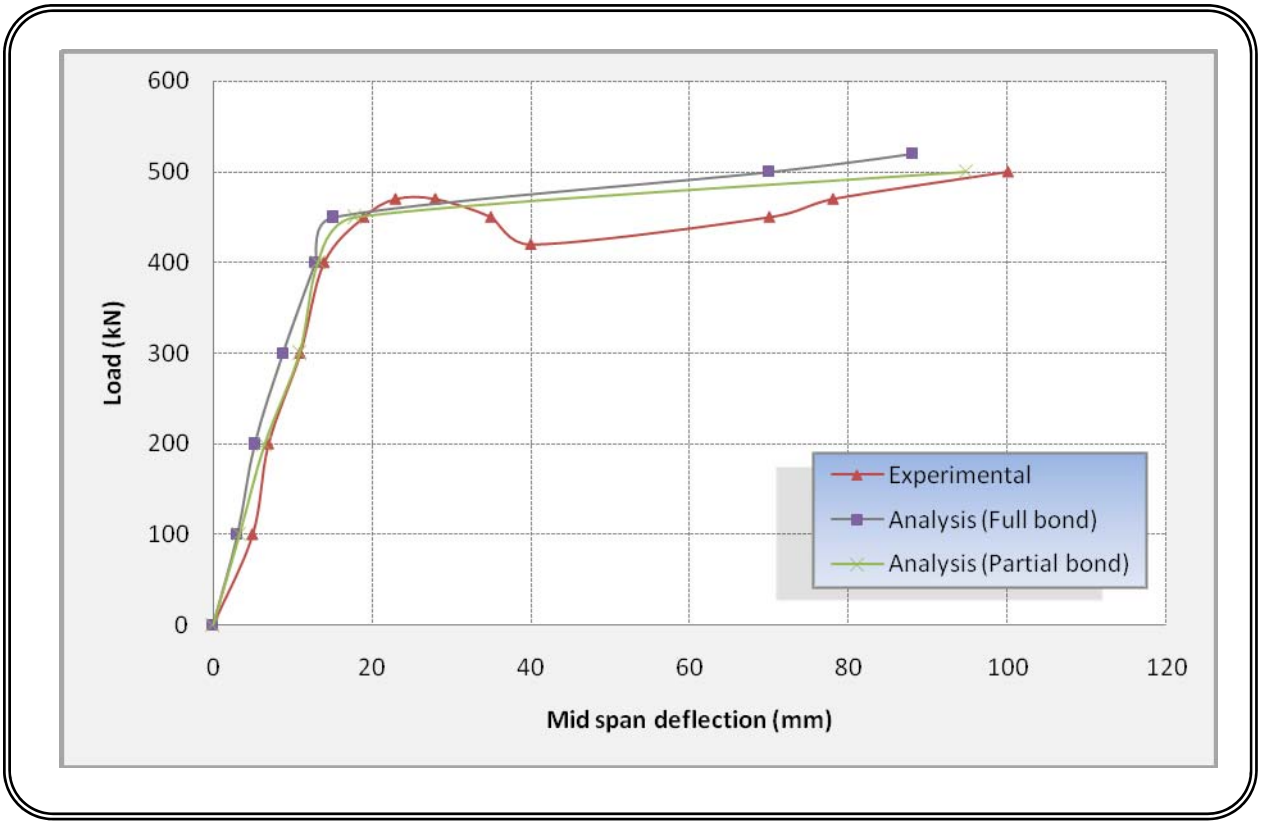

Figure 5.19 *Load-deflection curve of composite beam 3.*

As shown in ***table 5.4*** the major difference between three beams is the area of structural steel used. When the area of steel section of beam 2 was equal to 0.7 area of steel section of beam 1, the reduction in the ultimate load is only about 5%. On the other hand, in beam 3, when the area of steel structure was about half area of steel structure of beam 1, the ultimate is reduced about 25%. Form finite element analysis results, the failure in beam 1and 2 is caused by the concrete failure while in beam 3 caused by steel structure failure. This means that the ratio of steel structure to concrete must be calculated and carried out to be used in design purposes.

5.5. Example 4: Concrete Filled Steel Tube Columns

Composite concrete filled steel tubes have been used increasingly as columns in frame structures. Their worldwide use has ranged from compression members in low-rise building, using cold-formed steel circular or rectangular tubes filled with precast or cast-in-situ concrete, to large diameter cast-in-situ members used as the primary lateral-resistance columns in multi-storey frames.

A total number of specimens were 81 columns tested by (Gupta et.al, 2007) **[27]** in three diameters. In analysis two columns have been analyzed under compression loading. The tubes are seam welded and the edges of the tubes are machine finished after cutting to avoid eccentricity during loading.

5.5.1. Model Geometry, Loading, and Boundary Condition

In order to study the behavior of the composite concrete filled steel tube column, 2 specimens of circular cross section with different concrete strength and wall thickness were tested under compressive loading. Details of the specimens are presented in ***table 5.5***.

Table 5.5 *Details of column members*

No	Section Dimensions (mm)			in (MPa)				ν concrete	ν steel
	Diameter	t	L	f'_c	f_y	E_c	E_s		
1	89.32	2.74	340	28.89	360	25262	200000	0.2	0.3
2	112.56	2.89	340	40	360	29725	200000	0.2	0.3

5.5.2 Finite Element Idealization

In all previous examples, the types of elements used and the mesh details are the same in this example. Brick element (SOLID65), brick element (SOLID45), and contact element (CONTAC52) used to represented concrete core, steel tube, and bond respectively. Details of finite element model of composite column is shown in ***Figure 5.20***

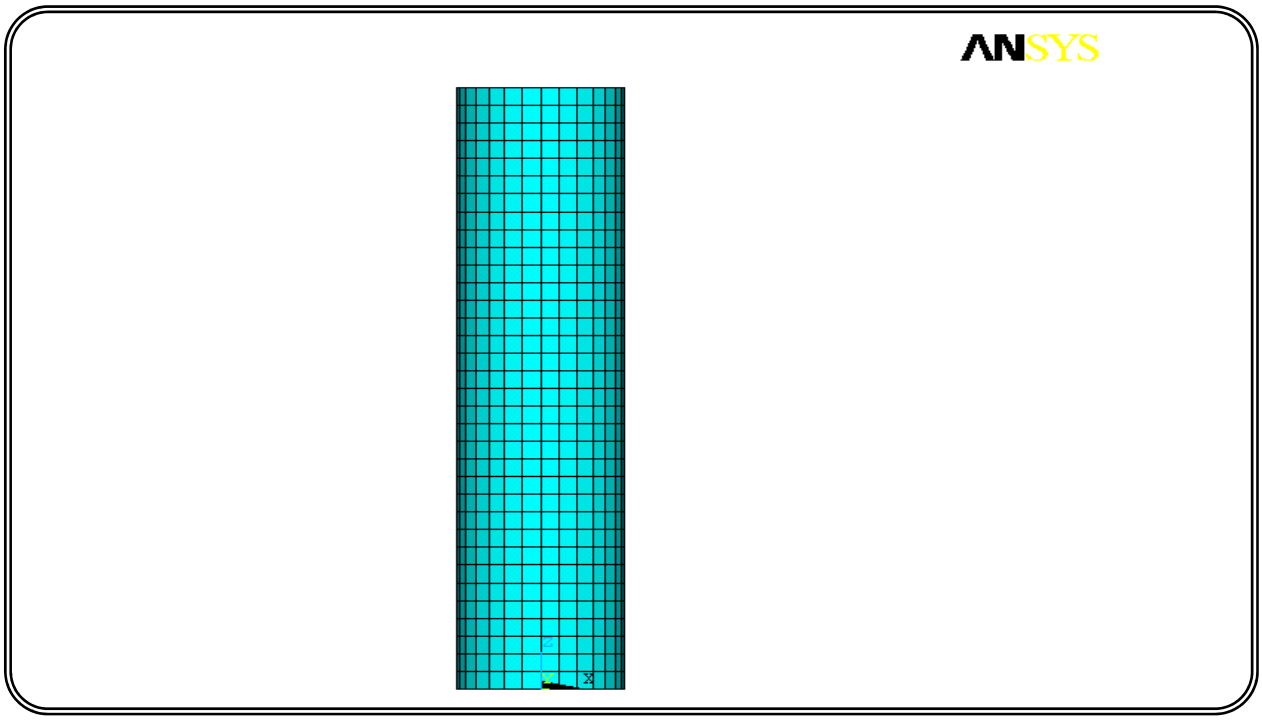

Figure 5.20 *finite element idealization of composite column.*

5.5.3. Results of Analysis

Result of finite element analysis as compared with experimental study is shown in ***Figure 5.21*** and ***5.22***, in analysis of finite element of composite columns partial bond adopted only because the full bond results can be said equal to partial bond results. This is caused by the support in the bottom of column that prevent concrete core from slip from steel tube. Finite element analysis by using partial bond gave good agreement with experimental study.

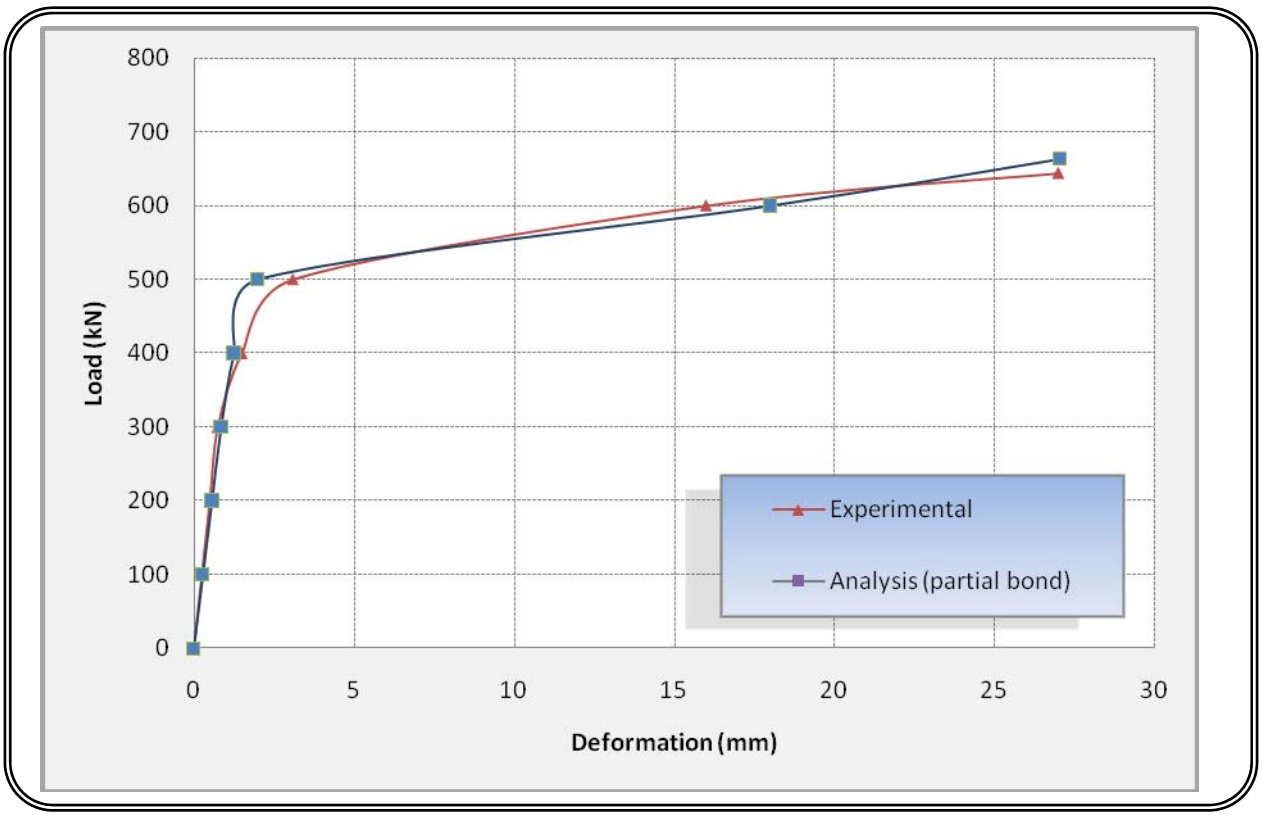

Figure 5.21 *Load deflection curve of composite column1.*

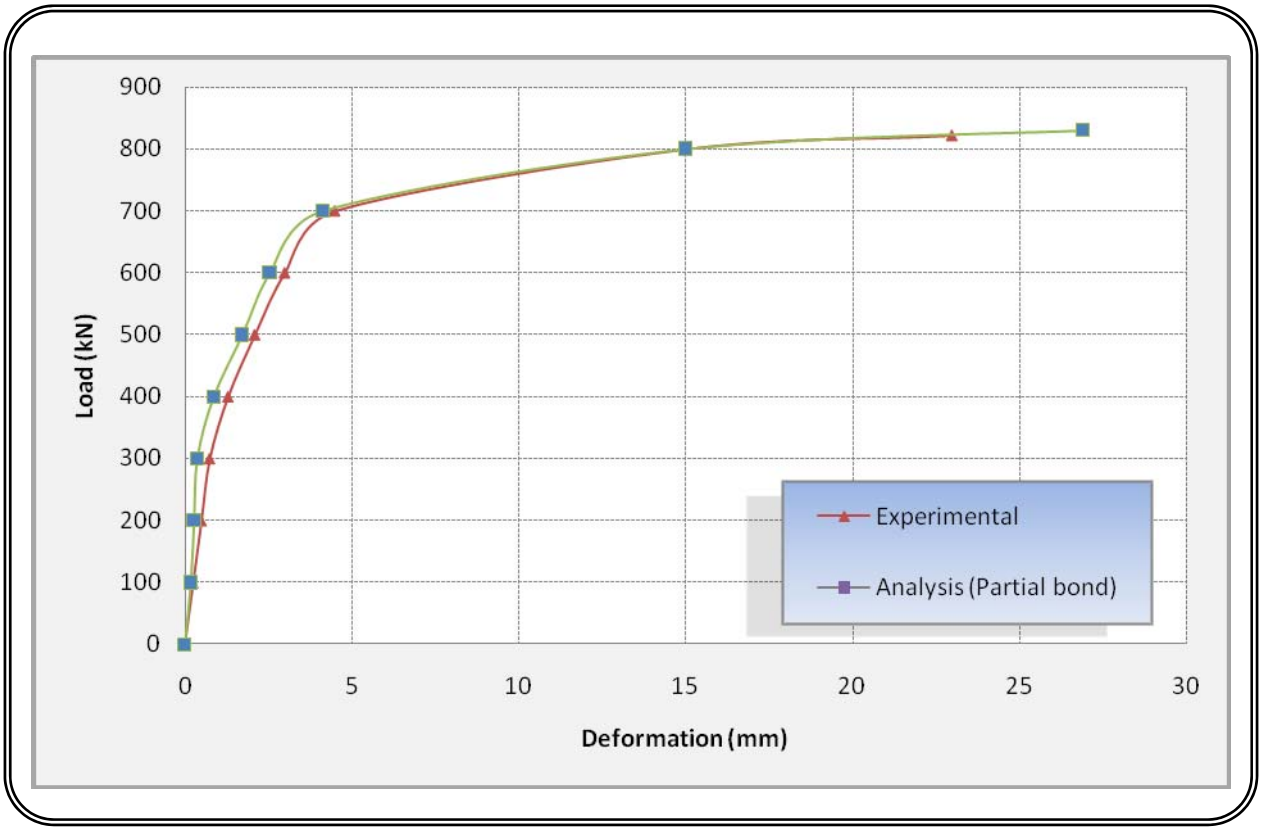

Figure 5.22 *Load deflection curve of composite column2.*

5.6. Example 5; Composite Frame

In this example, three types of frames are analyzed as follows:

- Composite Frame: all members used (beam and columns) in frame are made of concrete filled steel tubes.
- Composite Frame: concrete encased steel I-sections are used in all members of frame.
- Reinforced Concrete Frame: All members are made of reinforced concrete.

In the three types of frames connection of beam to column is assumed as of full bond as explained by (Brahmachari, 1997) **[23]** "it can be concluded that a reliable rigid connection can be achieved if the weld is designed properly to transfer the load".

5.6.1. Model Geometry, Loading, and Boundary Condition

In all frames, the area of steel is kept constant for all beams and columns that means, the area of steel tube (for concrete filled steel tube beam) is equal to the area of steel I-section (for concrete encased steel beam)and equal to the area of reinforced steel (for reinforced concrete beam). Also the volume of concrete is kept constant for all cases. This will lead to study the comparative performance of composite frame compared with reinforced concrete frame, also between composite frame that composed of concrete filled steel tube members and that composed of concrete encased steel section members. Section dimensions of frames are shown in ***Figure 5.23.***

5.6.1.1. Type of Frame

As stated above, three types of frame are adopted in analysis as follows:

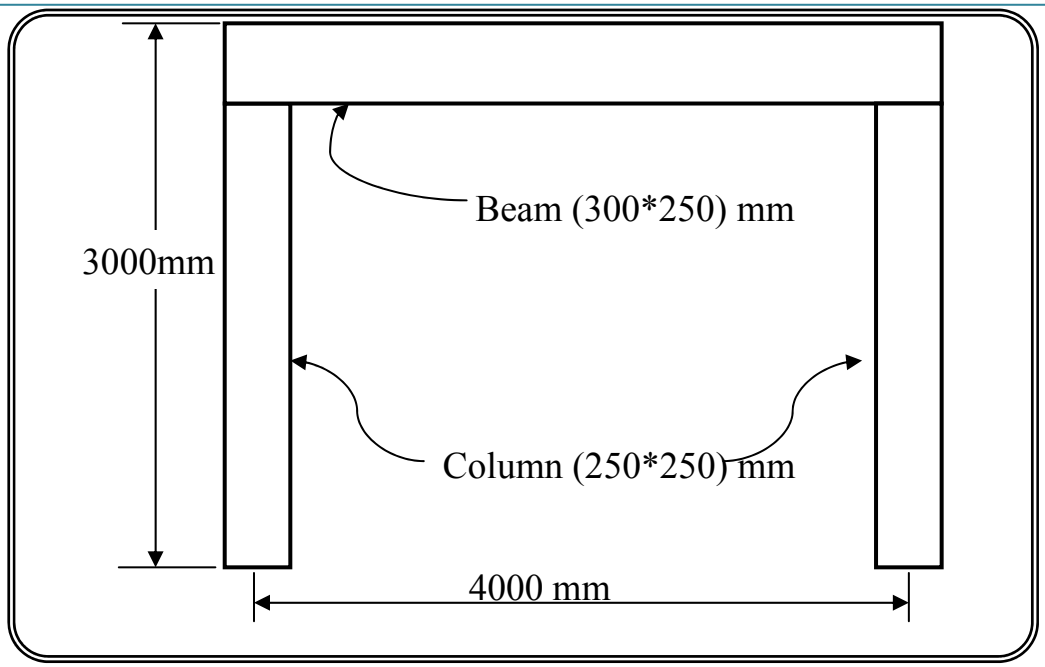

Figure 5.23 *Frame geometry*

5.6.1.1.1 Composite Frame composed of CFST members.

In this type, the steel tubes thickness is equal to 5 and 2.5 mm for columns and beams respectively as detailed in ***Table 5.6***.

Table 5.6 *Details of composite frame, concrete filled tube*

Members Type	Steel Dimensions (mm)			In (MPa)				μ	μ
	width	height	thickness	f'_c	f_y	E_c	E_s	concrete	steel
Columns	250	250	5	30	400	25750	200000	0.2	0.3
Beams	250	300	2.25	30	400	25750	200000	0.2	0.3

5.6.1.1.2 Composite Frame composed of CES members

All steel dimensions of beam and column are detailed in ***Table 5.7***. The symbols used in table explained in example three.

Table 5.7 *Details of composite frame, concrete encased steel*

Members Type	Steel Dimensions (mm)				In (MPa)				μ concrete	μ steel
	h	b	t_w	t_f	f'_c	f_y	E_c	E_s		
Columns	174	154	8	12	30	400	25750	200000	0.2	0.3
Beams	174	154	4	6	30	400	25750	200000	0.2	0.3

5.6.1.1.3. Reinforced Concrete Frame

In this case, all members of the frame are made of reinforced concrete members, the amount of steel reinforcement of reinforced concrete frame depends on the area of steel in composite frame, as in ***Table 5.8.***

Table 5.8 *Details of reinforced concrete frame*

Members Type	Steel Reinforcement		In (MPa)				μ concrete	μ steel
	Main Rein	Sec. Rein.	f'_c	f_y	E_c	E_s		
Columns	8 φ 25	$\varphi 10@20mm$	30	400	25750	200000	0.2	0.3
Beams	4 φ 25b 2 φ 16t	$\varphi 10@20mm$	30	400	25750	200000	0.2	0.3

5.6.1.2. Loading Conditions

5.6.1.2.1 Distributed Load

In this case, load has been distributed on the upper surface of beam. Loads value differs from frame to other depending on the ultimate loading capacity of each frame as shown in ***Figure 5.24.a***

5.6.1.2.2. Concentrated Load

As shown in ***Figure 5.24.b***, concentrated load is applied on mid span of beam.

5.6.1.2.3. Lateral Load

For all frames, lateral concentrated load is applied on the top of left column. This load condition is shown in ***Figure 5.24.c***.

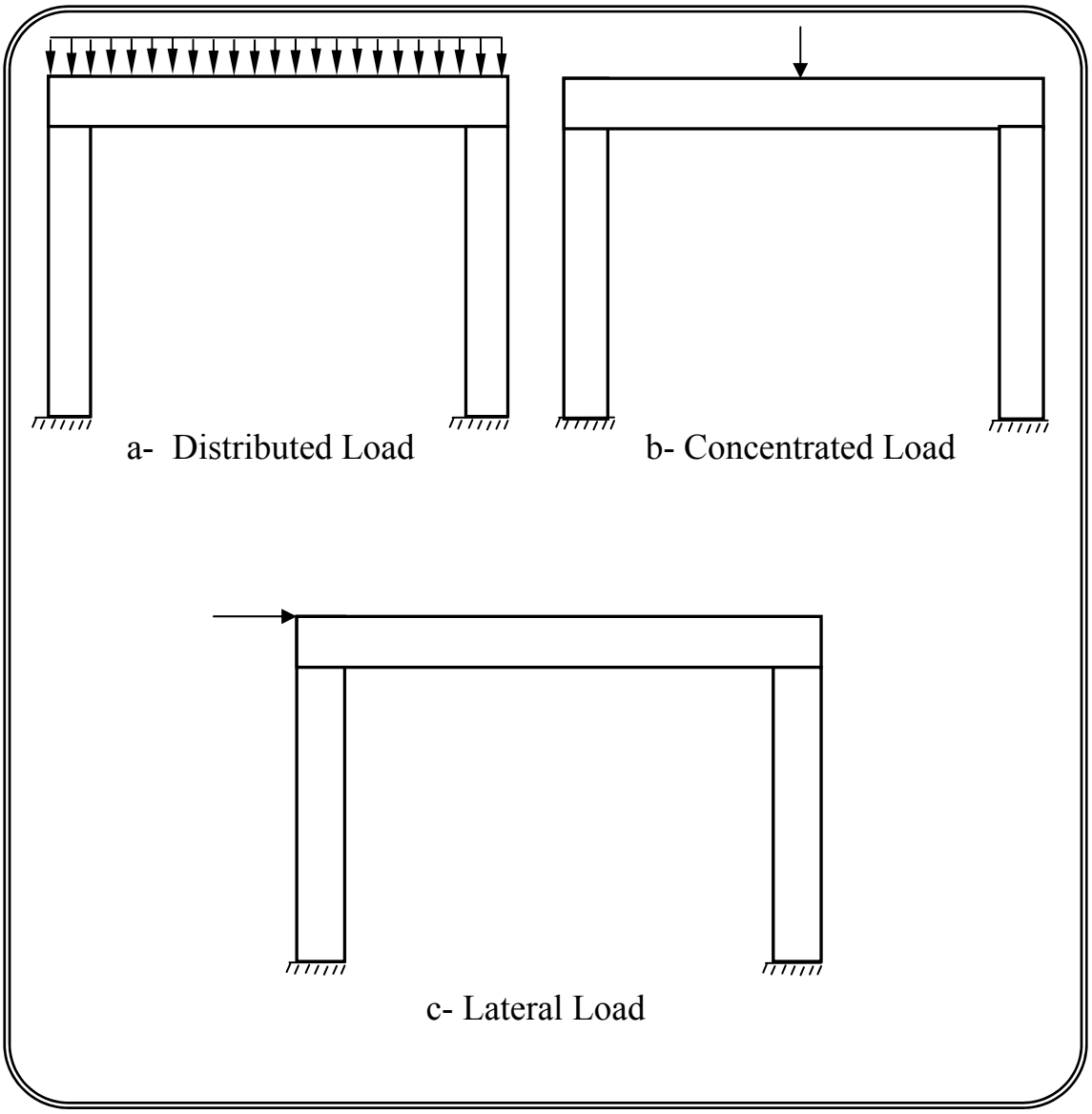

Figure 5.24.*Loading Conditions*

5.6.2. Finite element Idealization

The model adopted in the analysis of this example is explained in all previous examples. The beam to column connection is modeled in analysis by using GLUE (as denoted in ANSYS) which give full contact between beam and columns. Partial bond between steel and concrete has been adopted in analysis for beams and columns in composite frames. Finite element idealization of frame is shown in ***Figure 5.25.***

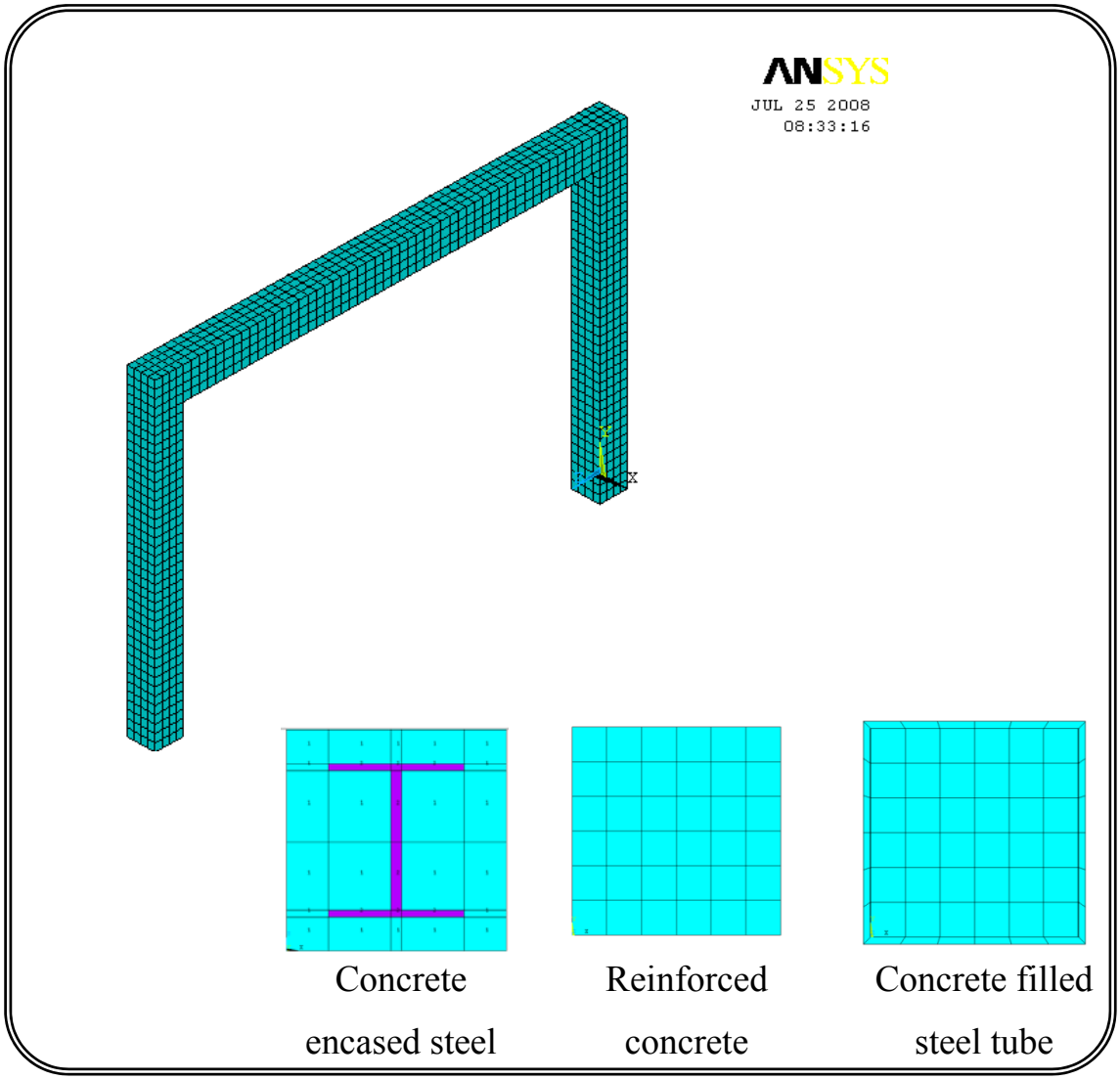

Figure 5.25 *finite element idealizations of frames.*

5.6.3. Results of Analysis

Results of finite element analysis of composite frames and reinforced concrete frame are shown in ***Figures 5.26, 5.27,*** and ***5.28***

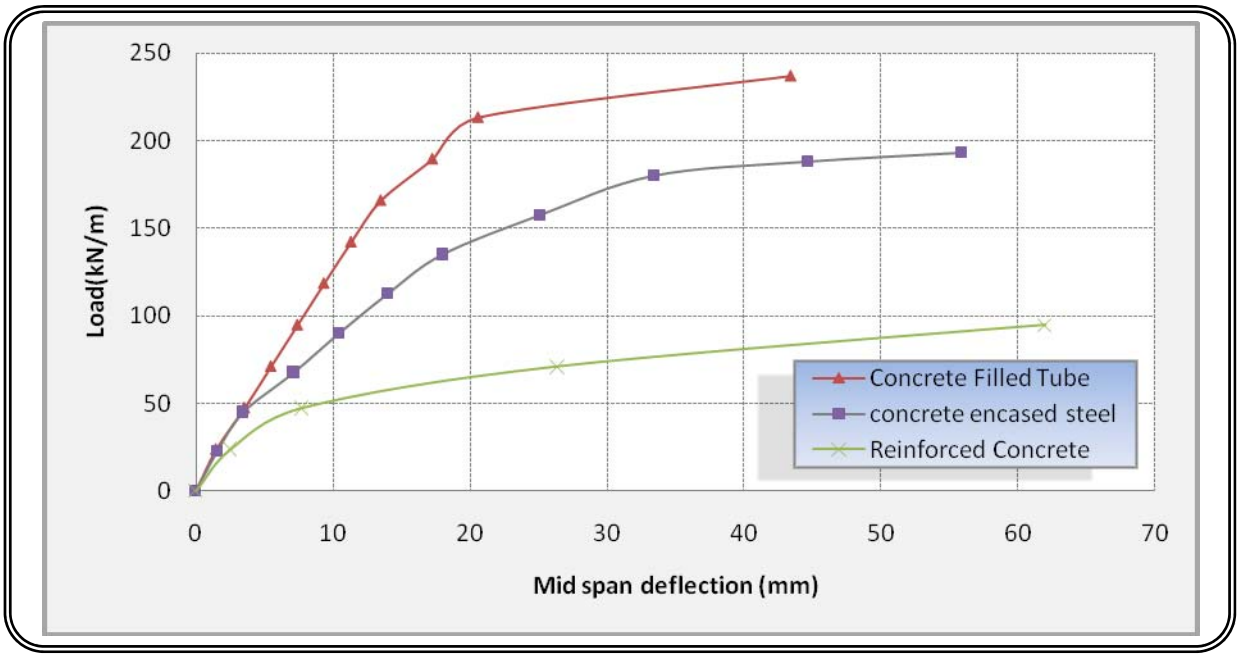

Figure 5.26 *load deflection curves of frames under distributed load.*

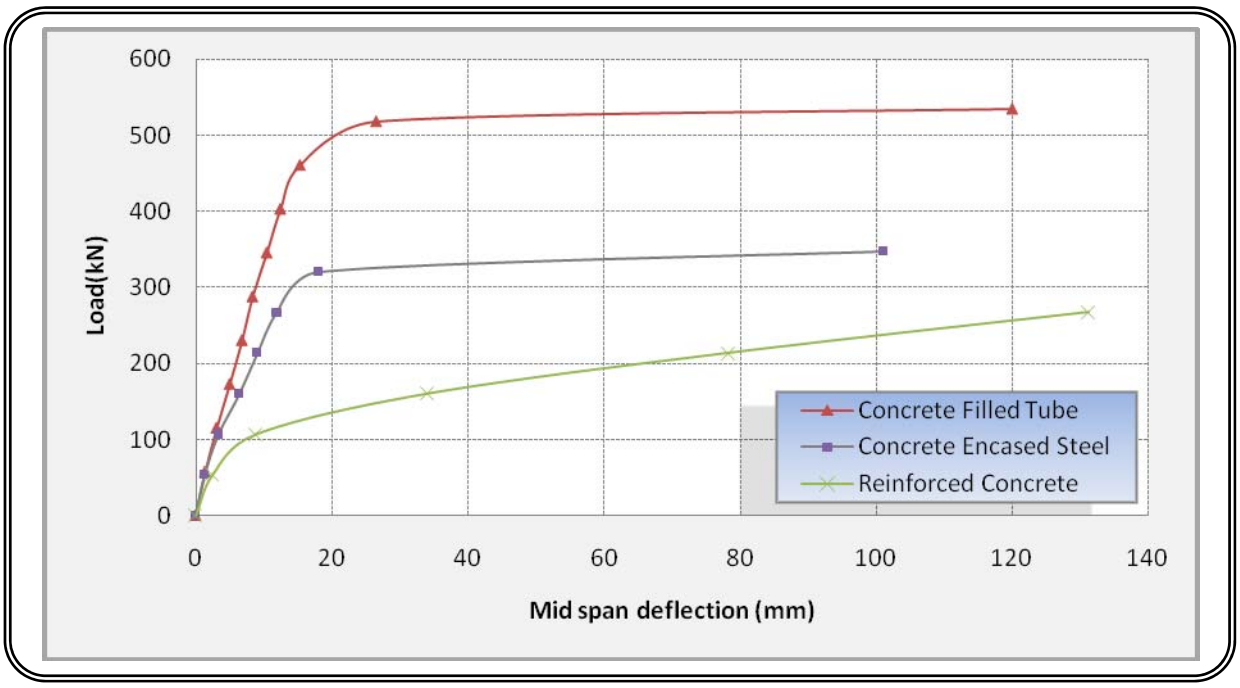

Figure 5.27 *Load deflection curves of frames under concentrated load.*

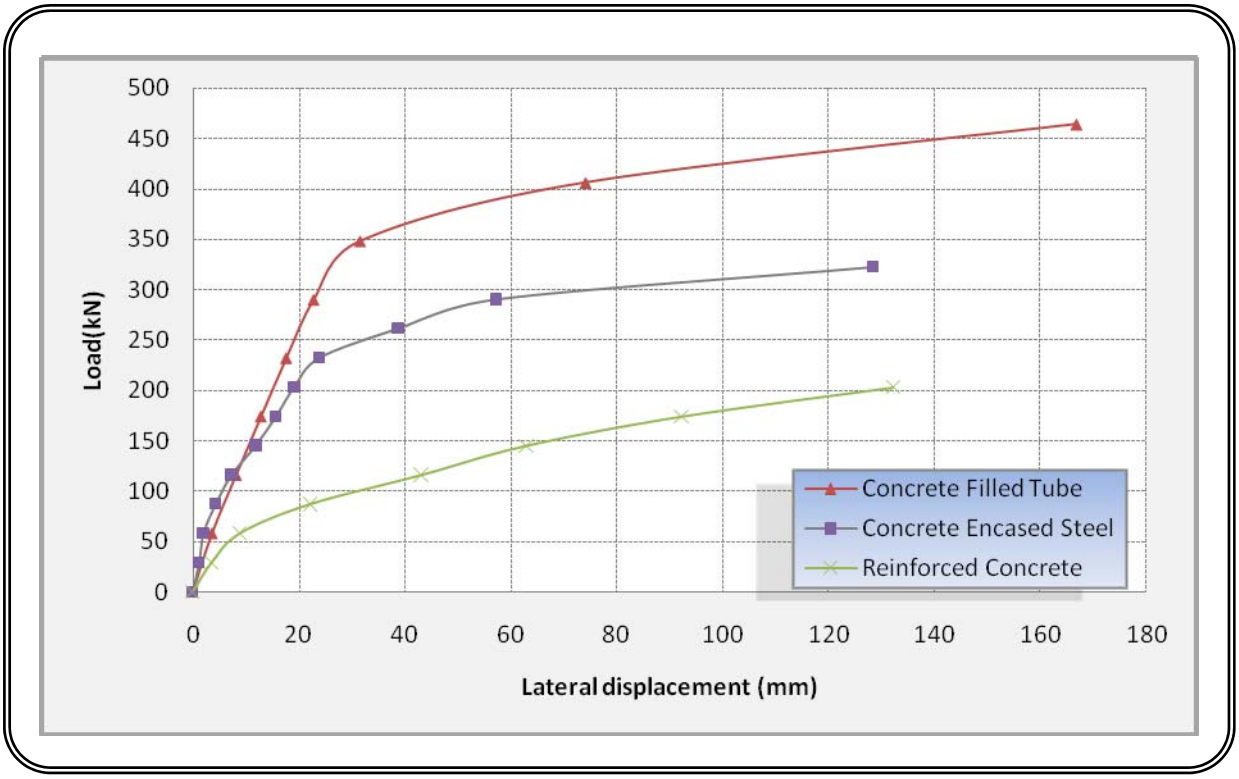

Figure 5.28 *Lateral load-displacement curves of frames.*

From results in ***Figure 5.26, 5.27***, and ***5.28***, the frame composed of concrete filled steel tube members gives best strength from other type of frames (for same steel area). This may be caused by confinement of concrete developed by steel tube and this is lead to increase in ultimate strain of concrete about 10 times ultimate strain of unconfining concrete as explained in chapter three.

5.6.4. Cracking Pattern

In case of distributed and concentrated load cracks were appeared in composite frames as well as reinforced concrete frame as shown in ***Figure 5.29.***

Figure 5.29 shows the location of cracks and crushed integration points along the beam and columns in the frame, utilizing plotting ability of ANSYS. The figure is selected at the critical load value (maximum load). As

shown, the cracks (red points represent the first crack, green points represent the second crack and the blue point represents the third crack at integration point) distributed at mid-span under the centerline of the beam then transformed gradually to top surface of the beam near the connection to column, also cracks appeared at columns. The crushed integration points (black points) are concentrated at mid-span section.

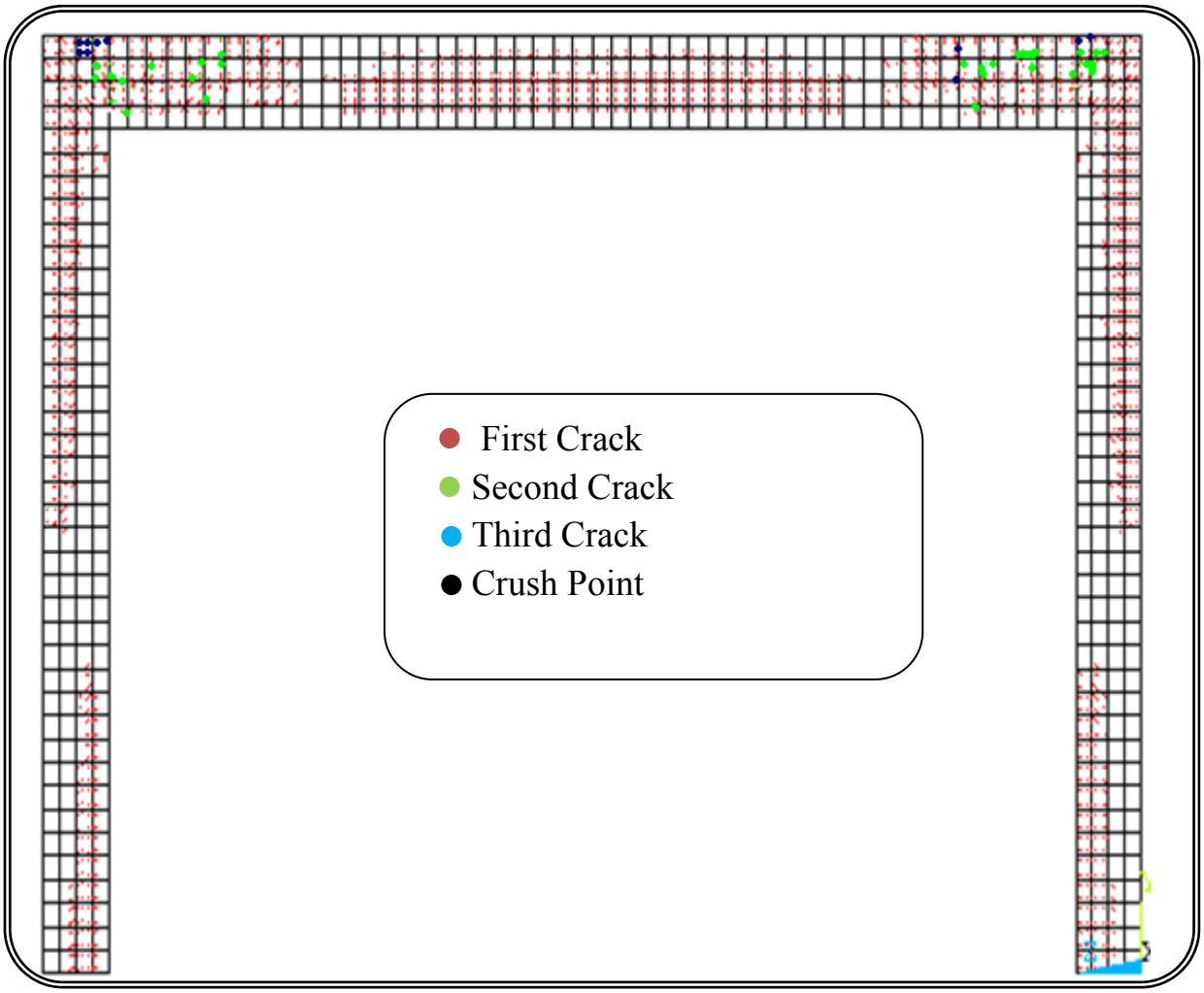

Figure 5.29 *cracking and crushing in frame under distributed and concentrated load.*

Under lateral loads cracks do not appear at mid-span of beam as in vertical load, the cracks always appear at region of beam to columns connection, where in columns, cracks located on the inner surface of right column and outer surface in left column and near support for the left and the

right columns. Crushing appeared at the right inner corner of frame, and appeared at opposite side of columns above support about one-third length of columns, all these cracks and crushing points are shown in ***Figure 5.30.***

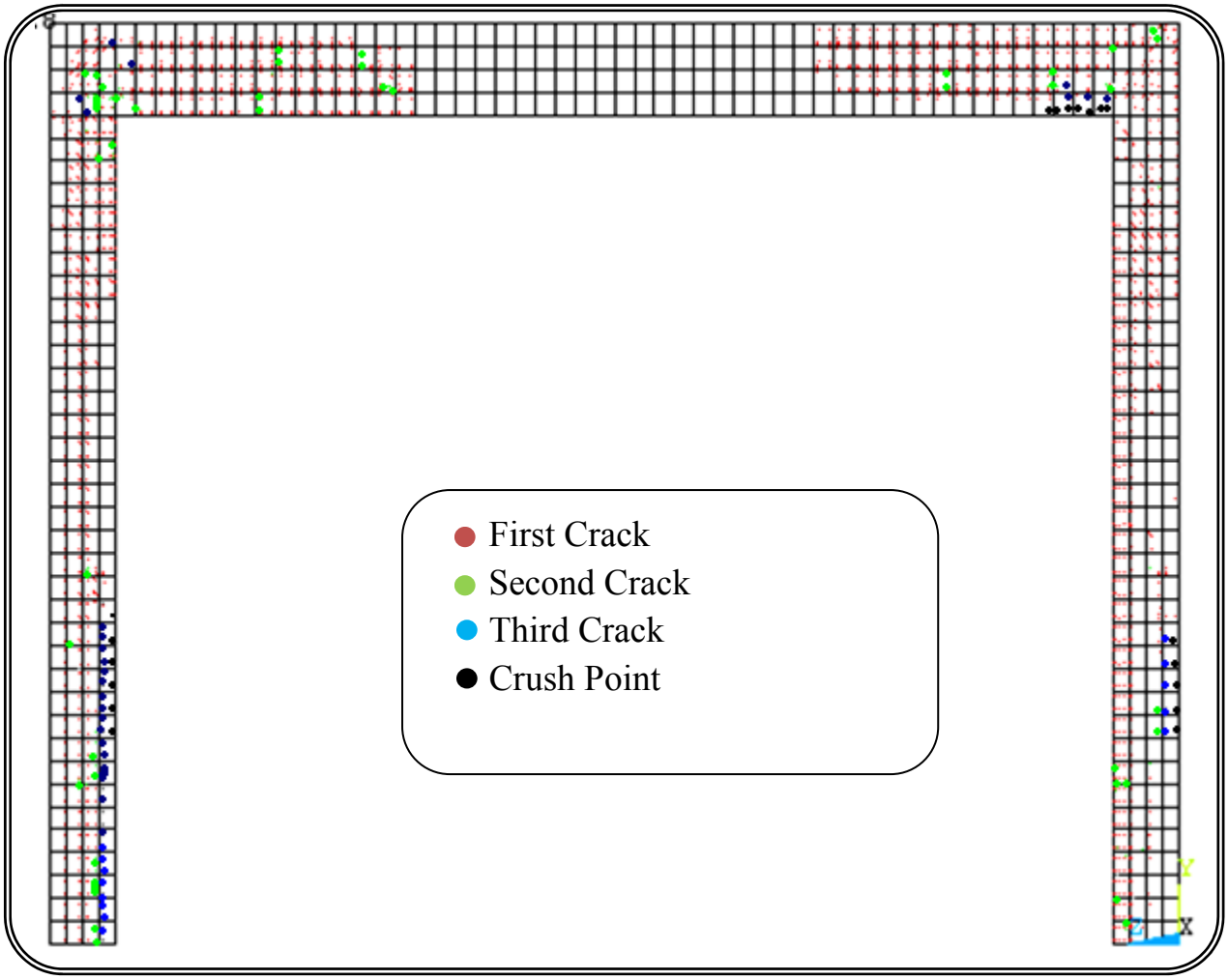

Figure 5.30*cracks and crushing points in frame under lateral load.*

5.7. Parametric Study

In order to investigate the effect of some geometrical and material parameters on nonlinear finite element analysis of composite frames, the following parameters are considered compressive strength of concrete, yield stress of steel, effect of cross section shape on composite members, and uniaxial stress-strain relationship model of unconfining concrete under compression.

5.7.1. Effect of compressive strength of concrete.

In order to study the effect of varying the value of compressive strength on the behavior of composite frame (example 5) under distributed load, many different values of compressive strength have been adopted in the analysis. ***Figure 5.31*** shows the load deflection curve of different compressive strength value.

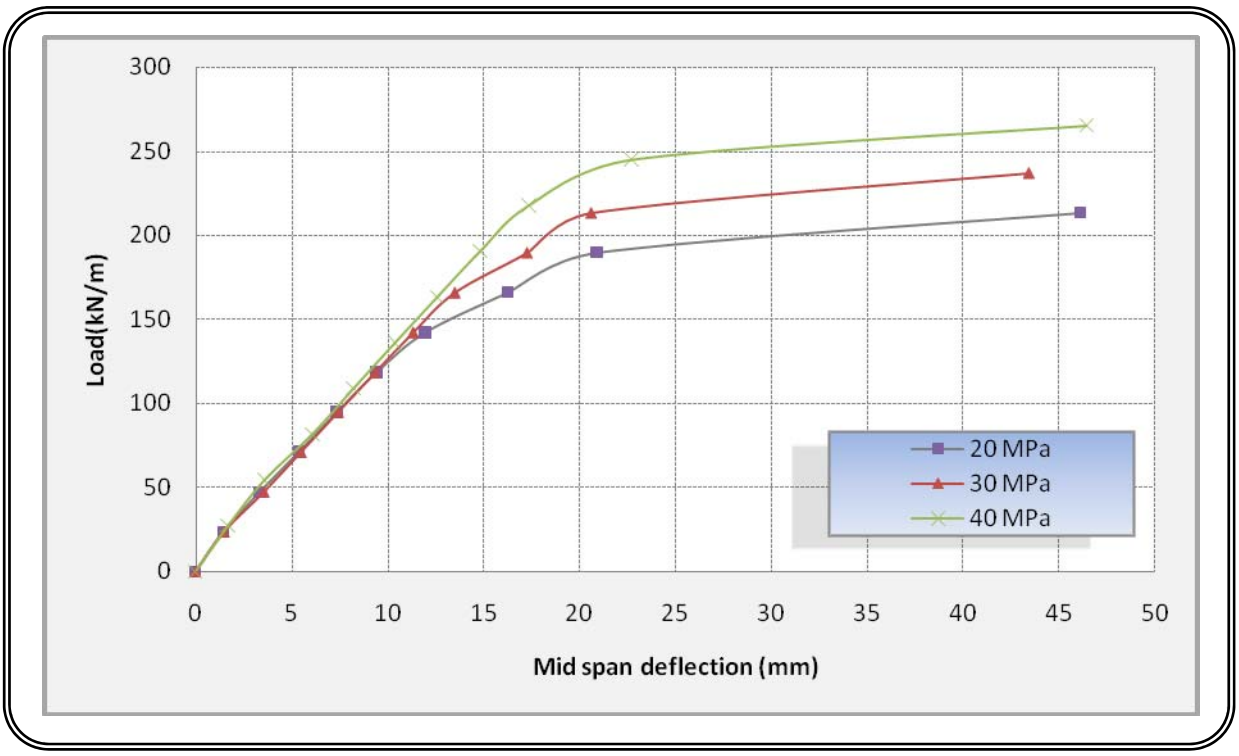

Figure 5.31*.Effect of compressive strength of concrete on composite frame*

The increase of compressive strength of concrete about 30% caused an increase ultimate load carrying capacity of composite frame about 13%, and decreases of compressive strength of concrete 30% cause a decrease of ultimate load carrying capacity of composite frame 10% under distributed load (lateral and concentrated load have same changing value). The failure of composite frame in case 3 (compressive strength of concrete 40 MPa) has been caused by failure in steel tube.

5.7.2. Effect of steel yield stress

In order to investigate the effect of yield stress of steel tube on the behavior of composite frame (example 5) under distributed load, three different values of yield stress of steel tube have been taken. ***Figure 5.32.***shows the effect of yield stress of steel tube on composite frame.

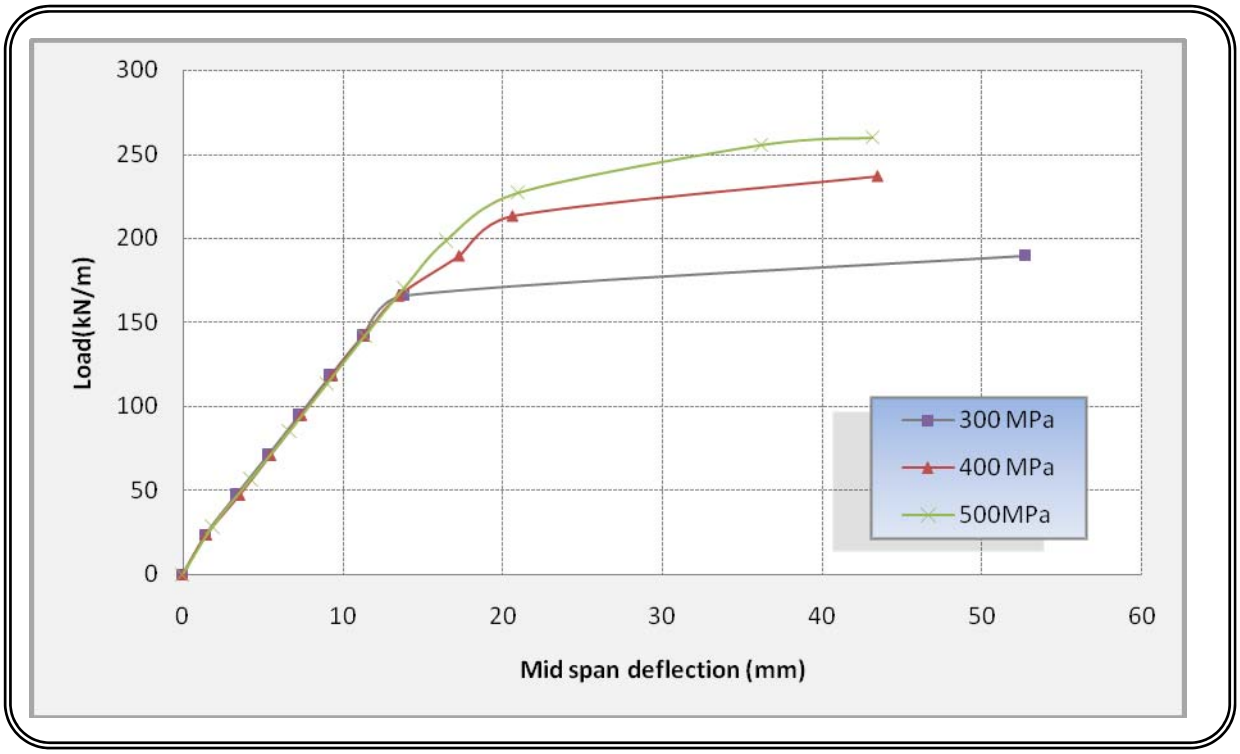

Figure 5.32.*Effect of steel yield stress on behavior of composite frame.*

The increase of yield stress of steel tube is about 25% and decrease is 25% that causes an increase of ultimate load about 8% and a decrease 33% respectively. The wide different value of ultimate load capacity (at failure) of composite frame in case of (f_y=300 MPa) was due to steel tube failure, while in other cases of yield stress the failure of composite frame began in concrete core.

5.7.3. Effect of cross-section shape of composite members

In order to choose best cross section shape of composite member, many cross section shapes have been taken in analysis with constant area of steel and concrete and materials properties (material properties as in example 5). ***Figure 5.33.***and ***5.34***.show the effect of cross section shape of composite beam and column respectively.

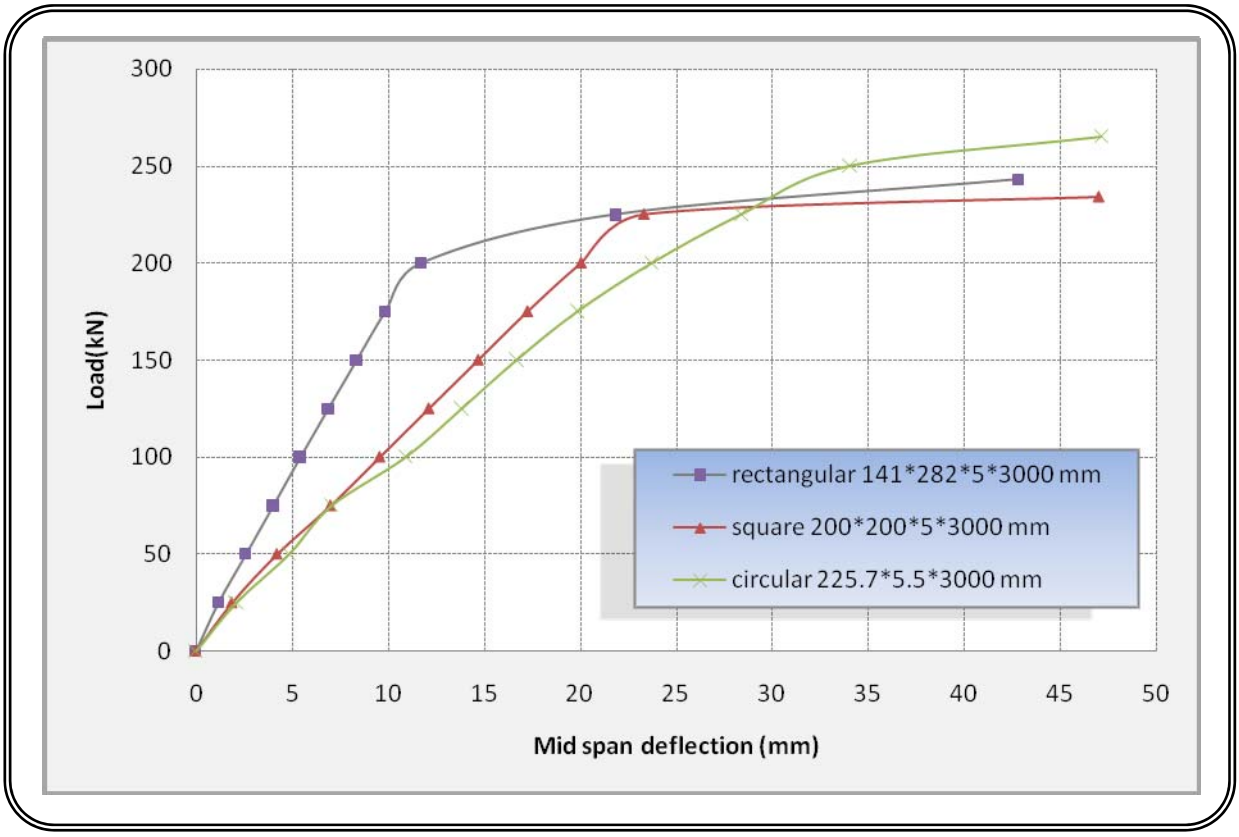

Figure 5.33*.Effect of cross section shape of composite beam.*

The circular composite beam gave greater load carrying capacity from other type of cross section shapes, and rectangular composite beam was better than square composite beam.

However, the square and rectangular composite beams are widely used while the composite circular beam is rarely used because the ability of the square and rectangular composite beam to be used in building and any other structures.

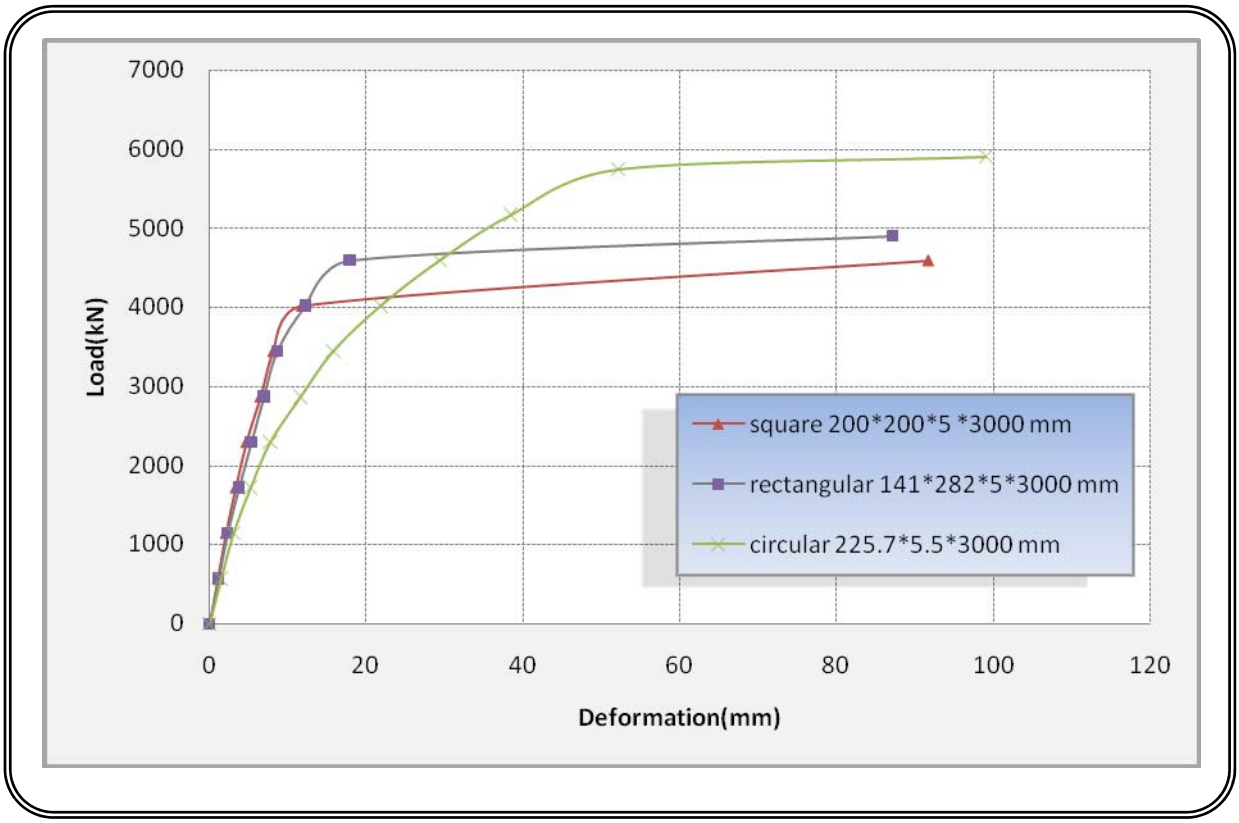

Figure 5.34*.effect of cross section shape of composite columns.*

With respect to composite columns, as shown in ***Figure 5.34***, the circular composite columns has higher load carrying capacity than square and rectangular composite columns, but square and rectangular composite columns has more rigidity in early age of loading. Circular composite columns have been widely used in last years from the other shapes of composite columns.

5.7.4 Effect of uniaxial stress-strain model of concrete

As given in chapter three, three model of stress-strain curve of unconfining concrete model have been explained. The composite beam composed of concrete encased steel member (beam 1) described in example 3 have been used to study the effect of stress-strain curve model of concrete as shown in ***Figure 5.35.***

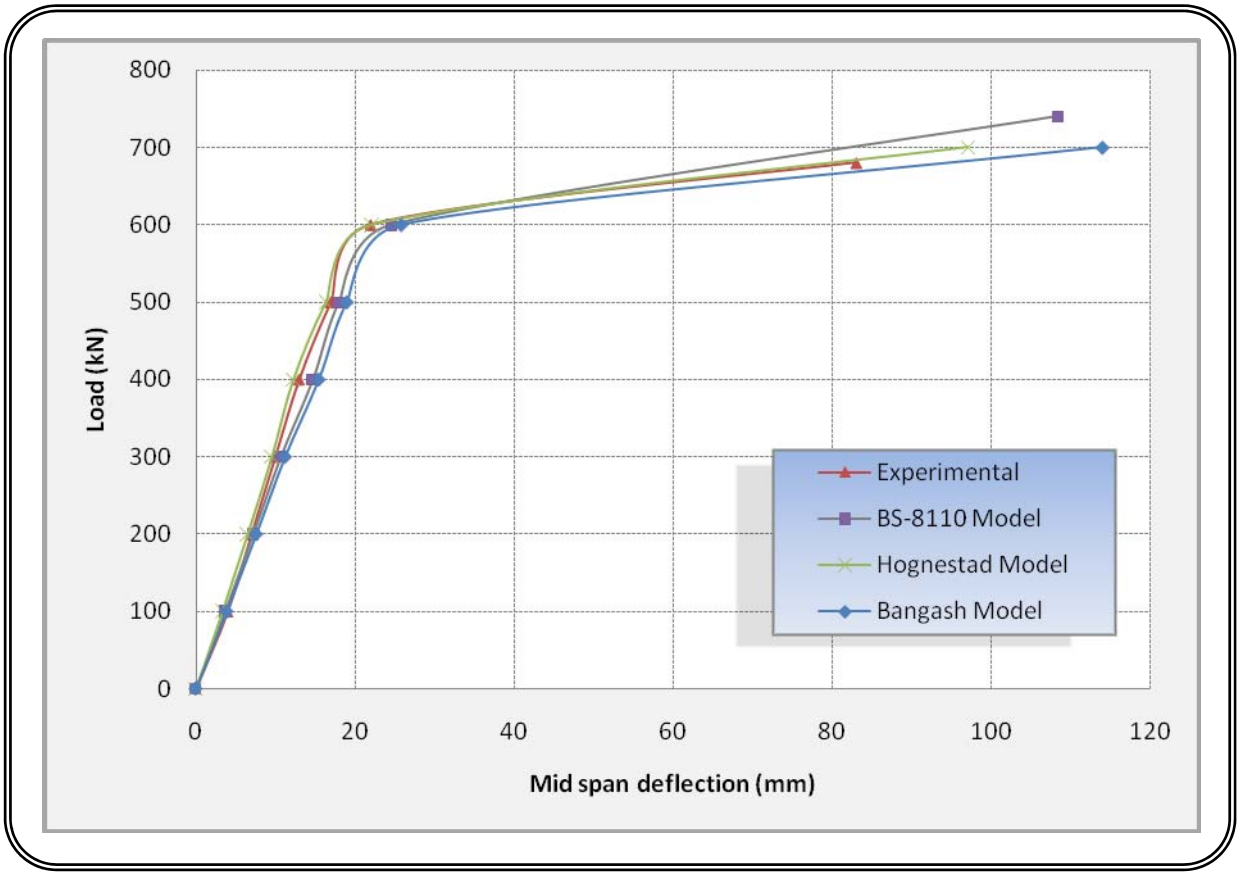

Figure 5.35 *Effect of uniaxial stress-strain curve model*

As shown in Figure (5.35) the Hognestad model is the best model with very good agreement with experimental results.

CHAPTER SIX

CONCLUSIONS AND RECOMMENDATIONS

6.1. Conclusions

Based on results obtained from the investigation, the following can be concluded:

1. The present nonlinear finite element analysis is a powerful tool and it can be provide the researchers with a lot of important information that cannot be supplied by the experimental tests.
2. Results from this study suggest that the concrete filled steel tube offer more load carrying capacity from concrete encased steel structure and reinforced concrete members.
3. The circular concrete filled steel tube member offers more load carrying capacity from square and rectangular concrete filled steel tube members (by amount reached 6% and 11% for rectangular and square composite beam respectively and about 17% and 22% for rectangular and square composite column respectively).
4. The present finite element modeling presents the steel part by brick element and considering contact (interface element) between steel and concrete, seems efficient and gives very good results through comparing with the experimental results.
5. The compressive strength of concrete affects the overall behavior of composite frame. As the compressive strength of concrete increases, the ultimate load capacity of composite frame increases. A 30% increase of concrete compressive strength causes an

increasing of ultimate load carrying capacity of composite frame about 13%.

6. As the yield stress of steel structure increases, the ultimate load capacity of composite frame increases. A change in the yield stress of 25% may cause a change in the load carrying capacity reaches 33%.
7. The Hognestad model of stress-strain curve (used by ACI) of unconfining concrete gives best agreement with experimental data than other model types (when model used for concrete encased steel section).

6.2. Recommendations for future work

1. The current analytical results of composite frame composed of composite members are required to be supplemented by experimental results by testing model or full scale composite frame (composed of concrete filled steel tube or concrete encased steel members)
2. An experimental and numerical research for beam to column connection in composite frame.
3. An effect of creep of concrete in the composite frame needs to be studied.
4. A change in the temperature effect on composite frame may be investigated using nonlinear finite element analysis.
5. A behavior of composite frames composed of composite members under cyclic load.
6. Concrete-filled steel tube frames have increasingly been used in earthquake resistance structure due to the large ductility that can be achieved. Therefore; dynamic and impact loads are important problems to be studied.

References

[1] Wakabayashi, M., “Japanese Standards for A Design of Composite Building; composite Construction of Steel and Concrete”, Engineering Foundation, 1988, pp53-70, Cited by Ref [72]

[2] Viest, I.M., Fountatain, R.S., and Singlton, R.C., “Composite Construction in Steel and Concrete”, McGraw-Hill, 1958.

[3] Godfrey, G.B., “Post War Development in German Steel Bridges and Structures”, Structural Engineer, Feb 1957, pp53-68. Cited by Ref. [72]

[4] Sattler, K., “Composite Construction in Theory and Practice”, Structural Engineer, Vol.4, No.2, April 1964, pp115-125.

[5] Eurocode 4, “Design of Composite Steel and Concrete Structures, Part 1.1- General Rules and Rules for Building”, European Committee for Standardization Brussels, 1994.

[6] Johnson, R.B., “Composite Construction of Steel and Concrete” Vol.1, 3rd edition, Blackwell Scientific Publication, Oxford, 2004.

[7] Cosenza, E., and Zandonini, R., “Composite Construction”, Structural Engineering Handbook, CRC Press LLC, 1999. Cited by Ref.[80]

[8] Faber, O., “More Rotational Design of Cased Stanchions”, Structural Engineer, Vol.34, March 1956, pp88-109. Cited by Ref. [45]

[9] Architectural Institution of Japan, “Recommendations for the Design and Fabrication of Tubular Structures in Steel”, Architectural Institution of Japan, 2001.

[10] Tort, C., and Hajjar, J.F., “A mixed Finite Element Approach for Nonlinear Dynamic Analysis of Composite Rectangular Concrete Filled Steel Tube Frames”, Computational Method in Structural

Dynamic and Earthquake Engineering, Conference Rethymno University, Greece, June 2007.

[11] Muhsen, H.N., "Three Dimensional Nonlinear Finite Element Analysis of Axially Loaded Concrete Filled Steel Tube Short Columns", M.Sc., Thesis, University of Technology, 2002,

[12] Knowel, R.B., and Park, R., "Strength of Concrete Filled Steel Tubular Columns", Journal of Structural Division, Vol.95, No.ST12, December 1969, pp 2565-2585.

[13] Sakino, K., Tomii, M., and Watanable, K., "Sustained Load Capacity of Plain Concrete Stub Columns by Circular Steel Tubes", Proceeding of the international Specialists Conference on Concrete Filled Steel Tubular Structure, 1985, pp112-118.

[14] ANSYS, "ANSYS Help", Release 9.0, Copyright 2004.

[15] David, A.N., "Composite Construction Stability and Strength" Elsevier Applied Science, 2004.

[16] Russell, W.A., "Structural Properties of Light Gage Tubular Columns", Housing Research Paper, No21,Housing and Home Finance Agency, October 1964, Cited by [22]

[17] Kloppel, K., and Goder, W., "Collapse Load Tests on Concrete Filled Steel Tubes and derivations of a Design Formula" Der Stahlbau, Vol.26, January and February 1957. Cited by [23]

[18] Furlong, R.W., "Strength of Steel-encased Concrete Beam Columns" Journal of the Structure Division, Vol.94, No.ST1, October 1967, pp267-281. Cited by [23]

[19] Knowles, R.B. and Park, R., "a Axial Load Design for Concrete Filled Steel Tubes", Journal of the Structure division, Vol.96, No. STI, October 1970, pp2125-2153.

[20] Tomii, M., Yoshimara K. and Morishima Y., "Experimental Studies on the concrete–Filled Steel Tubular Stub Columns Under

Concentric Load", Proceeding of the International Colloquium Stability of Structural Under Static and Dynamic Loads, 1977, pp718-741

[21] Shakir-Khalil, H., and Zeghich, J., "Experimental Behavior of Concrete Filled Rolled Rectangular Hollow Section Columns", Structural Engineer, Vol.67, No.3, October 1989, pp 346-353.

[22] Lu, Y., and Kennedy, D.J., "The Flexural Behavior of Concrete Filled Hollow Structural Section", the Structural Engineering Report, No.178, April 1992.

[23] Brahmachari, K., "Connection and Flexural Behavior of Steel RHS Filled with High Strength Concrete", Ph.D., Thesis, University of Western, Sydney, 1997.

[24] Huang, C.S., Yeh, Y., Liu, G., Hu, H., Tsai, K.C., Weng, Y.T., Wang, S.H., and Wu, M., "Axial Load Behavior of Stiffened Concrete Filled Steel Tube", Journal of Structural Engineering, Vol.128, No.9, September 2002, pp222-230.

[25] Prickett, B.S., and Driver, R.G., "Behavior of partial Encased Composite Columns Made with High Performance Concrete", Structural Engineering Repot, No.292, University of Alberta, January 2006.

[26] Baig, M.N., "Strength of Concrete Filled Steel Tubular Columns", Tsinghua Science and Technology, Vol.11, No.6, December 2006, pp 657-666.

[27] Gupta, P.K., Sarda, S.M., and Kumar, M.S., "Experimental and Computational Study of Concrete Filled Steel Tubular Columns under Axial Load", Journal of Constructional Steel Research, Vol.63, 2007, pp 183-193.

[28] Mouli, M., and Khclafim H., "Strength of Short Composite Rectangular Hollow Section Columns Filled with Lightweight

Aggregate Concrete", Engineering Structures, Vol. 24, 2007, pp 1791-1797

[29] Elghazouli, A.Y., and Treadway, J., "Inelastic Behavior of Composite Member under Combined Bending and Axial Load", Journal of Constructional Steel Research, Vol. 64, 2008, pp 1008-1019.

[30] Shakir-Khlil, H., and Mouli, M., "Further Tests on Concrete Filled Rectangular Hollow Section Columns', the Structural Engineer, Vol.68, No.20\16, October 1990, pp 405-413.

[31] Schiller, P.H., and Hajjar, J.F., "A distributed Plasticity Formulation for Three-Dimensional Rectangular Concrete Filled Steel Tube Beam-Columns and Composite Frames", Structural Engineering Report, No.ST-96-5, University of Minnesota, November 1996.

[32] Hajjar, J.F., and Gourley, B.C., "Representation of Concrete Filled Steel Tube Cross-Section Strength", Journal of Structural Engineering, Vol. 122, No. 11, November 1996, pp 1327-1336.

[33] Al-Rodan, A., and Al-Tarawnah, S., "FE Analysis of The Flexural Behavior of Rectangular Tubular Section Filled with High Strength Concrete", Emirates Journal for Engineering Research, Vol.8, No.1, March 2003, pp 71-77.

[34] Hock, L.G., and Cheong, F.S., "A Computerized Estimation of Moment Force Interaction for Externally Strengthened RC Composite Columns", Journal of Institution of Engineering, Vol.44, issue 1, 2004, pp 20-38.

[35] Han, L., "Flexural Behavior of Concrete Filled Steel Tubes", Journal of Constructional Steel Research, Vol.60, 2004, pp313-337.

[36] Giakoumelis, G., and Lam, D., “Axial Capacity of Circular Concrete Filled Tube Columns”, Journal of Constructional Steel Research, Vol. 60, 2004, pp 1049-1068.

[37] Bahjet, A.S., “Analysis of Composite Beams Concrete Encased Steel Sections”, Al-Nahrain University, 2005.

[38] Mohamed, L., Khandaker, M.A., and Vasilios, B., “Axial Load Behavior of Self-Consoliding Concrete Filled Steel Tube Columns”, Construction and Service Stages, ACI Structural Journal, Vol. 231. No. 5, January-February 2006.

[39] Pi, Y., and Brain, U., “Second Order Nonlinear Inelastic Analysis of Composite Steel Concrete Members”, Journal of Structural Engineering, Vol. 132, May 2006, pp 751-761.

[40] Sapountzikis, E.J., and Mokos, V.G., “3-D Beam Element of Composite Cross-section Including Warping and Shear Deformation effects”, Computer and Structure, Vol.85, 2007, pp 102-116.

[41] Xiong, D., and Zha, X., “A numerical Investigation on the Behavior of Concrete Filled Steel Tubular Columns under Initial Stresses”, journal of Construction Steel Research, Vol63, 2007, pp599-611.

[42] Han, L., Yao, G., and Tao, Z., “Behavior of Concrete Filled Steel Tubular Member Subjected to Combined Loading”, Thin Wall Structures, Vol.45, June 2007, pp600-619.

[43] Liang, Q.Q. Uy, B., and Liew, J.Y., “Local Buckling of steel Plates in Concrete Filled Thin Walled Steel Tubular Beam-columns”, Journal of Construction Steel Research, Vol.63, 2007, pp369-405.

[44] Dundar, C., Tokgoz, S., Tanrikulu, A.K., and Baran, T., “Behavior of Reinforced and Concrete Encased Composite Columns

Subjected to Biaxial Bending and Axial Load", Building and Environment, Vol. 43, 2008, pp 1109-1120.

[45] Ewak, H., Filippou, F., "Finite Element Analysis of Reinforced Concrete Structures under Monotonic Loads", Structural Engineering Mechanics and Materials, No.90/14, University of California, November 1990.

[46] Ferguson, P.M., "Reinforced Concrete Fundamentals", John Wiley and Sons, 4th Edition, 1981.

[47] Hognestad, E. "A Study of Combined Bending and Axial Load in Reinforced Concrete Members", University of Illinois Engineering Experiment Station, Bullenit Series No.399, Bullenit No.1, 1951. Cited by Ref. [45]

[48] Park, R., and Paulay, T., "Reinforced Concrete Structures", Wiley-Interscience, New York, 1975. Cited by Ref [51]

[49] BS8110: Part1 and 2, "Structural Use of Concrete", British Standard Institution, London, 1993.

[50] Bangash, M.Y.H., "Concrete and Concrete Structures", Numerical Modeling and Applications, Elsevier Science Publishers Ltd, London, England, 1989.

[51] ACI318-08, "Building Code Requirements for Reinforced Concrete", American Concrete Institute, Detroit, 2008.

[52] Chen, W.F., "A plasticity In Reinforced Concrete", McGraw-Hill Book Company, 1981.

[53] Hughes, B. P. and Chapman, G. P., "Deformation of Concrete and Micro Concrete in Tension and Compression", magazine of Concrete Research, London, March 1966, Vol.18, No.54, pp19-24.

[54] Kupfer, H., Hilsdorf, H.K., and Rusch, H., "Behavior of Concrete under Biaxial Stress", ACI Journal, Vol. 66, No.62, pp656-666.

[55] Richart, F. E., Brandzaeg, A., and Brown, R.L., "The Failure of Plain and Spirally Reinforced Concrete in Compression", Bulletin No.190, University of Illinois, Engineering Experiment Station, April 1929, 74 pp.

[56] Balmer, G. G., "Shearing Strength of Concrete under High Triaxial Stress", U.S. Bureau of Reclamation, Structural Research Lab, Report No. SP-23, Denver, CO., 1949. Cited by Ref [45]

[57] Ngo, D., and Scordelist, A. C., "Finite Element Analysis of Reinforced Concrete Beams", American Concrete Institute Journal, Vol. 64, No. 3, March 1967, pp152-163. Cited by Ref [52]

[58] Rashid, Y.R., "Ultimate Strength Analysis of Prestressed Concrete Pressure Vessels", Nuel. Eng. Des. , 1968, Vol. 7, pp334-344.

[59] Vebo, A., and Ghali, A., "Moment-Curvature Rotation of reinforced Concrete Slabs", Journal of Structural Division, ASCE, 1977, Vol. 103, No. ST3, pp 515-531. Cited by Ref [45]

[60] Bazant, Z. P., and Cedolin, L., "Fracture Mechanics of Reinforced Concrete", Journal of Engineering Mechanics, ASCE, 1980, Vol. 106, No.EM6, pp 1287-1306

[61] Hillerborg, A., Modeer, M., and Petersson, P.E., "Analysis of Crack Formulation and Growth in Concrete by Means of Fractures Mechanics and Finite Element", Cement and Concrete Research, 1976, Vol.6, No.6, pp 773-782.

[62] Bazant, Z.P., and Cedolin, L., "Finite Element Modeling of Crack Bond Propagation", Journal of Structural Engineering, ASCE, 1983, Vol.109, No. 1, pp 69-93. Cited by Ref [80]

[63] Broek, D., "Elementary Engineering Fracture Mechanics", Sijthoff and Noordoff, London, 1974, Cited by [72]

[64] Jenq, Y. S., and Shah, S.P., "Crack Propagation in Fiber-Reinforced Concrete" Journal of Structural Engineering, ASCE, 1986, Vol.112, No.1, pp334-344.

[65] High Strength Concrete, Published Jointly by Cement and Concrete Association of Australia and Notional ready Mixed Concrete Association of Australia, 1992. Cited by [23]

[66] Huyse, L., ,Hemmaty, Y., and Vandewalle, L., "Finite Element modeling of Fiber Reinforced Concrete beam", Proceeding of the ANSYS Conference ,vol.2. Pittsburgh, Pennsylvania, May 1994. .

[67] Hemmaty, Y., "Modeling of the Shear Force Transformed Between Cracks in Reinforced Concrete Structures" Proceeding of the ANSYS Conference, Vol.1Pittsburgh, Pennsylvania, August 1998.

[68] Desayi, P., and Krishnan, S., "Equation for the Stress Strain Curve of Concrete", ACI Journal, March 1964, Vol.61, pp345-350. Cited by [45]

[69] Gene, J.M., and Timoshenko, S.P., "Mechanics of Materials", PWS Publishing Company, Boston, Massachusetts, 1997.

[70] William, K.J., and Warnk, E.P., "Constitutive Model for the Triaxial Behavior of Concrete", Proceeding, International Associated for Bridge and Structure Engineering, Vol. 19, ISMES, Bergamo, Italy, 1975.

[71] Shah, S.P., Swartz, S.E., and Ouyang, C., "Fracture Mechanics of Concrete", John Wiley & Sons. Inc. New York, 1995.Cited by [72]

[72] Kochlakev, D., Miller, T., Yim, S., Chansawat, K., and Potisuk, T., "Finite Element Modeling of Reinforced Concrete Structures Strengthened with FRP Laminates", Oregon Department of Transportation, No. SPR316, May 2001.

[73] Rangand, B.V., and Joyce, M., "Strength of Eccentrically Loaded Slender Steel Columns Filled with High Strength Concrete", ACI

Structural Journal, Vol.89, No. 6, November-December 1992, pp 676-681. Cited by [23]

[74] Prion, H.G.L., and Boehme, J., "Beam-Column Behavior of Steel Tube Filled with High Strength Concrete", Canadian Journal of Civil Engg., Vol.21, 1994, pp207-218.

[75] Hajjar, J.F., Schiller, P.H., and Molodan, A., "A Distributed Plasticity Model for Concrete Filled Steel Tube Beam-Columns with Interlayer Slip", Engineering Structures, Vol. 20, No.8, 1998, pp663-676.

[76] Virdi, K.S., and Doweling, P.J., "Bond Strength on Concrete Filled Steel Tube", Proceedings, IABSE, pp125-139, 1980.

[77] Shakir-Khalil, H., and Hassan, N.K.A., "Push-out Resistance on Concrete Filled Tubes", Proceeding of the 6th International Symposium on Tubular Structures, Melbourne, Australia, December 1994, pp285-291.

[78] Syamy, P.N. and Anand, K.L, "Shrinkage and Creep Properties of High Strength Concrete", Civil Engineering and Public Works Review, October 1973, pp 859-868.

[79] Zienkiewicz, O.C., and Taylor, C.L., "Finite Element Method Volume 1- Its Basic and Fundamentals", 6th Edition, Butterworth-Heinemann, 2006.

Appendix A

Contact Algorithms

There are many approaches which can be used to represent the contact algorithm: **[79]**

A.1. Pure Lagrange multiplier

A pure Lagrange multiplier approach is given simply by multiplying the gap condition given in Equation (A.1) by the multiplier. Accordingly, we can write for each nodal pair for which a contact constraint is assigned a variational term

$$g = \tilde{x}_2^s - \tilde{x}_2^m = (\tilde{X}_2^s + \tilde{u}_2^s) - (\tilde{X}_2^m + \tilde{u}_2^m) = (\tilde{X}_2^s - \tilde{X}_2^m) + (\tilde{u}_2^s - \tilde{u}_2^m) \qquad \text{(A.1)}$$

$$\Pi_c = \int_{\Gamma_c} \mathbf{t}_\Gamma^T (\mathbf{x}^s - \mathbf{x}^m)\, d\Gamma \approx \lambda_n g \qquad \text{(A.2)}$$

where $\mathbf{t}_\Gamma$ is the surface traction, $\mathbf{x}^s$ is the position on the surface of the slave body, $\mathbf{x}^m$ is the position on the surface of the master body, λ_n is a Lagrange multiplier force and g is the gap given by Equation (A.1). We then add the first variation of Π_c to the variational equations being used to solve the problem. The first variation to Equation (A.2) is given as

And thus we identify λn as a 'force' applied to each node to prevent penetration. Linearization of Equation (A.3) produces a tangent matrix term for use in a Newton solution process. The final tangent and residual for the nodal contact element may be written as

$$\delta\Pi_c = \delta\lambda_n g + (\delta\tilde{u}_2^s - \delta\tilde{u}_2^m)\lambda_n = \begin{bmatrix} \delta\tilde{u}_2^s & \delta\tilde{u}_2^m & \delta\lambda_n \end{bmatrix} \begin{Bmatrix} \lambda_n \\ -\lambda_n \\ g \end{Bmatrix} \qquad \text{(A.3)}$$

$$\begin{bmatrix} 0 & 0 & 1 \\ 0 & 0 & -1 \\ 1 & -1 & 0 \end{bmatrix} \begin{Bmatrix} d\tilde{u}_2^s \\ d\tilde{u}_2^m \\ d\lambda_n \end{Bmatrix} = \begin{Bmatrix} -\lambda_n \\ \lambda_n \\ -g \end{Bmatrix} \qquad \text{(A.4)}$$

and is accumulated into the global equations in a manner identical to any finite element assembly process. It is evident that the equations in this form introduce a new unknown for each contact pair. Also, as for any Lagrange multiplier approach, the equations have a zero diagonal for each multiplier term, thus, special care is needed in the solution process to avoid division by the zero diagonal.

In a contact state, one could select one of the parameters, say $\tilde{x}^s_2$, as a primary variable and directly satisfy the gap constraint by making $\tilde{x}^m_2 = \tilde{x}^s_2$. This approach is called constraint elimination and may be used to reduce the number of overall unknowns. In the simple frictionless node-to-node contact case it is simple to implement as no transformations are needed to write the constraint equation. In a general case, however, the approach can become quite cumbersome and it is often simpler to use the pure Lagrange multiplier form directly or to consider other related approaches. If the global tangent matrix has its non-zero sparse structure defined for the case when all the specified contact elements are active (e.g. the tangent matrix defined by Equation (A.4) can be inserted without adding new non-zero terms) then a full contact analysis may be performed using Eq. (A.4) when

$g \leq 0$ and using the alternate tangent matrix and residual.

$$\begin{bmatrix} 0 & 0 & 0 \\ 0 & 0 & 0 \\ 0 & 0 & 1 \end{bmatrix} \begin{Bmatrix} d\tilde{u}^s_2 \\ d\tilde{u}^m_2 \\ d\lambda_n \end{Bmatrix} = \begin{Bmatrix} 0 \\ 0 \\ 0 \end{Bmatrix} \qquad \text{(A.5)}$$

For nodal pairs when $g > 0$ However, if a large number of possible contact pairs are inactive (i.e. $g > 0$) it is more efficient to recompute the sparse structure of the global tangent matrix to just accommodate the active contact pairs (i.e. those for which $g \leq 0$). This step can be performed by determining all the active pairs prior to computing the tangent arrays.

A.2. Perturbed Lagrange Multiplier

The problem related to the zero diagonal may be resolved by considering a perturbed Lagrangian form where

$$\Pi_c = \lambda_n g - \frac{1}{2\kappa}\lambda_n^2 \tag{A.6}$$

In which κ is a parameter to be selected. As κ→∞ the perturbed Lagrangian method converges to the same functional as the standard Lagrange multiplier method. The first variation of Π_c becomes

$$\delta\Pi_c = \delta\lambda_n \left(g - \frac{1}{\kappa}\lambda_n \right) + [\delta\tilde{u}_2^s - \delta\tilde{u}_2^m]\lambda_n \tag{A.7}$$

And again we identify λn as a 'force' applied to each node to prevent penetration.

Linearization of Eq. (A.3) produces a tangent matrix term for use in a Newton solution process. The final tangent and residual for the nodal contact element may be written as:

$$\begin{bmatrix} 0 & 0 & 1 \\ 0 & 0 & -1 \\ 1 & -1 & -1/\kappa \end{bmatrix} \begin{Bmatrix} d\tilde{u}_2^s \\ d\tilde{u}_2^m \\ d\lambda_n \end{Bmatrix} = \begin{Bmatrix} -\lambda_n \\ \lambda_n \\ -g + \lambda_n/\kappa \end{Bmatrix} \tag{A.8}$$

which is added into the equations in a manner identical to the Lagrange multiplier form. It is also possible to eliminate λ_n directly from Equation (A.7) giving

$$\lambda_n = \kappa g = \kappa(\tilde{x}_2^s - \tilde{x}_2^m) \tag{A.9}$$

Substitution into Equation (A.8) and eliminating $d\lambda_n$ gives the reduced form

$$\begin{bmatrix} \kappa & -\kappa \\ -\kappa & \kappa \end{bmatrix} \begin{Bmatrix} d\tilde{u}_2^s \\ d\tilde{u}_2^m \end{Bmatrix} = \begin{Bmatrix} -\lambda_n \\ \lambda_n \end{Bmatrix} \tag{A.10}$$

In a perturbed Lagrangian approach the final gap will not be zero but becomes a small number depending on the value of the parameter κ selected. Thus, the advantage of the perturbed Lagrangian method is somewhat offset by a need to

identify a value of the parameter that gives an acceptable answer. Indeed, in a complex problem this is not a trivial task, especially for problems involving contact between structural elements (e.g. rods, plates, or shells) and solid elements. This can be avoided in part by modifying Equation (A.8) to read

$$\begin{bmatrix} 0 & 0 & 1 \\ 0 & 0 & -1 \\ 1 & -1 & -1/\kappa \end{bmatrix} \begin{Bmatrix} d\tilde{u}_2^s \\ d\tilde{u}_2^m \\ d\lambda_n \end{Bmatrix} = \begin{Bmatrix} -\lambda_n \\ \lambda_n \\ -g \end{Bmatrix} \tag{A.11}$$

Here this form is called a perturbed tangent method and is a combination of the perturbed Lagrangian tangent matrix with the Lagrange multiplier residual. As such it is not a consistent linearization of any functional and there is some loss in convergence rate in solving the overall non-linear problem. Moreover, it is not possible to directly solve for λ_n in each element and an iterative update must be used with

$$\begin{aligned} d\lambda_n &= \kappa \left(g + d\tilde{u}_2^s - d\tilde{u}_2^m \right) \\ \lambda_n &\leftarrow \lambda_n + d\lambda_n \end{aligned} \tag{A.12}$$

In the above the incremental displacements are those from the last global solution;

however, the same form may be used in Equation (A.11) to give the reduced problem

$$\begin{bmatrix} \kappa & -\kappa \\ -\kappa & \kappa \end{bmatrix} \begin{Bmatrix} d\tilde{u}_2^s \\ d\tilde{u}_2^m \end{Bmatrix} = \begin{Bmatrix} -\lambda_n - \kappa g \\ \lambda_n + \kappa g \end{Bmatrix} \tag{A.13}$$

The method does, however, converge to a solution in which g approaches zero when κ is large enough. Thus the difficulty of selecting an appropriate value for κ is still not fully resolved.

A.3. Penalty Method

An alternative approach which avoids the difficulties of dealing with a zero diagonal from a Lagrange multiplier method is the classical penalty method. In this method the contact term is given by

$$\Pi = \tfrac{1}{2}\kappa g^2 \tag{A.14}$$

where κ is a penalty parameter. The matrix equation for a nodal pair is now given by

$$\begin{bmatrix} \kappa & -\kappa \\ -\kappa & \kappa \end{bmatrix} \begin{Bmatrix} d\tilde{u}_2^s \\ d\tilde{u}_2^m \end{Bmatrix} = \begin{Bmatrix} -\kappa g \\ \kappa g \end{Bmatrix} \tag{A.15}$$

For the scalar problem considered here the penalty and the perturbed Lagrangian methods lead to identical reduced problems. However, when multi-point constraints are considered and independent approximations are taken for λ_n and **u** the two methods are different unless the limitation principle is satisfied (i.e. the λn includes all the terms in the expression for g). Thus, in practice, the use of the perturbed Lagrangian method is preferred. This is especially crucial for more complex methods in treating contact problems, such as mortar methods or other surface-to-surface treatments.[79]

A.4. Augmented Lagrangian

A compromise between the perturbed Lagrangian or penalty methods and the Lagrange multiplier method may be achieved by using an iterative update for the multiplier combined with a penalty-like form. We write the augmented form as

$$\begin{bmatrix} \kappa & -\kappa \\ -\kappa & \kappa \end{bmatrix} \begin{Bmatrix} d\tilde{u}_2^s \\ d\tilde{u}_2^m \end{Bmatrix} = \begin{Bmatrix} -\lambda_n^k - \kappa g \\ \lambda_n^k + \kappa g \end{Bmatrix} \tag{A.16}$$

Where an update to the Lagrange multiplier is computed by using (79)

$$\lambda_n^{k+1} = \lambda_n^k + \kappa g \tag{A.17}$$

Such an update may be computed after each Newton iteration or in an added iteration loop after convergence of the Newton iteration. In either case a loss of quadratic convergence in solving the global non-linear problem results for the simple augmented strategy shown. Improvements to super-linear convergence are possible as shown, and a more complex approach which restores the quadratic convergence rate may be introduced at the expense of retaining an added variable. [79]

In general, however, use of a fairly large value of the penalty parameter in the simple scheme shown above is sufficient to achieve good solutions with few added iterations. In summary, we find the Lagrange multiplier form to be the only one that does not require the identification of an appropriate value for the κ parameter. Furthermore, in a Newton solution algorithm the Lagrange multiplier form leads to optimal satisfaction of the impenetrability condition in a minimum number of iterations.

اضافة الى ذلك، تم اجراء دراسة مقارنة اثبت ان الزيادة في مقاومة الانضغاط للخراسنة او اجهاد الخضوع للحديد يسبب زيادة في الحمل الاقصى للمقطع المركب،وكذلك استخدام مقطع دائري بالمقارنة مع المقاطع الاخرى (مربع او دائري) يعطي اكثر قابلية تحمل لنفس مساحة المقطع العرضي بنسبة تصل الى (12%)

الخلاصة

الهياكل المركبة (يتم انشاءها من خرسانة مالئة لانبوب معدني او من هيكل معدني مغلف بالخرسانة) والتي توفر صلابة اكثر، فضاء اوسع، وكذلك اكثر اقتصادية بالنسبة للبنايات المرتفعة والمتوسطة الارتفاع.

خلال هذه الدراسة تم استخدام التحليل اللاخطي بطريقة العناصر المحددة للتنبؤ بعلاقة الحمل بالهطول بالنسبة للهيكل المركب تحت تأثير ظروف مختلفة من الاحمال الساكنة وذلك باستخدام برنامج ANSYS V.9، وقد تم استخدام العناصر الطابوقية لتمثيل الخرسانة (المسلحة والغير مسلحة) ولتمثل المقطع الحديدي (انبوبي او مقطع-I)، اضافة الى ذلك تم تمثيل الروابط بين الخرسانة والحديد باستخدام العناصر البينية ذوات العقدتين. تم حل المعادلات التوازن اللاخطية باستخدام طريقة (Full Newton-Raphson). تم اخذ التصرف اللاخطي للمواد، والذي يشمل التشقق والتهشم للخرسانة والخضوع لحديد التسليح والاضلاع الحديدية بنظر الاعتبار، اذ تم تمثيل الخرسانة المتشققة بالشد باستخدام نموذج التشقق المنتشر الثابت مع الاخذ بنظر الاعتبار انتقال قوى القص بعد التشقق.

حللت عدة مقاطع مركبة (اعتاب واعمدة) وتم مقارنة نتائج التحليل مع النتائج العملية. فوجد ان التحليل باستخدام طريقة العناصر المحددة تعطي نتائج متقاربة مع النتائج العملية. في الدراسة الحالية، تم تحليل ثلاث انواع من الهياكل(هيكل مركب تتكون عناصره من خرسانة مالئة للأنبوب المعدني، هيكل مركب تتكون عناصره من مقطع معدني مغلف بالخرسانة، وهيكل خرساني مسلح) بنفس ماسحة المقطع العرضي للحديد والخرسانة، بالنسبة للنوع الاول من الهياكل (هيكل مركب تتكون عناصره من خرسانة مالئة للأنبوب المعدني) يمثل اكثر قابلية تحمل للأحمال من بقية الانواع، وكذلك النوع الثاني للهياكل (هيكل مركب تتكون عناصره من مقطع معدني مغلف بالخرسانة) يمتلك قابلية تحمل اكثر من الهيكل الخرساني المسلح.

جمهورية العراق
وزارة التعليم العالي والبحث العلمي
جامعة بابل- كلية الهندسة
قسم الهندسة المدنية

التحليل اللاخطي باستخدام طريقة العناصر المحددة للهياكل المستوية المتكونة من الاعضاء المركبة

رسالة مقدمة الى

قسم الهندسة المدنية في كلية الهندسة في جامعة بابل كجزء من متطلبات نيل شهادة ماجستير علوم في الهندسة المدنية

من قبل

ماجد محمد علي كاظم محيي الدين

بكلوريوس في الهندسة المدنية 2006

اشراف

الاستاذ الدكتور نمير عبد الامير علوش

د.مصطفى بلاسم داوود

تشرين الثاني- 2008